

DESIGN AND EXPERIMENTAL VALIDATION OF A CARBON FIBRE SWINGARM TEST RIG

Reno Kocheappen Chacko

A research report submitted to the Faculty of Engineering and the Built Environment, of the University of the Witwatersrand, in partial fulfilment of the requirements for the degree of Master of Science in Engineering

March 2013

Declaration

I declare that this research report is my own unaided work. It is being submitted to the Degree of Master of Science to the University of the Witwatersrand, Johannesburg. It has not been submitted before for any degree or examination to any other University.

.....

(Signature of Candidate)

..... day of,

Abstract

The swingarm of a motorcycle is an important component of its suspension. In order to test the durability of swingarms, a dedicated test rig was designed and realized. The test rig was designed to load the swingarm in the same way the swingarm is loaded on the test track. The research report structure is as follows: relevant literature related to automotive component testing, current swingarm test rig models and composite swingarms were outlined. The Leyni bench, a rig specifically developed by Ducati to test swingarm reliability was shown to be effective but lacked the ability to apply variable loads. The objective of this research was to design and experimentally validate a swingarm test rig to evaluate swingarm performance at different loads. The methodology, the components of the test rig and the instrumentation required to achieve the objectives of the research were presented. The elastic modulus of the carbon fibre swingarm material was calculated using classical laminate theory. The strains and stresses within a swingarm during testing were analysed. The test rig was shown to be versatile, accurate and efficient, with potential for future application. This research has shown the benefit of test rigs for testing motorcycle components.

To Ryan Chacko Preno

Acknowledgment

First of all, to the almighty God, who strengthened me day in and day out. I take this opportunity to thank Dr Frank Kienhofer, lecturer and researcher, within the school of Mechanical, Industrial and Aeronautical Engineering, The University of the Witwatersrand for providing me with all the support and guidance to carry out my project successfully and for making my contribution to BlackStone Tek (BST) possible.

I express my sincere gratitude to my internal guides in BST, Mr Craig Goodrum and Mr Damien Hawken who provided me with moral support and stood by me throughout the entire duration of my project.

I express my profound sense of gratitude to the lecturers and the lab assistants of the University of the Witwatersrand and Mr Hendrick and Mr Lawrence of BST. I am grateful to the staff and management of the University of the Witwatersrand and BST for providing the necessary facilities and encouragement for conducting the project.

Table of Contents

Declaration.....	i
Abstract.....	ii
Acknowledgment.....	iv
Table of Contents.....	v
List of Figures.....	viii
List of Tables.....	x
List of Symbols.....	xi
Nomenclature.....	xiv
Chapter 1: Introduction.....	1
1.1 Background.....	1
1.2 The Swingarm and Its Evolution.....	1
1.3 Ducati 1098 Single-Sided Swingarm.....	3
1.4 Composites and its Development.....	4
1.5 Chapter Summary.....	5
Chapter 2: Literature Review.....	6
2.1 Automotive Components Development in South Africa.....	6
2.2 Development of Rigs for Testing.....	6
2.2.1 Automotive Component Test Rigs.....	7
2.3 Research Projects on Swingarm.....	9
2.3.1 Swingarm Test Rigs.....	9
2.4 Swingarm Development Using Lighter and Stronger Materials.....	12
2.5 Motivation to Develop a New Swingarm Test Rig.....	13
2.6 Significance of Research.....	13
2.7 Project Objectives.....	14
2.7.1 Phase 1- Design of Test Rig.....	14
2.7.2 Phase 2- Evaluation of Rig Performance.....	14
2.7.3 Phase 3- Evaluation of Results.....	14
2.8 Organization of the Dissertation.....	15
2.9 Chapter Summary.....	15
Chapter 3: Methodology.....	17
3.1 Product Requirement Specification (PRS).....	17

3.1.1 Requirements	17
3.1.2 Constraints	20
3.1.3 Criteria	22
3.2 Design Approach	26
3.3 System and Facility Requirements.....	26
3.3.1 Mechanical Components.....	26
3.3.2 Data Acquisition (DAQ) System	27
3.3.3 Higher Reliability Procedures or Modifications	31
3.4 Limitations of the Test Rig	31
3.5 Methodology to Calculate the Effective Elastic Constants of the Carbon Fibre Swingarm	32
3.5.1 Design Approach	34
3.5.2 Assumptions.....	34
3.5.3 Young's Modulus, Volume Fraction, the Thickness and the Poisson's Ratio of Lamina	34
3.5.4 New Stiffness Values for Toray 700G According to the Orientation of Ply in Tension and Compression.....	37
3.5.5 Effective Elastic Constants of the Swingarm for the 12 Layers	38
3.6 Chapter Summary	39
Chapter 4: Results and Discussion.....	41
4.1 Introduction.....	41
4.2 Variation of Effective Elastic Constants with Fibre Orientation for the 12 Layers.....	41
4.3 Effect of Thickness	44
4.4 Effect of Volume Fraction	45
4.5 Evaluation of Test Rig	46
4.5.1 Static Test.....	47
4.5.2 Dynamic Test.....	47
4.6 Static Test Results.....	48
4.6.1 Load vs. Time	51
4.6.2 Strains vs. Time	52
4.6.3 Stresses vs. Time.....	52
4.6.4 Stress vs. Strain.....	53
4.7 Dynamic Test Results	54
4.7.1 Load vs. Time	55
4.7.2 Transmission History	56
4.7.3 Strain in One Second	56
4.7.4 Stresses in One Second	57
4.7.5 Stresses vs. Number of Cycles.....	59

4.7.6 Stress vs. Strain.....	60
4.8 Chapter Summary	61
Chapter 5: Conclusions and Future Work.....	63
5.1 Conclusions.....	63
5.2 Recommendations for Further Work	64
References.....	65
Appendix A.....	69
A.1 Cost of Machined Components.....	69
A.2 Load Design	70
A.3 Spring Design.....	71
A.4 Motor Design	74
A.5 Eccentric Bolt Design	75
A.6 Eccentric Shaft Design.....	77
A.7 Thread for the Hexagonal Bolt Design	79
A.8 Bearing Design.....	81
A.8.1 Bearing Over the Eccentric Shaft Design	81
A.8.2 Bearing Reactions	82
A.8.3 Bearing-2 Design	83
Appendix B	85
B.1 Strain Gauge Calibration.....	85
B.2 Load Cell Calibration	86
B.3 Equations for Strain Gauge Measurements	88
Appendix C.....	89
C.1 Young's Modulus, Volume Fraction, the Thickness and the Poisson's Ratio of Lamina	89
C.2 New Stiffness Values According to the Orientation of Ply in Tension and Compression	90
C.2.1 Equations Used.....	90
C.2.2 Variation of Elastic Constants with Fibre Orientation	90
C.3 Effective Elastic Constants of the Swingarm for the 12 Layers	93
Appendix D.....	94
D.1 Effect of Thickness	94
D.2 Effect of Volume Fraction	95
D.3 Variation of Dynamic Load	96
D.4 Classical Laminate Theory.....	97
Appendix E	100
E.1 The English code	100

List of Figures

Figure 1.1 Ducati 1098 single-sided swingarm	3
Figure 2.1 A rolling bench test rig (42)	10
Figure 3.1 Six degrees of freedom of the swingarm in a real-life test.....	20
Figure 3.2 The six degrees of freedom of the swingarm during the test	21
Figure 3.3 CAD model of the swingarm test rig for dynamic testing.....	23
Figure 3.4 The swingarm static test rig.....	24
Figure 3.5 Layout for data acquisition	28
Figure 3.6 Attachment of strain gauges on the swingarm-1	29
Figure 3.7 Attachment of strain gauges on the swingarm-2	29
Figure 3.8 Graphical user interface panel	31
Figure 3.9 The swingarm layup, which has $+45^{\circ}/-45^{\circ}$ and $0^{\circ}/90^{\circ}$ orientations	33
Figure 3.10 Principle material axes in a unidirectional lamina (53).....	35
Figure 4.1 Variations of effective Young's modulus and Poisson's ratio with orientation.....	42
Figure 4.2 Variations of effective shear modulus with orientation	43
Figure 4.3 Variations of effective elastic constants for compression with orientation.....	44
Figure 4.4 Variations of effective Young's modulus with volume fraction	45
Figure 4.5 Variations of effective transverse and shear modulus with volume fraction	46
Figure 4.6 Mechanical spring arrangement inside spring housing	47
Figure 4.7 Variation of dynamic load to the eccentric radius.....	48
Figure 4.8 Resultant forces and moments acting on the laminate	49
Figure 4.9 Load applied during the static test.....	51
Figure 4.10 Strains experienced during the static test	52
Figure 4.11 Stresses experienced during the static test.....	53
Figure 4.12 Stress-strain graphs for static testing.....	53
Figure 4.13 Effective load applied in one second.....	55
Figure 4.14 Strain readings from the dynamic test	56
Figure 4.15 Effective strains in one second	57
Figure 4.16 Stresses experienced in each second during the dynamic test.....	58
Figure 4.17 Stresses experienced during the dynamic test	59
Figure 4.18 Stress-strain graphs for dynamic testing.....	60

Figure A.1 Dimensions of a spring	71
Figure A.2 Eccentric mechanism components and the electric motor.....	74
Figure A.3 Eccentric system of the test rig.....	75
Figure A.4 Eccentric shaft and its components	77
Figure A.5 Hexagonal bolt and its components.....	80
Figure A.6 Dimensions of a double row angular contact ball bearing	81
Figure A.7 Bearing reactions	82
Figure A.8 Dimensions of a deep groove ball bearing	83
Figure B.1 Load vs voltage graph.....	87
Figure C.1 Variations of Young's modulus for Toray 700G with orientation	91
Figure C.2 Variations of shear modulus for Toray 700G with orientation.....	91
Figure C.3 Variations of Poisson's ratio for Toray 700G with orientation	92
Figure C.4 Variations of elastic constants for Toray 700G with orientation.....	92
Figure D.1 Variations of effective elastic constants with thickness of composite	95
Figure D.2 Laminate geometry and ply numbering system.....	97

List of Tables

Table 3.1 Capital cost analysis of electrical test rig.....	25
Table 3.2 Capital cost analysis of hydraulic test rig	25
Table 3.3 Technical data sheet.....	36
Table 3.4 Stiffness values of each laminate.....	37
Table 3.5 Elastic constant values with orientation of ply for Toray 700G	38
Table 3.6 Effective elastic constants of the swingarm for the 12 layers.....	39
Table A.1 The cost of machined components within the factory	69
Table A.2 Cost of components purchased	70
Table B.1 Strain gauge calibration chart.....	85
Table B.2 Load cell calibration data	86
Table D.1 Effect of thickness on elastic constants	94
Table D.2 Effect of volume fraction on elastic constants	96
Table D.3 Variation of dynamic load to the eccentric radius	97
Table D.4 Calculated values for laminate thickness.....	98

List of Symbols

A	Area under which the stress acts
AC	Alternating current
C	Specific capacity
C_0	Basic static load rating
D	Diameter of shaft/bolt
D	Outer diameter
d	Inner diameter
D_d	Coil diameter
D_h	Diameter of guide sleeve
D_m	Mean coil diameter
E	Young's modulus,
E_f	Elastic modulus of fibre
E_m	Elastic modulus of matrix
E_{11}	Longitudinal modulus of elasticity
E_{22}	Transverse modulus of elasticity
F	Torsional frequency
F	Maximum load
F_a	Axial force
F_a	Alternating force
F_m	Constant mean load for a period of fluctuating load
F_c	Cyclic load
f_n	Natural frequency of the spring
F_{max}	Maximum force
F_{min}	Minimum force
F_p	Total preload
F_r	Radial force
F_{rc}	Rear wheel cyclic load
F_{rp}	Rear wheel total preload
g	Acceleration due to gravity
G_{12}	Longitudinal in-plane shear modulus
GF	Gauge factor of strain gauge

hp	Horse power
Hz	Hertz
K	Spring rate
K_t	Stress-concentration-factor for bending
K_{ts}	Stress-concentration-factor for torsion
kW	Kilowatt
L_h	Life in working hours
L_0	Free length of spring
L_n	Life in millions of revolutions
L_s	Solid length of the spring
M	Bending moment
N	Speed of shaft
N_a	Number of active coils
n_f	Total number of spring coils
P	Pitch of thread
Rf	Rated frequency
R_G	Nominal resistance value of strain gauge
R_L	Lead resistance
RPM	Rotations per minute
S_e'	Endurance limit
S_e	Cyclic stress
Sf	Factor of safety
S_{sa}	Fatigue strength in reversed shear
S_{sm}	Ultimate shear strength
S_{se}	Yield strength in shear
S_{ut}	Ultimate tensile strength
t	Laminate thickness
T_{c1}	Thickness of composites
τ_a	Alternating torsional stresses
τ_m	Midrange torsional stresses
τ_{min}	Minimum torsional stresses
τ_{max}	Maximum torsional stresses
τ_{xy}	Shear stress in the x - y plane
V_{c1}	Volume fraction of composites

V_{EX}	Excitation voltage.
V_f	Volume fraction of fibre
ν_f	Poisson's ratio of fibre
ν_m	Poisson's ratio of matrix
V_m	Volume fraction of matrix
$V_{O (strained)}$	Measured output when strained
$V_{O (unstrained)}$	Measured output voltage when unstrained
ν_{12}	Major Poisson's ratio
ν_{21}	Minor Poisson's ratio
W	Wahl correction factor
W_b	Motorcycle weight
W_r	Weight of rider and passenger
σ	Stress
σ_x	Longitudinal stress
σ_y	Transverse stress
σ_m	Midrange axial stresses
σ_a	Alternating axial stresses
σ_{min}	Minimum axial stresses
σ_{max}	Maximum axial stresses
ϵ	Strain
ϵ_s	Calibration strain
ϵ_i	Indicated strain
ϵ_x	Longitudinal strain
ϵ_y	Transverse strain
ϵ_{xy}	Average shear strain on the x faces along the y direction, and on the y face along the x direction
γ_{xy}	Shear strain in the x - y plane
θ	Angle to the reference axis
ρ	Density
ρ_m	Density of matrix
ρ_f	Density of fibre

Nomenclature

BST	BlackStone Tek
CAD	Computer Aided Design
EDS	Electro Dynamic Shaker
FEM	Finite Element Model
LabVIEW	Laboratory Virtual Instrumentation Engineering Workbench
LVM	LabVIEW Measurement
MIDP	Motor Industry Development Programme
NI	National Instruments
NPD	New Product Design and Development
OE	Original Equipment
PRS	Product Requirement Specification
R&D	Research and Development
RBT	Rolling Bench Test
TÜV	Technischer Überwachungsverein

Chapter 1: Introduction

1.1 Background

Motorcycles are one of the most affordable forms of motorised transport in many parts of the world. For most of the world's population, they are also the most common type of motor vehicle. The swingarm is the main component of the rear suspension of a modern motorcycle. It supports the rear axle while pivoting vertically to allow the suspension to absorb bumps on the road.

Motorcycle manufacturers are continually striving to improve their products and make components (e.g. the swingarm) lighter, stronger and cheaper. This research report details the development of an innovative suspension rig to test the durability of a swingarm. The rig will be used to develop improved swingarms.

This project has been completed with the industrial support of BlackStone Tek (BST). BST is an aftermarket and original equipment (OE) supplier of carbon fibre motorcycle components [1]. BST has recently developed a carbon fibre swingarm for the Ducati 1098 motorcycle which will be tested on the suspension rig detailed in this report.

Before a new design is allowed into the market, it first has to undergo certain quality tests. Since BST is approved by the German TÜV, quality tests have to be undertaken to ensure that the swingarm adhere to all the necessary safety standards ([Appendix E](#)). One of these tests is a fatigue test where a component has to run for 500 000 cycles at a given loading. After the test, no fatigue cracks or failure of mechanical fastenings may be present [2].

1.2 The Swingarm and Its Evolution

Automobile suspension systems and swingarms play a vital role in influencing ride comfort as well as handling dynamics [3]. The handling qualities of motorcycles are often of great importance [4]. They affect the pleasure to be gained from the rider-machine interactions and the safety of the rider. The right handling makes any move easy: it depends on several elements such as gravity centre position, total weight, stiffness, steering geometry, wheel size and driver-machine coupling [5].

Today's state of the art suspension designs evolved over the years, through numerous iterations [3] [6]. Investigations of the dynamics and the stability of motorcycle components have been conducted to improve the handling of motorcycles [7] [8] [9]. Comfort is also important to minimize the driver's stress; and thus suspension performance is crucial [6] [10]. Excessive flexibility of motorcycle components causes a phase lag which is difficult for the driver to control. Because of low stiffness values, the driver feels the motorcycle as being very heavy [11]. Motorcycles with a higher stiffness will have a greater responsiveness and handling.

The functions of a motorcycle frame (chassis and swingarm) are of two basic types: static and dynamic. In the static sense the frame has to support the weight of the rider or riders, the engine and transmission and the necessary accessories such as fuel and oil tanks [12]. For precise steering the frame must resist twisting and bending sufficiently to keep wheels in their proper relationship to one another regardless of the considerable dynamic loads imposed by power transmission, bumps, cornering and braking.

The main components linked to the chassis are the swingarm on the rear and the fork, which steers and damps, on the front. As a motorcycle travels down the road, bumps and road surface irregularities send dynamic loads through the rear wheel, forcing it upward. These dynamic loads push against the swingarm, which moves vertically against its pivot point. The vertical motion is dampened and absorbed by the suspension system, which rebounds and pushes the swingarm back towards the ground to prevent a loss of traction [5] [13].

An excessive strain either on the swingarm or of the chassis has a bad effect on the steering manoeuvre producing a thrust which is felt by the rider [14]. A procedure to measure these strains on a swingarm is a necessity to identify the forms of instability that can compromise the safety of the rider. The swingarm links the suspension to the wheel so its elasticity can significantly change the vehicle set-up. Adding another spring in series to the shock absorber can produce an unpredictable behaviour of the vehicle, thus reducing rider confidence. Therefore the swingarm must have the maximum possible stiffness without compromising its weight. Nowadays the structural optimisation of the swingarm is strategic for motorcycle performance improvement [13].

Over the last twenty years a non-stop evolution has led to stronger and stiffer swingarms due to the increased engine power [8]. At the beginning, a swingarm was simply a fork with two tubed arms and pick up points for the dampers, and a crossed cylinder as pivot location [3] [6]. This kind of swingarm was very weak, as all arms could swing freely from each other causing large deformation. Over the time the size of the arms (diameter and thickness) progressively grew until Yamaha made a new trellis scheme swingarm which was much stiffer.

Nowadays swingarms are mostly made with two boxed beams and many stiffening elements and ribs, and it is more and more uncommon to see a trellis model. Racing motorcycle swingarms have to be a lot stiffer because of the static and dynamic loads they take.

1.3 Ducati 1098 Single-Sided Swingarm

Unlike most traditional constructions, essentially symmetric (forks), the Ducati 1098 swingarm exhibits a single-sided configuration as show in Figure 1.1, in that it entirely develops along the left side of the wheel. The advantages that the single-sided swingarm enjoys over the fork solution are the suggestive appearance and the fast wheel access. The time reduction for changing the tyre and for testing different ratios of the chain transmission is particularly useful in competitions [13]. Also the torsional stiffness can be made insensitive to tightening of the wheel spindle, thus eliminating the disturbing attribute of the classical design [15].

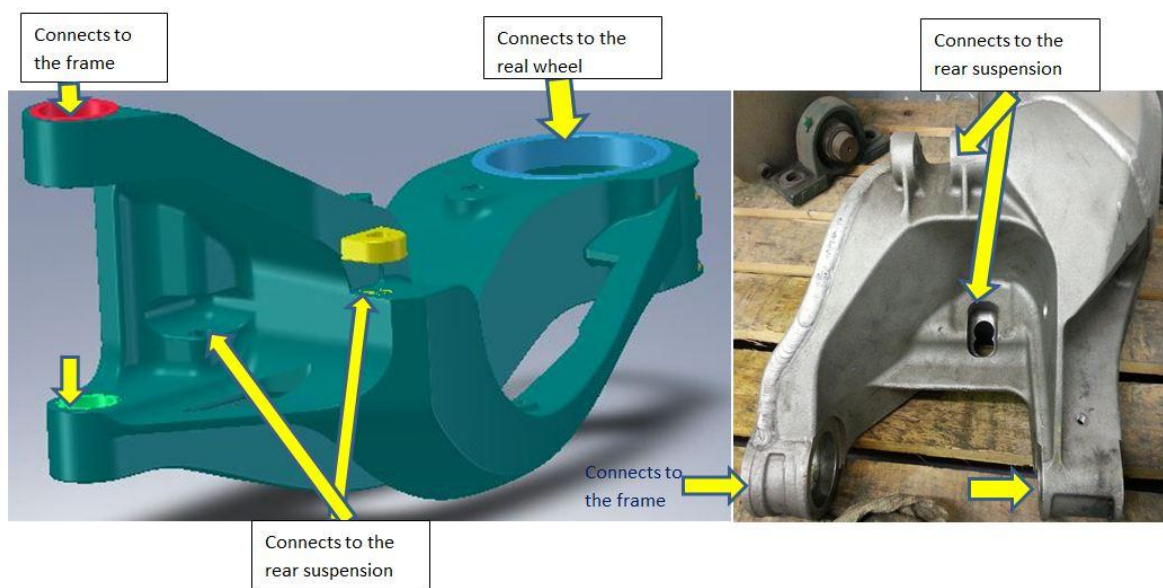


Figure 1.1 Ducati 1098 single-sided swingarm

The disadvantage of the single side swingarm is the reduction of the lateral bending stiffness at the same weight condition. This can significantly degrade the curve stability and the handling. The swingarm structure consists essentially of five connection points (Figure 1.1). The two spreads are provided with holes supporting the swingarm pivot which joins the swingarm to the frame with a swingarm pivot. The rear suspension is connected to the middle of the arm by means of a two pins: two slots house the end of the shock absorber and the extremity of the tie rod. Lastly the hub connects the swingarm to the rear wheel.

The stresses in swingarms are mainly affected by the rear suspension load; the most dangerous stress level occurs when the load of the strut and the shock absorber are maximum [13]. This happens slightly before the maximum shortening of the shock absorber because of the damper effect and the complex interaction between the tyre and the road, i.e. the load condition becomes more critical when riding over bumps.

Composite materials offer significant weight reduction opportunities and minimise stress concentration areas while making the product stiffer. A study done by Bruderick et al. [16] shows that the 2003 Dodge Viper was the first automotive to have its body structure redesigned in carbon fibre. Mass reductions and stiffness improvements in the body structure were the key achievements.

This process and material gave the design team great flexibility in consolidating the parts and increasing the function of the system. A carbon fibre swingarm was thus developed [17]. This new product enables the geometric freedom to improve frame design, resulting in improved vehicle performance.

1.4 Composites and its Development

For motorcycles, the chassis needs to be lighter to improve both fuel efficiency and operating performance. Some components of super sport models are currently being made of aluminium or magnesium alloys [18] [19]. Composites have about two-third of the specific weight of aluminium alloys and the high specific strength, provides a better solution [15] [17]. A high degree of rigidity is required for a motorcycle swingarm because torsional, vertical and horizontal bending forces are applied to it during its life.

In modern terms the word “composite” is often referred to a matrix material which is reinforced with fibres [20]. The compositions are combined on a microscopic scale through physical rather than chemical means, where the matrix is more soft and ductile than the reinforcing fibre. Metals are usually isotropic in nature i.e. their properties are not dependent upon direction whereas composites are anisotropic or at best orthotropic. Thus they show variation in their mechanical properties according to the direction of the orientation of fibre. [21].

The manufacturing method used can have a marked impact on the composite, thus manufacturing takes on increased significance. A carbon fibre is a long and thin filament which is about 5-10 μm in diameter and has a crystal bonding of carbon atoms which are more or less aligned parallel to the longitudinal axis of the fibre. This type of bonding makes the fibre very strong.

1.5 Chapter Summary

The introduction presents background information on swingarms and their evolution. The Ducati 1098 single-sided swingarm was described along with some fundamental concepts of composite materials. This work aims to show the design and validation of a test rig to perform quality tests on a carbon fibre swingarm.

A detailed literature review is given hereafter in Chapter 2 to establish what research has been carried out in the following areas:

- Automotive components development and development of rigs for testing.
- Research projects on swingarm and swingarm test rigs.
- Swingarm development using lighter and stronger materials.

Chapter 2: Literature Review

The literature review summarises research conducted on automotive test rigs and composite swingarms and testing. The initiative to introduce a test rig to assess the durability of swingarms is subsequently discussed along with the project objectives and the organization of the dissertation.

2.1 Automotive Components Development in South Africa

South Africa has a history of automotive assembly since 1920. Today, the country is the leading producer on the continent. There are approximately 250 first tier suppliers and in excess of 300 second and third tier suppliers. Investment in vehicle assembly and component manufacture has also increased at an annual rate of 12% [22].

The automotive industry is a volume driven industry and certain critical mass is a pre-requisite for attracting the much needed investment in research and development (R&D) and new product design and development (NPD). R&D investment is needed for innovations which is the life-line for achieving and retaining the competitiveness in the industry [23].

Simulation and testing at component level form an important part of automotive product development. The objective of any component level testing is to bring the road conditions to the lab. A procedure to derive an input excitation profile capable of generating damage similar to the road is required in any lab test.

2.2 Development of Rigs for Testing

In the highly competitive automotive world, automotive manufacturers are focussing their efforts on shortening product development cycle without compromising performance and reliability [4] [24]. This means reducing the testing time by identifying the failure modes early in the development cycle and avoiding the overdesign of components by optimising them to the required life [25] [26] [27]. Researches have also shown that a greater level of stability can be achieved by properly optimizing the design parameters without compromising the requirement of ride comfort [3] [4] [28].

It is very difficult to predict the future loading history of a motorcycle. One solution is to fit strain gauges and other transducers on a motorcycle ridden on a variety of road-track conditions. With sufficient testing, one can thus build up a picture of the load cycles of a typical machine over its expected lifetime. The second solution is to build a test rig that can simulate the road conditions [12]. The first is not an option since BST did not have any motorcycles for testing purposes but they are willing to invest in a test rig.

Physical testing must be conducted to validate designs and to determine the accuracy of simulation or virtual testing. Virtual testing cannot replace physical testing [29]. Physical testing can be performed on test rigs to validate simulations if it reproduces the failures realistically as it happens on the field [30]. A similar approach is required in this research to develop a test rig that simulates exact road conditions to test the durability and performance of swingarms.

2.2.1 Automotive Component Test Rigs

Durability test rigs have been built to test motorcycle components such as a rig to test the effect of disk braking on the durability of front shock absorber tubes [31], the fatigue life of centre stands [26], the fatigue life of motorcycle handlebars [28] [32], the fatigue analysis of motorcycle front fenders [27] [33] and the fatigue life of exhaust systems [34]. Results are generally obtained by measuring the strain on the component and then calculating the corresponding stresses. Different parameters like strain and acceleration play a crucial role in durability prediction, as they are required across the process from test track/lab testing, to virtual testing, to fatigue life prediction [30].

Kharul et al. [27] [33] used an electro dynamic shaker (EDS) to test a motor cycle front fender. Strain data were collected on the components while it was being tested on the test rig. The results obtained from experimental and FE-based fatigue life prediction were compared with the estimated target life. The component design was then optimised using the FEA simulation. A durable design of the fender was developed within a short time eliminating the design cycle time and product development cost.

Correlations between customer usage and laboratory testing of automotive components were conducted by Kharul et al. [24] [30]. Three full vehicle evaluation test rigs that evaluate various components in a vehicle were selected for establishing a correlation with road usage.

All three test rigs had different loading patterns and rig 1 in this analysis was a rolling test bench. Two different approaches, namely, failure data based analysis and experimental data based analysis were adopted to arrive at a final correlation between the structural test rigs and the customer usage on the road. The results indicated a good comparison between the approaches. The conclusion was drawn that a well-designed test rig can accurately predict the failure of a component being tested and gives a real test track response.

Similarly Muthuveerappan et al. [35] showed that test rigs for determining the performance of automobile parts with dynamic loading offer a versatile means of simulating the actual working condition of parts. The data obtained from the data acquisition systems from test rigs were more reliable in predicting the life of the parts and in establishing the safe working regime for the materials used in manufacturing the parts as compared to pure simulation. In conclusion, a well-designed test rig provides real test track response and makes the system more versatile in accurately predicting the failure of the component being tested.

Crump et al. [36] demonstrated the use of a test rig to replicate a full-scale pressure loading on a composite aircraft wing structure. Their work clearly demonstrated that test rigs can be designed to accurately impart representative loads to obtain the mechanical performance from composite structures using strain measurement techniques.

In a 2011 study, Ismail et al. [37] showed that the development of a test rig setup with LabVIEW could achieve test automation which reduced product validation time and provided accurate results to test for fault tolerance of a system. The testing although not precise was considered to be more accurate than analytical model predictions [38].

Carroll and Carver [39] presented a process for defining the mechanical parameters of laboratory test systems used in evaluating durability and performance properties of motorcycle components. They stated that in order to evaluate various properties of motorcycles, the process often leads to track testing, laboratory testing, or some combination of the two [30]. Also, a successful test begins with a good mechanical design which involves many complex factors to arrive at an optimal balance among cost, complexity, simulation accuracy, and ease of use. By considering those design factors, the mechanical engineer is more likely to arrive at a design that will recreate the desired test environment, measure

useful responses, and provide useful data for analysis and future work. All these factors were considered in this research.

2.3 Research Projects on Swingarm

A survey of the literature showed that there has not been extensive research into the testing of motorcycle swingarms using a test rig and even less into the development of composite swingarms but there are some studied on using FEM on swingarms for optimisation process [14] [40].

A study was done using FEM for radiation noise analysis of an electric scooter swingarm. The study was able to reduce the radiation noise by 10 dB [41].

Armentani et al. [14] developed a finite element model (FEM) of a swingarm to test for its torsional and lateral stiffness. Because of the gravity centre position, the weight distribution they used was 60% on the rear wheel and 40% on the front wheel. Five experimental static tests were carried out: three to test the lateral deflection and two to obtain the flexional and torsional stiffness.

2.3.1 Swingarm Test Rigs

Motorcycles are subjected to a series of physical tests to ensure survivability when subjected to static and cyclic loadings. The bump test is one of the critical life tests performed on a motorcycle for evaluating the fatigue life of the frame [25]. Unlike automobiles, in laboratory simulations of motorcycles, test rigs must hold the Motorcycle upright. During normal riding, gyroscopic effects of the tyres and wheels hold the vehicle upright [4].

A specially designed test bench was made to test three motorcycle swingarms by Risitano et al. [11]. It was designed especially for determining the torsional stiffness of the components, the symmetries and similarities in behaviour between clockwise and counter clockwise stress. The rig consisted of a rigid steel platform on which the swingarm was constrained. Potentiometers and dynamometers were used to measure the movements and the loads applied by a hydraulic jack. The rear suspension was replaced with non-deformable rigid strut fixed to the test bench. The pin-wheel and the wheel hub were mounted on the swingarm for all tests. The torque was applied at points where there are holes in the chain tensioner. The experimental results were validated with FEM analysis and the average percentage error was

less than 4%. This rig was limited to torsional stiffness test on swingarms that are symmetrical.

2.3.1.1 Comfort Bench Test or Rolling Bench Test (RBT)

Rolling bench test (RBT) is a common test widely spread throughout motorcycle/scooter companies whose rules have not been standardized yet; thus being different from one company to another. The RBT is a severe test designed for reliability study of some motorcycle parts: indeed, by the RBT it is possible to apply high stresses on the vehicle performing accelerated fatigue cycles. This test replaces the on road tests, with ensuing time and cost-saving. During the RBT the vehicle frame complete with front and rear suspension is placed above rolling drums as shown in Figure 2.1. A variable number of shaped obstacles are arranged on the external surface of one of the two rollers.

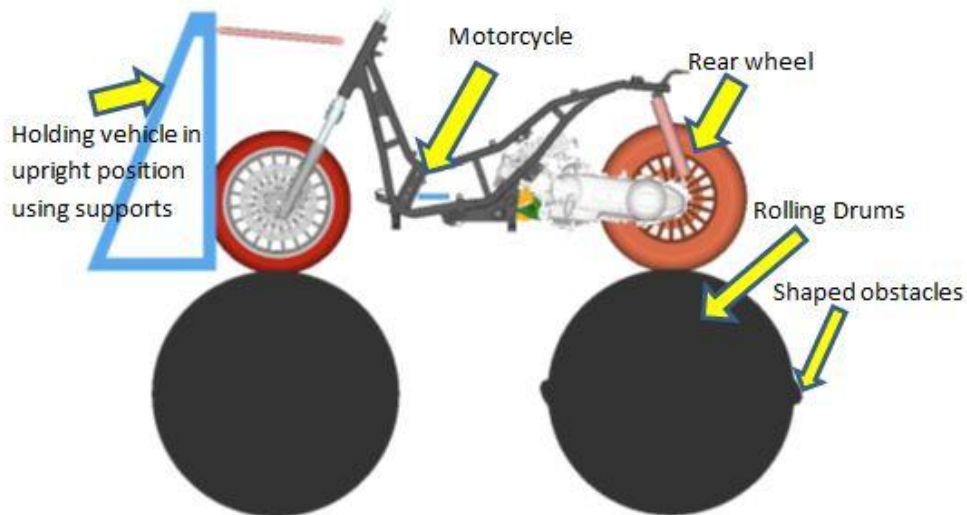


Figure 2.1 A rolling bench test rig [42]

The RBT was simulated by means of commercial multi-body software by Ardiri et al. [42]. The aim of their paper was to obtain the spectral stresses acting upon the swingarm of a scooter during the RBT, so as to evaluate its fatigue strength. The correlation between experimental data and computed results were good with a discrepancy of less than 5%. Their work demonstrated the accuracy and reliability of numerical simulation to drastically reduce the time of real experiments and tests.

Kumar [5] presented an FEM analysis of a motorcycle swingarm in different loading conditions for optimisation. The results were validated through experimental analysis using an RBT.

Carfagni et al. [10] built a numerical model that reproduced the test of a scooter on a RBT. The model simulated the dynamic behaviour of the chassis and the rear suspension of the motorcycle. A shortcoming with the RBT [25] is that the static weight applied doesn't count the weight of the rider and passenger. Thus a modified roller bench called the Leyni test bench that includes the static weight was designed by Ducati.

2.3.1.2 Leyni test bench

The Leyni test bench is used to conduct fatigue tests to verify the reliability of the main bodies of a motorcycle. The rig incorporates a rolling rig for testing a motorcycle on which a dummy is placed [12] [13] [18]. A compression beam is lowered on to the dummy pushing down with a load of 1960 N (the weight of the pilot and his passenger).

Stefano and Simone [43] developed a structural optimisation method which Ducati used to design an efficient swingarm structure, with a high stiffness to weight ratio, respecting the constraints given by the stylists. The purpose was to maximize the swingarm torsional stiffness while minimizing its mass. The study was carried out by simulating a Leyni test to test the behaviour between the swingarm and the other components of the motorcycle including the chassis and the suspension system.

By means of numerical simulations (using FEM analysis) and experimental tests (using the Leyni test bench) the stress field of a Ducati Monster S4 R single-sided swingarm and the dynamic behaviour of a Ducati chassis were tested by Cassani and Mancuso [13] and Piazza [12] respectively. They both concluded that the numerical results agreed with the failures seen at the Leyni bench tests after many hundred thousands of loading cycles.

Gaiani [18] redesigned the carbon steel swingarm to an aluminium swingarm for the Ducati Monster S4 R. Different welding solutions were compared to optimise the design. He used the Leyni bench to test the reliability of the new component by an accelerated fatigue test. Finally he was able to apply automatic MIG-welding technique to assemble the parts of the swingarm and thus increasing daily production from 28 units to 110 units. It was observed during the Leyni test he conducted that, in a standard test, a maximum external loading of 5900 N on the motorcycle (excluding the weight of the motorcycle) occurs during the impact

of the step (Appendix E, test factor (K_r) of 1.431). This standard maximum load will be used in this research.

The main advantages of the Leyni test bench are its flexibility, cheapness, the speed of testing and repeatability. The drawbacks are the impossibility to apply horizontal forces and variable loads. It is not possible to obtain fatigue stress curves at different load levels because the applied forces are controlled by the motorcycle suspension dynamics and determined by the interactions between the stepped drum, tyre, suspension frame, constraint and preload systems [12].

2.4 Swingarm Development Using Lighter and Stronger Materials

Based on the stress analysis of a swingarm of a certain model, Iwasaki et al. [19] designed a magnesium swingarm that had the same degree of deflection when subjected to a torsion load as an aluminium swingarm. A prototype magnesium swingarm was designed and produced by press forming and TIG-welding the rolled AZ31 and extruded AZ31 magnesium alloys respectively, because they were easier to find on the market. They concluded that the prototype magnesium swingarm was 10% lighter and had 60% more torsional rigidity and the static strength of the prototype magnesium swingarm was similar or superior to that of the conventional aluminium swingarm.

Modern swingarms are mostly made with two boxed beams and many stiffening elements and ribs for it to be stronger and lighter. Racing motorcycle swingarms have increased stiffness and strength because of the increased static and dynamic loads they bear. Composite materials offer significant weight reduction opportunities and O'Dea showed that a 3.9 kg aluminium swingarm could be redesigned to weigh 2.7 kg using carbon fibre [17].

A magnesium alloy Ducati 916 single-sided swingarm was redesigned with composite materials for reduction in mass and mass moment of inertia at comparable stiffness by Dragoni and Foresti [15]. The structural behaviour of the composite arm was optimised by FEM in view of high stiffness and low weight. The final composite design exhibits an increased torsional stiffness (+10%), together with reduced mass (-30%) and mass moment of inertia (-40%). The mass reduction contributed to a brisker performance and to a more responsive handling of the machine while the decrease in mass moment of inertia added to

the bumping, the rebounding characteristics of the rear suspension, improving road holding on irregular tracks.

2.5 Motivation to Develop a New Swingarm Test Rig

A search of the relevant literature revealed that there are few published experiments quantifying the performance and durability of a swingarm. A summary of existing models and their shortcomings are as follows:

1. Ardiri et al. [42], Kumar [5] and Carfagni et al. [10] validated their results by conducting experimental analysis using a RBT. But the static weight applied on an RBT never counts the weight of the rider and pilot and limiting the accuracy of the load applied to a real-life test.
2. Risitano et al. [11] model was limited to torsional stiffness test for symmetrical swingarms.
3. Dragoni and Foresti [15] validated their single-sided Ducati 916 composite swingarm with an FE model but were never compared to any experimental results for accuracy.
4. The simulated Leyni test bench by Stefano and Simone [43], Cassani and Mancuso [13] and Piazza [12] validated their results by conducting experimental analysis using the Leyni test bench which counts the weight of the rider and pilot. But the accuracy of the model was limited due to the impossibility to apply horizontal forces and variable loads.

Considering the above points, this study seeks to identify and validate a suitable accelerated approach for durability and performance testing of motorcycle components, in particular swingarms. The Leyni test bench developed by Ducati did not evaluate swingarm performance at different loads, and therefore it is desirable to have a simplified test rig that can quickly and easily predict swingarm performance and counter the drawbacks of the Leyni test bench. A dedicated test rig has to be designed to replicate the loading that a swingarm could experience on the test track. The rig will then be used to test the durability and performance of swingarms.

2.6 Significance of Research

A normal procedure for any automotive component which undergoes any testing is as follows [25] [26] [27] [38]: a test simulation is made using software like ADAMS or BikeSim.

Subsequently, the data obtained from this model are used in FEM software and the stresses are predicted. The stress pattern helps in identifying the critical areas. The critical areas identified are validated through experimental strain measurement. The validated model is further used to optimise the design by reducing the stresses at critical areas to below the acceptable limit. The final optimised frame will clear the test without any failure. This kind of approach saves the need to conduct expensive iterative tests.

This project is part of a larger project to develop an optimised swingarm. The FEA and optimisation were considered to be beyond the scope of this project, which is a 50/50 MSc. A 50/50 MSc is made up to 50% coursework and 50% research. The development and design of a new swingarm test rig was considered sufficiently novel as discussed in section 2.5.

2.7 Project Objectives

To design and experimentally validate a swingarm test rig to be used for durability testing of carbon fibre swingarms at varying loads.

2.7.1 Phase 1- Design of Test Rig

Design a test rig for the fatigue testing of a carbon fibre swingarm.

The test rig should:

- Replicate the suspension of a Ducati 1098.
- Apply the required loads for the static and the dynamic test.

2.7.2 Phase 2- Evaluation of Rig Performance

The system should be capable of:

- Counting the number of cycles performed.
- Capturing and storing the load and all strains experienced by the swingarm during fatigue testing.
- Controlling the speed of the motor.

2.7.3 Phase 3- Evaluation of Results

- The Swingarm should undergo 1.2 million cyclic loads ($S_f > \text{two}$, more than twice the BS code requirement) for BST management approval.
- Determine the stresses within a swingarm during testing and show that the swingarm will withstand a real-life test without failure.

2.8 Organization of the Dissertation

The article is organized as follows:

Chapter one provides an introduction to this research, the background, the research problem, research question and the hypothesis. It provides the overall research setting.

Chapter two presents a review of relevant literature related to automotive component testing, current swingarm test rig models and composite swingarms. The project objectives are outlined in this chapter.

Chapter three provides details on the methodology used in this research for the design of the rig and to calculate the modulus of the carbon fibre swingarm. The chapter contains details of how the rig was designed to make it as realistic as a real-life test and the detailed design of the major components of the rig.

Chapter four presents the results and discussion of this research, including detailed outcomes and assumptions. This section also covers details of the variable loading system for the static and dynamic test rig to overcome the drawbacks of the current swingarm test rig models.

Chapter five provides a conclusion of the results of this research and recommendations for further research.

2.9 Chapter Summary

The review of the literature began with a look at the current state of automotive component development. Research examples of successively developed automotive test rigs were described. A number of research projects on swingarms and the swingarm test rigs were reviewed. Lastly, studies on swingarm development using lighter and stronger materials and the need to develop a new test rig to assess the durability of swingarms were discussed along with the project objectives and the organization of the dissertation.

In the light of the published literature, the significance of this research lies in the following areas:

1. A research gap exists to develop a test rig, which incorporates the benefits and overcomes the shortcomings of the Leyni test bench, which can assess carbon fibre

swingarm performance at varying loads. The test rig is able to include the loading of the motorcycle pilot and passenger as a variable load.

2. There are no published results of a carbon fibre swingarm test and as a result the safety of using such is unknown. Published carbon fibre test results would further the application of composites in South Africa.

From these discussions on automotive component testing and test rigs, it is clear that the accuracy of parameters like strain, acceleration etc. play a crucial role in durability prediction since exposure to vibration may result in injuries to the rider/occupant and affect the reliability and performance of the whole motorcycle. These results measured using a data acquisition system can be used for refining a finite element analysis for future design improvements.

Chapter 3: Methodology

This section covers details of the methodology used in this research using a well-defined product requirement specification (PRS) technique. The different concepts considered for the design of the rig and the detailed final concepts were defined. Finally the methodology to calculate the effective modulus of the carbon fibre swingarm is presented.

3.1 Product Requirement Specification (PRS)

The Product Requirement Specification (PRS) [39] [44] will discuss the test and all functional requirements of the rig to be designed. Relevant aspects of performance, manufacture, operability and cost are considered to decide on the final concept from the various alternative designs. The mechanical concepts of the test rig are outlined and all additional development of the final concept, showing the comparison of functions during a real-life test and while using the test rig, with respect to the product being tested. Lastly, the limitations of the test rig are discussed.

3.1.1 Requirements

3.1.1.1 Describing the Test

The specimen to be tested is a Ducati 1098 single-sided carbon fibre swingarm as shown in Figure 1.1 whose five connection points were described in chapter 1. The connection points have aluminium inserts to enable the carbon structure to be attached to the motorcycle suspension, frame and wheel system.

The goal of this test is to replicate the suspension of a Ducati 1098 to find the durability of the swingarm through a static and dynamic test; both by reproducing the same loads the arm experiences during a real-life test. For motorcycles, which are typically considered fair-weather vehicles, environmental considerations are often secondary concerns. For durability purposes, taking in to account the environmental factors, a higher safety factor ($S_f > \text{two}$, i.e. 1.2 million cycles, more than twice the BS code requirement for BST management approval) is considered in this research.

3.1.1.2 Loading design

The static load due to the rider and the passenger is 1960 N (assuming weight of 100 kg per person). The static load due to the weight of the motorcycle is 2158 N. The total static load is therefore 4118 N ([Equation A.2](#)). The weight distribution was estimated as 60% on the rear wheel and 40% on the front wheel [14] therefore total static load on the rear wheel is 2471 N (Equation A.4).

A maximum external loading of 5900 N on the motorcycle (excluding the weight of the motorcycle) occurs during the impact of the step of the Leyni test bench [18] (Appendix E). The cyclic loading was thus calculated as 3940 N (Equation A.1). Therefore the maximum load on the rear wheel is 4835 N (Equation A.5). Therefore in experimental testing, the minimum and maximum loads applied in the vertical direction are 2471 N and 4835 N respectively.

Specifications of the Test Rig

For dynamic test rig

- No of cycles = 1.2 million cycles per test
- Maximum preload on swingarm = 2471 N
- Maximum cyclic load on swingarm = 2364 N
- Minimum load applied on swingarm = 2471 N
- Maximum load applied on swingarm = 4835 N
- Dynamic loading frequency = 210 RPM

For static test rig

- Maximum load on swingarm = 7350 N

3.1.1.3 Functional Requirements

Defining the test process and the constraints early in the system development stage will reduce the number of design iterations and avoid expensive and time consuming mechanical changes after the system is built. Recreating the exact conditions of a real-life test in the laboratory test by reproducing the same loads the arm experience, will generate a more accurate test result. Consequently the laboratory test must replicate the degrees of freedom of the real-life scenario.

Degrees of Freedom

The six degrees of freedom of the swingarm in a real-life test during its operation are identified (Figure 3.1):

- The arm swings along the vertical direction during bumps or road surface irregularities, and the vertical motion is determined by amount of road force acting on the swingarm through the rear wheel forcing the arm upwards.
- The arm is rigidly connected to the frame through the two spreads of the swingarm pivot and thus preventing all horizontal motion (in the direction the motorcycle travels) of the arm.
- The arm is rigidly connected to the frame and the suspension system through the two spreads of the swingarm and the shock absorber respectively to prevent any lateral motion to the arm.
- The arm swings about the lateral axis (pitch motion) with respect to the swingarm pivot due to the bearing in the two spreads of the swingarm during its motion over bumps.
- The arm is rigidly connected to the frame and the suspension system through the two spreads of the swingarm and the shock absorber respectively to prevent any roll motion (rotation about the longitudinal axis) and yaw motion (rotation about the vertical axis) to the arm for all non-cornering motions of the motorcycle. But during cornering the wheel undergoes roll and yaw motion creating a bending and twisting moment on the arm.

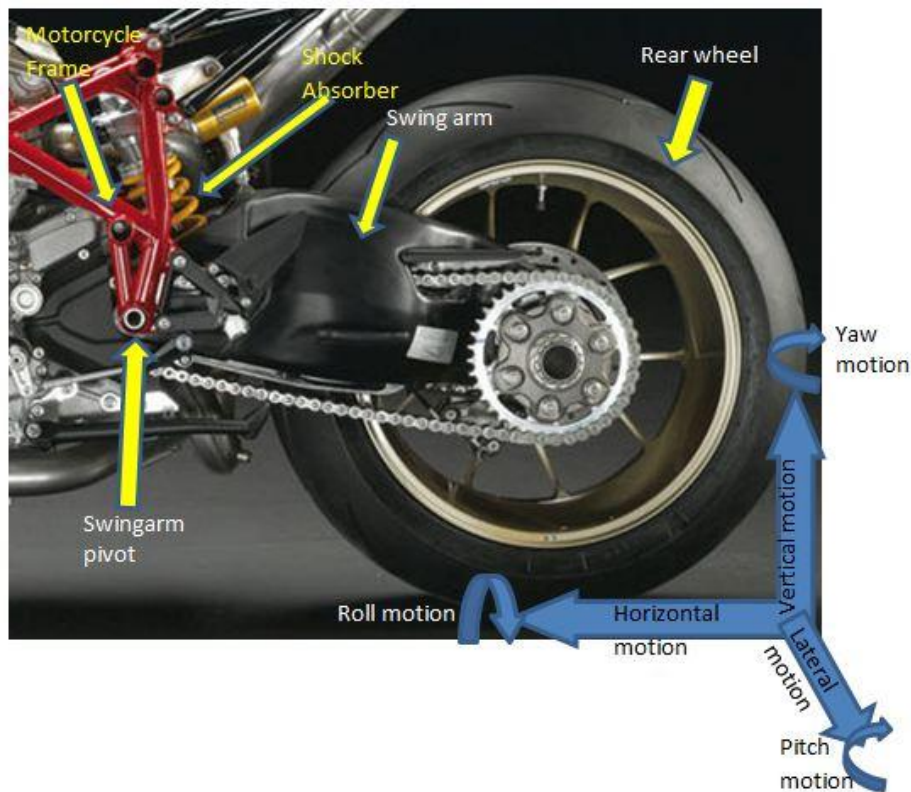


Figure 3.1 Six degrees of freedom of the swingarm in a real-life test

3.1.2 Constraints

The test is intended to have only one specimen tested at a time to 1.2 million cycles. The test rig at BST will be operated by a skilled engineer or a technician at all times. The machine will be used in a testing research environment; the installation of the test piece can be done by some manual assembly and installation time. The test is not a non-stop continuous process, as in the real-life case, the system can have scheduled maintenance in between and is capable of accepting any down time for unexpected failures of the test equipment. The test rig will also be bolted to the existing base of a lathe.

The test rig has to be designed in such a way that BST can perform the test accurately. But the more accurate the machines have to be, the more expensive it becomes. So the engineer is faced with a dilemma and in the end has to find a balance between the accuracy and cost of the testing machine.

3.1.2.1 Test Rig Functional Constraints

Defining the test rig functional limits and constraints can avoid expensive and time consuming mechanical changes after the system is built. The degrees of freedom during the test are defined for better comparison with a real-life test.

The exact six degrees of freedom of the swingarm during the test are identified as controlled, restrained, or free (Figure 3.2):

- The vertical motion of the swingarm hub is restrained by a horizontal slider.
- The horizontal/longitudinal motion (in the direction the motorcycle travels) is restrained by angle plate 2 which is attached to the base plate. The angle plate is connected to the arm through the swingarm pivot and the two plummer blocks.
- The lateral motion is restrained by the angle plate 1 which is attached to the base plate. The angle plate is connected to the arm through the two rods replicating the suspension system and the rocker arm.
- The pitch motion (rotation about the lateral axis) is restrained by the slider mechanism as it swings about the swingarm pivot.
- Yaw motion (rotation about the vertical axis) and roll motion (rotation about the longitudinal axis) is restrained by the swingarm pivot, the two plummer blocks, the two rods replicating the suspension system and the rocker arm, which are all attached to the two base plates along with the slider mechanism.

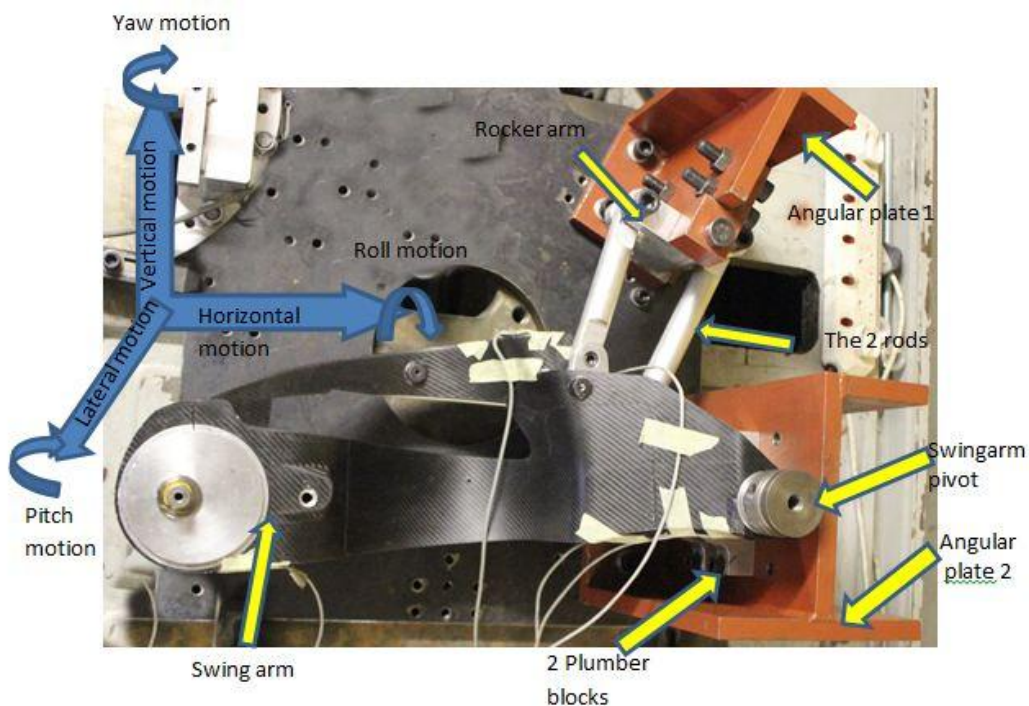


Figure 3.2 The six degrees of freedom of the swingarm during the test

The condition of bending and twisting moment acting on the arm during cornering of the motorcycle is not taken in to consideration during both the tests. Since the road bump load is much higher than the bending or twisting moment acting on the arm, the moments were

neglected. Normally a specially designed test bench like the one by Risitano et al. [11], is designed to apply moments. Hence a separate project as future work will be initiated to modify the rig.

3.1.3 Criteria

3.1.3.1 Proposed Methods of Test Rigs

The rig should test the swingarm specimen for 1.2 million cycles and thus all designed rig parts should be capable to withstand many times more (effectively infinite) cycles for the dynamic test. The rig should also be capable of applying variable loads.

Concept 1: Electrical Swingarm Test Rig

For dynamic testing

The test rig will consist of the following main components:

- 3 phase 4 kW AC motor.
- Electronic motor controller.
- Plummer blocks.
- An eccentric mechanism to convert rotational to translational movement ([Figure A.2](#)).
- A spring mechanism and housing.
- A slider mechanism.
- Angle plates to hold the swingarm (Figure 3.2).

A CAD model of the basic layout of the swingarm electrical test rig for dynamic testing is shown in Figure 3.3, revealing the orientation of the motor, plummer blocks, springs, swingarm etc. These components are to be mounted on a base plate, which is to be bolted to the existing base of a lathe.

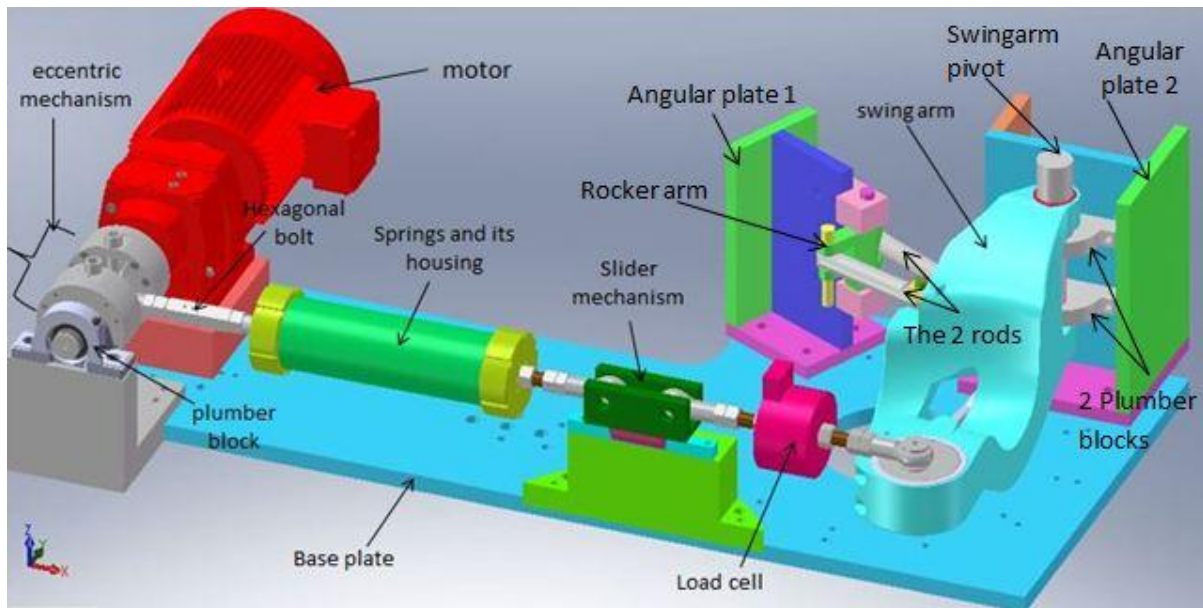


Figure 3.3 CAD model of the swingarm test rig for dynamic testing

Concept 2: Hydraulic Swingarm Test Rig

For dynamic testing

The hydraulic test rig will have many components similar to the electric test rig but will replace the electric motor along with the eccentric mechanism with a hydraulic system. The eccentric mechanism is not used because direct force from the hydraulic piston will be applied to the spring housing.

The test rig will consist of the following main components:

- Hydraulic power system.
- Hydraulics electronic control box.
- Hydraulic cylinder.
- A spring mechanism and housing.
- A slider mechanism.
- Angle plates to hold the swingarm.

No CAD models were made since this concept was rejected by BST management as explained in section 3.1.3.2.

For static testing

The static test rig for both concepts will be the same. Although the static test rig is similar to the dynamic test rig, a hydraulic jack with a hydraulic ram attached to an angle plate for proper alignment, along with a chain will replace the electric motor, the eccentric mechanism, the springs and its housings as shown in Figure 3.3. Thus the range of static load applied on

the swingarm will depend of the hydraulic ram capacity. The swingarm and its connection to the base plate through the angle plates are exactly as in the dynamic test rig. The hydraulic jack was chosen to be part of the test rig because of its availability in the bearing assembly department of BST enabling cost reduction to the test rig.

The test rig will consist of the following main components:

- Hydraulic jack.
- Hydraulic ram.
- Chain.
- Angle plates to hold the swingarm.

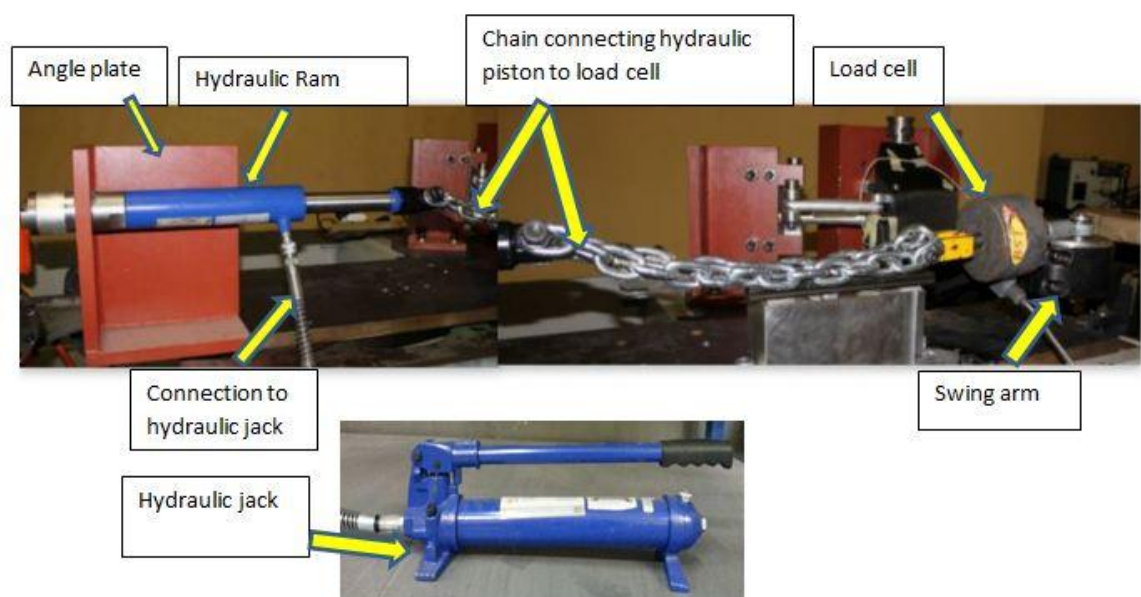


Figure 3.4 The swingarm static test rig

3.1.3.2 Decision Factor

The decision was evaluated relative to budget, available materials and equipment, manufacturing techniques, schedule, etc. BST have access to steel/aluminium rods or blocks of any size from nearby factory outlets and CNC machines available within the factory, which enables all aluminium/steel components to be machined with low cost. Thus with proper design, low cost components of the rig can be made within the factory. The capital cost of machined components with-in the factory followed by the cost of components purchased which are common for electric and hydraulic test rig are given in [Appendix A.1](#).

Capital Cost Analysis of Concept 1: Electrical Test Rig

Table 3.1 Capital cost analysis of electrical test rig

Components and specifications	QTY	Price (Inc. VAT)	Total (R) (Inc. VAT)
4 kW electric motor, 1400 RPM	1	1825	1825
Movitrac motor controller	1	2600	2600
2 plummer bearings for eccentric mechanism	2	324	648
Bearing for con-rod	1	220	220
Total cost of purchased components (R)			10343
Total cost of machined components (only for electrical test rig)			1125
Total cost of machined components (common for electrical and hydraulic)			1501
Total cost of Electrical test rig			18262

Capital Cost Analysis of Concept 2: Hydraulic Test Rig:

Table 3.2 Capital cost analysis of hydraulic test rig

Components and specifications	QTY	Price (Inc. VAT)	Total (R) (Inc. VAT)
Hydraulic power system, 5 hp, featuring reservoir, electric motor and pump	1	30000	30000
Hydraulics electronic control box	1	6000	6000
Hydraulic cylinder, double-acting, 4in. Bore, 8in. Stroke	1	3500	3500
Hydraulic hose, 1/2in. * 30in.l, 3500 psi	2	300	600
Other hydraulic accessories		1500	1500
Total cost of purchased components (R)			10343
Total cost of machined components (common for electric and hydraulic)			1501
Total cost of Hydraulic test rig			53444

From the above capital cost analysis, the hydraulic test rig costs almost three times the cost of the electrical test rig. Even though most fatigue testing machines use hydraulic actuators to perform the test, the Technical Director of BST wanted their rig to consist mostly of off-the-

shelf products for cost reduction. Thus the electrical test rig was considered as the final concept which consisted of a cylinder with two springs with an eccentric that has a continuous adjustment to cater for varying load ranges.

As BST needed to pass the BS code for fatigue test as early as possible for mass production, it was advisable from the BST management to move forward with the electrical test rig due to a shortage of funds and also the delivery of the hydraulic system and its components could take up to 3 months or more.

3.2 Design Approach

1. Determine the static and dynamic loads that a swingarm must withstand and that must be reproduced by the test rig.
2. Design and fabricate the bearings and other components used for the test rig to produce the above loading.
3. Assemble the test rig and attach all instruments for the evaluation of the rig performance.
4. Preload the swingarm to the desired static load.
5. Start the dynamic machinery of the rig to apply the dynamic load.
6. Evaluate the performance of the rig to apply the static and dynamic loads representative of the loading experienced on the test track.

3.3 System and Facility Requirements

The success of any overall test system is highly dependent on the correct integration of the mechanical and electrical hardware, with the associated electronics, data acquisition, software, and analysis [38].

3.3.1 Mechanical Components

The mechanical design of the swingarm test rig components are given in [Appendix A](#). The following components are the crucial components of the test rig and are the significant contributors to the cost of the whole test system and is therefore worth the time to properly evaluate it as it is done.

- Spring Design ([Appendix A.3](#))
- Motor Design ([Appendix A.4](#))
- Eccentric Bolt Design ([Appendix A.5](#))

- Eccentric Shaft Design ([Appendix A.6](#))
- Thread for Hexagonal Bolt Design ([Appendix A.7](#))
- Bearing Design ([Appendix A.8](#))

Take Heed

Since the dynamic test is a high velocity test, especially with high specimen mass, care must be taken in the design to ensure that the specimen can be stopped if control of the test system is lost. The acceleration requirement is important since the test runs on the basis that the total load is applied throughout each test cycles. Thus a Movitrac electronic motor controller which can control the acceleration and equipped with an emergency STOP button was used. Vibrations from the test rig can be transmitted into building structures, disrupt nearby instrumentation, and disturb people working in the area. Thus the test rig was bolted to the existing base of a lathe which has good vibration isolation.

3.3.2 Data Acquisition (DAQ) System

The main components of the DAQ system used to evaluate the performance of the swingarm are:

1. Strain gauges/ load cell.
2. Data acquisition hardware – (consisting of NI SCXI-1000 chassis, SCXI-1600 control card, SCXI-1521B strain gauge card, SCXI-1317 module).
3. The computer.
4. LabVIEW software.

A basic layout is shown in Figure 3.5 revealing the orientation of the load cell/strain gauges and DAQ system.

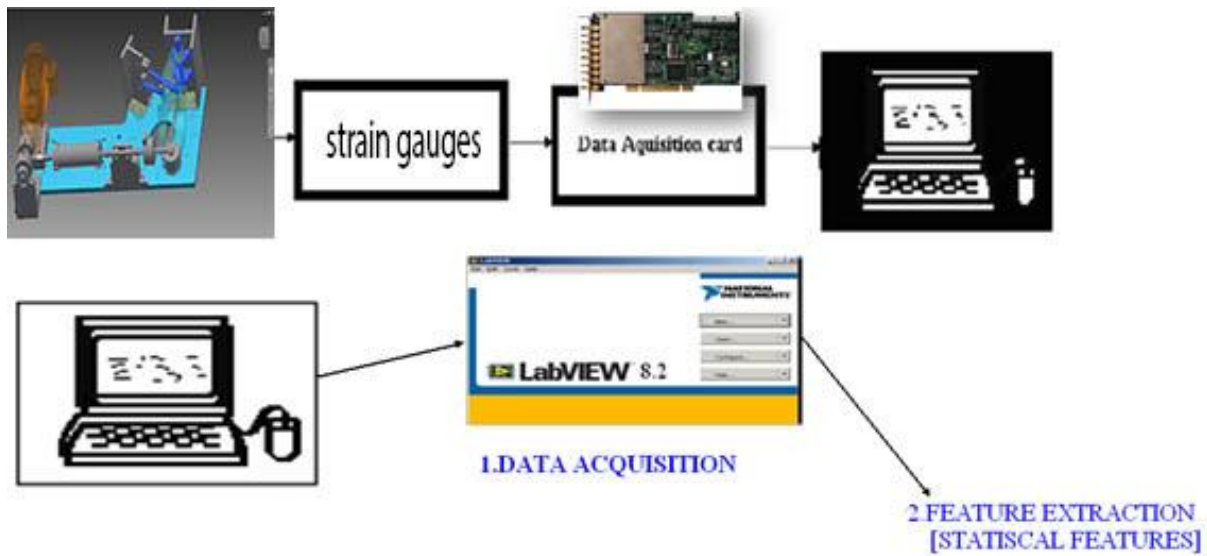


Figure 3.5 Layout for data acquisition

3.3.2.1 Strain Gauges and Load Cell

Strain is the amount of deformation of a body due to an applied force. Strain gauges produce electrical signals that the DAQ system measures. Signal conditioning accessories amplify low-level signals and then isolate and filter them for more accurate measurements [45]. A bonded resistance strain gauge is capable of measuring the minute changes in resistance corresponding to strain [46]. Calibration of the strain gauges was done using the National Instruments LabVIEW software features and the results are given in [Appendix B.1](#).

Position of Strain Gauges

Five strain gauges were mounted on the swingarm for testing purpose as shown in Figure 3.6 and Figure 3.7.

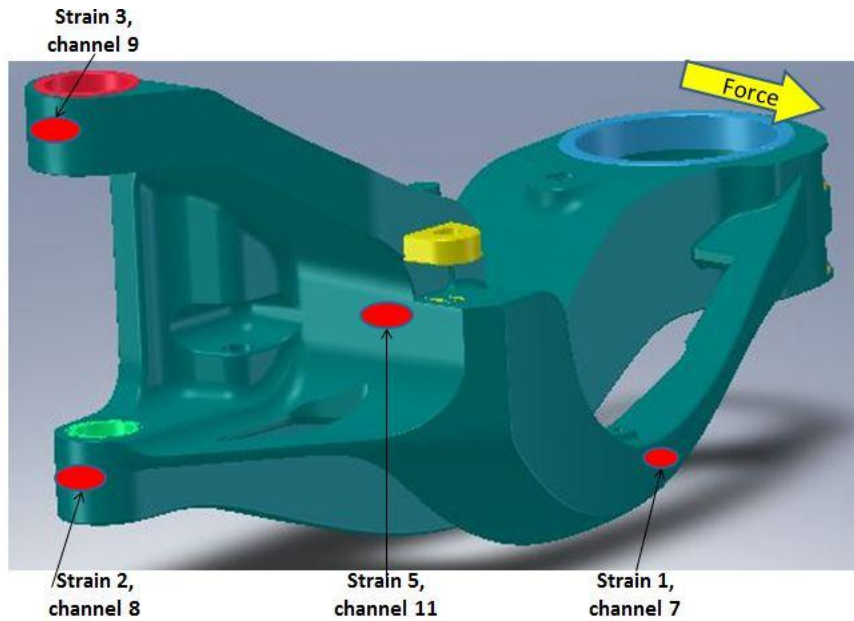


Figure 3.6 Attachment of strain gauges on the swingarm-1

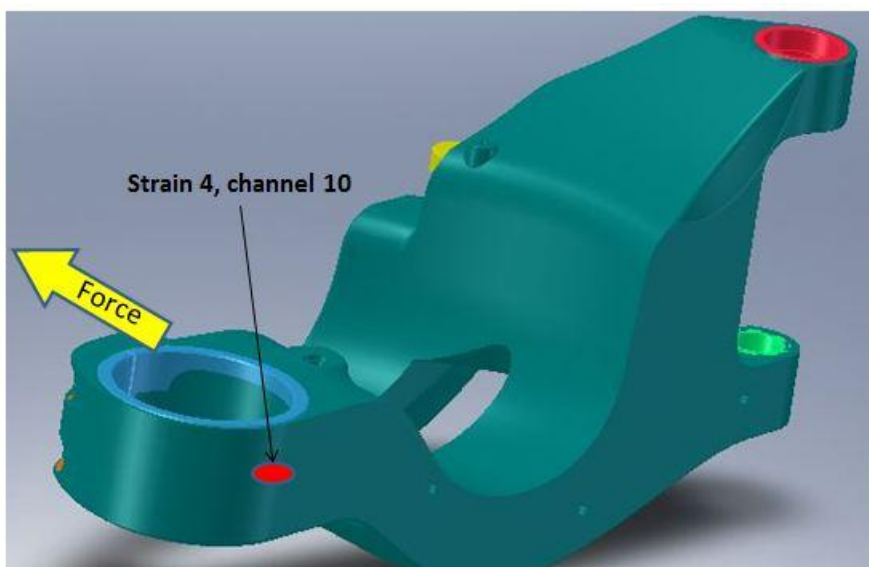


Figure 3.7 Attachment of strain gauges on the swingarm-2

The critical areas where the strain gauges were placed were based on previous testing of a swingarm tested at BST. A static test rig was used to apply a static load of 9135 N until a crack developed, at the position where strain 5 is attached now. It is known that minute irregularities such as grinding scratches or surface scales may produce a high value for the stress due to stress concentration and serve as the starting point for the micro crack [47]. Thus the rest of the areas having surface scales on the swingarm were categorized as critical areas. Strain gauges attached to these critical areas of the frame are shown in Figures 3.6 and 3.7. Experimental stresses are calculated using strains measured from these points in this research.

The most commonly used load cell today is the strain gauge load cell. As their name implies, strain gauge load cells use an array of strain gauges to measure the deformation of a structural member and convert it into a voltage. A load cell with a maximum capacity of 5 ton was placed as shown in Figure 3.3 to measure the load value applied to the arm. The load cell was placed as close as possible to the test specimen for more accuracy.

The voltage signal was measured using the DAQ. Calibration of the load cell was done using the NI LabVIEW software and the results are given in [Appendix B.2](#). The equations used in the strain gauge measurements are given in [Appendix B.3](#)

Take Heed

Lead wire resistance can cause a reduction in sensitivity because of the long wires used with small gauge wires in it, which have greater resistance than the bridge completion wiring within the measurement system. Strain gauge imperfections, lead wire resistance, and a pre-strained installation condition will generate some nonzero initial voltage offset.

3.3.2.2 Software

LabVIEW is the platform and development environment for a visual programming language from National Instruments. The graphical language is named "G". Execution is determined by the structure of a graphical block diagram (the LV-source code) on which the programmer connects different function-nodes by drawing wires. LabVIEW programs or subroutines are called virtual instruments (VIs).

The graphical user interface panel used in this research for data acquisition using LabVIEW is shown in Figure 3.8. When the stop button is clicked, the predetermined number of samples is acquired and stored on the computer hard disk as a LabVIEW measurement file (.LVM).

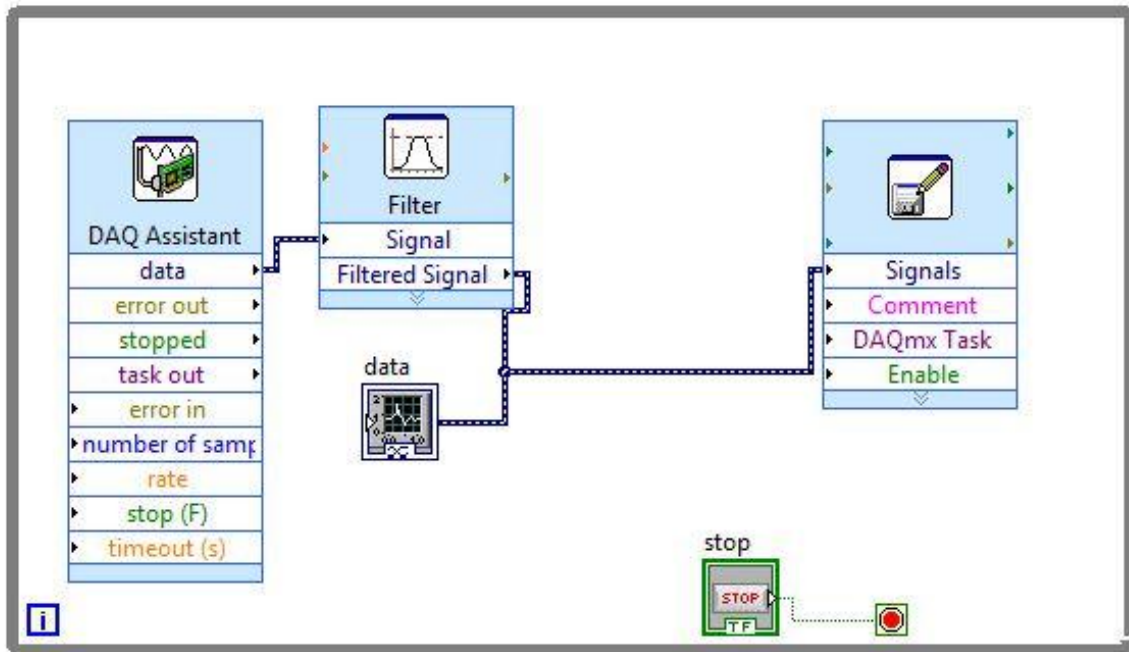


Figure 3.8 Graphical user interface panel

3.3.3 Higher Reliability Procedures or Modifications

The test was never a non-stop continuous process, and had scheduled maintenance in between due to unexpected failures of the test rig components. And since the reliability of the whole system depends on the reliability of each component in the system [48], modifications were done to some components to increase the reliability of the whole system. Some of these modifications or procedures to ensure higher reliability are listed below:

- The single plummer block system (Figure 3.3) was replaced with the two plummer block system (Figure A.2). The new shaft rotating inside the two plummer blocks, which extends from the eccentric hub was press forged by heating the eccentric hub to 180 °C and cooling the shaft to -30 °C. The two plummer block system lasted for over 1 million cycles compared to the 200 000 cycles of the single plummer block system.
- A hydraulic press (available in BST bearing assembly department) was used to press fit most components of the rig. All tolerances for the fit were designed according to ISO standards.

3.4 Limitations of the Test Rig

- It is difficult to simulate interaction between rider and vehicle. In a real-life test, the vehicle response is substantially influenced by the posture, weight distribution and characteristics of the rider and pillion. Also while moving over a bump, the rider is

separated from the vehicle (momentarily will be in air) and lands again onto the seat. This phenomena causes tyre force variation [6].

- The force of gravity acts on the vertical plane of the swingarm in a real-life test as shown in Figure 3.1 but since the swingarm was placed laterally on the test rig (Figure 3.3, since it was the only option available to apply forces accordingly) the force of gravity acting will be on the lateral side of the swingarm.
- Neither of the two tests in this research included the dynamics of cornering, running engine, wind, or temperature, since each additional condition adds considerable complexity and cost to the test rig.

3.5 Methodology to Calculate the Effective Elastic Constants of the Carbon Fibre Swingarm

A study on each layer was done to determine the stiffness of the layers (since data from Toray was limited to Table 3.1) and combined to formulate the effective elastic constants of the swingarm in tension and compression. Using the calculated values of the effective elastic constants of the swingarm in classical laminate theory and Hooke's law [49] [50], the stresses in the swingarm can be calculated.

Unlike isotropic materials, carbon fibre composites are a man-made material that can be made to satisfy virtually any mechanical property without changing the overall structural shape of the part, they are entirely anisotropic. The ability to customize your fibre direction allows you to only use as much material and fibre as you need; rather than waste material, costs, strength, and weight in directions you don't need. The high importance of laying down patches of carbon fibre pre-preg in different orientations is due to carbon fibre having maximum strength only along the lengths of the fibres.

Carbon fibre fabric comes in a variety of weaves that have different strength properties like woven fabric or unidirectional fabric. The carbon fibre swingarm is made of 12 layers of two different composites packed together at different orientations at BST, i.e. by placing 6 layers of Toray 700S (unidirectional carbon) in $0^{\circ}/90^{\circ}$ orientation and 6 layers of Toray 700G (woven fabric) in $+45^{\circ}/-45^{\circ}$ orientation as shown in Figure 3.9. Toray carbon fibres are the suppliers of carbon fibre sheets for the swingarm production in BST.

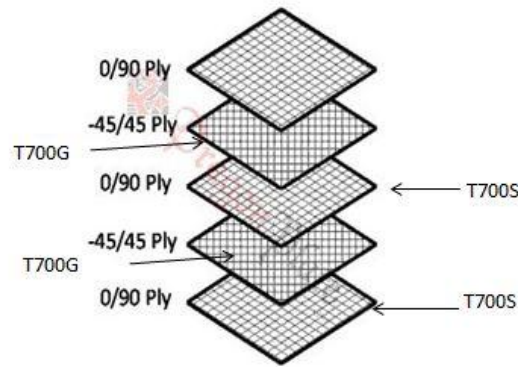


Figure 3.9 The swingarm layup, which has $+45^{\circ}/-45^{\circ}$ and $0^{\circ}/90^{\circ}$ orientations

Unidirectional carbon fibre is a reinforcement where all (or almost all) of the carbon fibres are aligned in the same direction. The only thing holding the fibres together will be occasional strands of either carbon or polyester running across the fibres at 90 degrees. A unidirectional weave creates a carbon fibre sheet that's very strong in the direction of the fibres, but weak in the opposite direction. On the other hand, a woven fabric contains fibres oriented on at least two axes, in order to provide great all-around strength and stiffness. A sheet of woven fabric once cured can take flexural and tensile loads on multiple axes, and even exhibits good stiffness properties off axis. A woven fabric was the norm for the outermost covering of any carbon component for its traditional "weave" look appearance.

If a hole is punched in a unidirectional fabric it will compromise strength for the entire length of the fibre, relying on the resin strength to distribute loading across the broken fibres. Unlike on the weave fabric, strands punctured in one place, will behave at full strength within a very short distance (typically one to two weave widths) from the damage [51]. But if a component requires 70% strength in the horizontal direction and 30% strength in the transverse direction, woven fibre would waste 40% additional material than unidirectional fibre to meet the same requirements [52]. Thus the combination of the two would be ideal for better performance and cost.

The swingarm is a complicated structure without symmetry but a high degree of rigidity and stiffness is required all-around the structure because torsional, vertical and horizontal bending forces are applied to it during its life (Figure 3.1). Thus a combination of a high strength, standard modulus unidirectional fibre (Toray 700S) and enhanced adhesion properties and tensile modulus woven fibre (Toray 700G) was used for the swingarm.

3.5.1 Design Approach

1. Determine the Young's modulus, volume fraction, the thickness and the Poisson's ratio of each layer.
2. Calculate the new stiffness values according to orientation of ply in tension and compression.
3. Determine the effective modulus and the Poisson's ratio for the swingarm in tension and compression.
4. Use the final effective elastic constant values in classical laminate theory along with the measured strain values to determine the stresses in the swingarm.

3.5.2 Assumptions

While designing composite structures, the main problems faced are [49] [53] [54]:

1. Fibre waviness and variation in thickness are the most common type of defects in composite material due to their complicated manufacturing process. This type of material imperfection increases the strain in the localised region and can lead to premature failure. Care should be taken in the manufacturing process to eliminate fibre waviness and variation in thickness.
2. Non-uniform fibre strength is a characteristic of most current high-strength fibres. Failure due to non-uniform fibre strength can be prevented by using a strong fibre-matrix interface or a soft ductile matrix which permits the redistribution of the high shear stresses.

Several assumptions were made when characterizing the lamina properties [50]:

1. The fibre and matrix material were assumed homogeneous.
2. The fibre and matrix material were assumed orthotropic.
3. The bonding between the fibre and matrix was assumed perfect, and thus strains experienced by the fibre, matrix and the composite are the same in all directions.

3.5.3 Young's Modulus, Volume Fraction, the Thickness and the Poisson's Ratio of Lamina

In the design of composite structures, it is often necessary to predict the strength of the laminate. Since the laminate strength depends on the strength of the individual lamina from which it is made. Most of the composite materials are made by stacking several distinct layers of unidirectional or woven lamina. Each lamina or ply is made of the same constituent

materials, matrix and fibre. Figure 3.10 represents a unidirectional lamina with respective longitudinal and transverse directions.

The stiffness of the lamina and laminate depends on three factors [53]:

1. Volume fraction of the constituent materials.
2. Thickness of each layer.
3. Orientation of the fibres with respect to a common reference axis [54].

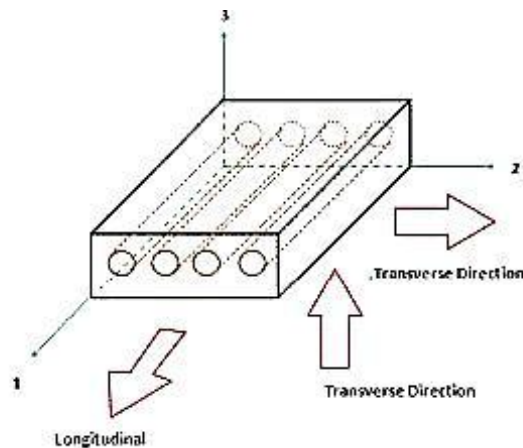


Figure 3.10 Principle material axes in a unidirectional lamina [53]

- X-Axis - an axis in the plane of the laminate, which is used as the 0 degree reference for designating the angle of a lamina.
- Y-Axis - the axis in the plane of the laminate which is perpendicular to the x-axis.
- Z-Axis - the reference axis, normal to the plane of the laminate.
- X-Y Plane - the reference plane, parallel to the plane of the laminate.

Given data

Different carbon composite structures are formed from different combinations of matrices and fibres, thus there were limited technical data about the carbon fibre composite used in this research. Table 3.3 provides all technical data's collected from Toray which were used for the calculations of the lamina strength [55] [56] [57].

Table 3.3 Technical data sheet

Material 1- Toray 700S (Unidirectional)	Material 2- Toray 700G (Woven)
Areal mass, $m_{700S} = 300 \text{ g/m}^2$	Areal mass, $m_{700G} = 380 \text{ g/m}^2$
No of lamina, $n_1 = 6$	No of lamina, $n_2 = 6$
Fibre	Fibre
Elastic modulus, $E_f = 230 \text{ GPa}$	Elastic modulus, $E_f = 240 \text{ GPa}$
Poisson's ratio, $\nu_f = 0.20$	Poisson's ratio, $\nu_f = 0.20$
Volume fraction, $V_f = 0.60$	Volume fraction, $V_f = 0.49$
Density, $\rho_f = 1800 \text{ g/m}^3$	Density, $\rho_f = 1800 \text{ g/m}^3$
Matrix (Epoxy Resins)	Matrix (Epoxy Resins)
Elastic modulus, $E_m = 4.5 \text{ GPa}$	Elastic modulus, $E_m = 4.7 \text{ GPa}$
Poisson's ratio, $\nu_m = 0.33$	Poisson's ratio, $\nu_m = 0.30$
Volume fraction, $V_m = 0.40$	Volume fraction, $V_m = 0.51$
Density, $\rho_m = 1250 \text{ g/m}^3$	Density, $\rho_m = 1250 \text{ g/m}^3$
Carbon Fibre [57]	Carbon Fibre
Shear modulus, $G_{12} = 4.4 \text{ GPa}$	Shear modulus, $G_{12} = 5.5 \text{ GPa}$

Results

The equations used to calculate the Young's modulus, volume fraction, the thickness and the Poisson's ratio of lamina are given in [Appendix C.1](#). The results are calculated by substituting the values from the above table in to the equations in Appendix C.1 and are shown in Table 3.4.

Table 3.4 Stiffness values of each laminate

	Toray T700S	Toray T700G
E₁	140 GPa	120 GPa
E₂	10 GPa	9 GPa
G₁₂	4.4 GPa	5.5 GPa
ν₁₂	0.25	0.25
T_c	2.440 mm	3.091 mm
Total Thickness		5.530 mm
V_c	0.441	0.559

The rule of mixture model was selected for the analysis in this research. It is observed that the elastic constants of a laminate are a function of the volume fraction, which in turn is a function of the thickness of the body [49]. The thickness is higher in T700G since more areal mass is present in it. The transverse modulus is matrix dominated and tends to be very low in comparison to the fibre dominated longitudinal modulus.

Since the composite structure is cured under vacuum in an autoclave at BST. No specimen tests were conducted to compare the results with respect to the calculated material properties because of the time and cost involved in the moulding and curing process for manufacturing the test specimen required.

3.5.4 New Stiffness Values for Toray 700G According to the Orientation of Ply in Tension and Compression

Composites are rarely used in the form of unidirectional laminates, since one of their greatest merits is that the fibres can be arranged so as to give specific properties in any desired direction. In order to calculate the properties of the woven fibre (T700G), which is orientated at $\pm 45^\circ$ direction to the unidirectional fibre (T700S), a method which can determine the stress-strain relations for a lamina at an arbitrary orientation to the reference axes is required [49] [50]. The equations used to calculate the new stiffness values according to the orientation of ply in tension and compression for Toray 700G followed by the variation of elastic constants with fibre orientation are given in [Appendix C.2](#).

Results

The results are calculated by substituting the values from Table 3.3 in to the equations in Appendix C.2 and are shown in Table 3.5.

Table 3.5 Elastic constant values with orientation of ply for Toray 700G

Old values			New values		
	Tension	Compression		Tension	Compression
E_1	140 GPa	120 GPa	E_1	14.016 GPa	13.464 GPa
E_2	10 GPa	9 GPa	E_2	14.016 GPa	13.464 GPa
ν_{12}	0.25	0.25	ν_{12}	0.274	0.224
G_{12}	5.5 GPa	5.5 GPa	G_{12}	9.032 GPa	8.089 GPa

For tension and compression, fibre behaviour dominates the $0^\circ/90^\circ$ behaviour, while matrix behaviour dominates the $+45^\circ$ direction and at 45° the value of E_1 and E_2 will be the same. It is observed that the good properties in a particular direction come at the expense of poor properties in another direction. These roles are reversed in the shear case, the $+45^\circ$ behaviour is fibre dominated and thus this is the ideal angle at which the lamina will resist maximum torsion. Hence a sensible approach to design a structure with all-around rigidity and stiffness (like the swingarm), would be to ensure that the transverse and shear modulus are at its maximum.

3.5.5 Effective Elastic Constants of the Swingarm for the 12 Layers

Since the swingarm has 12 layers of two different composites packed together at different orientations, the resulting elastic constants will clearly be affected by the distributions of the different species of fibre. Thus the results from the above two tables are combined to formulate the effective elastic constants as a function of the volume fraction of the swingarm in tension and compression. The equation used is given in [Appendix C.3](#).

Results

The results are calculated by substituting the values from Table 3.4 and Table 3.5 in to the equation in Appendix C.3 and are shown in Table 3.6.

Table 3.6 Effective elastic constants of the swingarm for the 12 layers

	Tension	Compression
E₁₁	67.391 GPa	67.083 GPa
E₂₂	12.244 GPa	11.936 GPa
ν_{12}	0.264	0.235
G₁₂	9.459 GPa	9.462 GPa

The combination of different lamina types and orientation results in a strength of 67 GPa in longitudinal direction (50% less than initial lamina strength) and 12 GPa in shear direction (more than 150% greater than the initial lamina strength) and thus creating a composite that has high stiffness in all directions, to resist torsional, vertical and horizontal bending forces acting on the arm, by taking advantage of the longitudinal strength of the unidirectional fibre.

3.6 Chapter Summary

The research methodology presents a structured approach in addressing the research problem using a well-defined product requirement specification (PRS) technique. This discussed all functional requirements of the rig to be designed. The different criteria were considered to decide on the final concept from the various alternative designs. All design details of the components in the test rig and instrumentation required to perform the desired objectives were outlined along with the limitations of the test rig.

This rig is the first of its kind for swingarm testing and has highlighted a number of unique aspects of the rig. There is significant scope for further work on this topic in performing error analyses by comparing the FE model results with the test results and also in developing a hydraulic test rig for improved reliability and accuracy. The final concept of the test rig offers the following advantages:

1. The model is capable of overcoming the shortcomings of the previous test rig, the Leyni test bench.
2. The model is capable of recreating all degrees of freedom and reproducing the same loads the swingarm experiences in the laboratory test as in a real-life test. This system is able to simulate road conditions in the laboratory for stress calculations.

3. Many complex factors were considered to arrive at an optimal balance among cost, schedule, available materials and equipment, manufacturing techniques, complexity, simulation accuracy, and ease of use.
4. With slight modification the model can test durability or even test torsional or bending stiffness of different carbon fibre components at BST.

Since no data were available regarding the effective elastic constants of the carbon fibre swingarm, a methodology to calculate this was developed. Using equations of composites, the stiffness of each layer at $0^\circ/90^\circ$ and 45° was calculated and then combined to formulate the effective elastic constants of the swingarm in tension and compression. These values are used in the classical laminate theory to determine the stresses in the swingarm. The design approach for each methodology was outlined, including the assumptions and limitations for each test. The next Chapter deals with the results and discussion of the analysis on the research data.

Chapter 4: Results and Discussion

4.1 Introduction

The discussion begins with a look at parameters that affect the final mechanical properties of composites and some of the major parameters are discussed here with its effect on the current design of the swingarm and thus validating how the swingarm test rig can guide the carbon fibre swingarm to an improved design. Lastly, the strain gauged results of the static and dynamic tests of the swingarm are discussed, validating that the swingarm can withstand a real-life test without failure. Even though there are no published results available for the carbon fibre swingarm in the literature of stresses and strains for comparison and error analysis, the results of the static and dynamic test were compared to arrive at a good correlation between the both.

4.2 Variation of Effective Elastic Constants with Fibre Orientation for the 12 Layers

A study is done to verify if the current model of the swingarm in which 6 layers of Toray 700S are $0^{\circ}/90^{\circ}$ orientated and 6 layers of Toray 700G are $+45^{\circ}/-45^{\circ}$ orientated, has maximum strength and stiffness in the shear and transverse direction. The values for the elastic constants of Toray 700S is taken from Table 3.4. These values are constants since their orientation is fixed at $0^{\circ}/90^{\circ}$. The values for the elastic constants of Toray 700G is varied according to fibre orientations from 0° to 90° using the equations from Appendix C.2. Then the values for the effective elastic constants of the swingarm for the 12 Layers orientated at angle from 0° to 90° are calculated using the equation from Appendix C.3 and the results are shown below.

4.2.1 For Tension

The effective longitudinal modulus, transverse modulus and Poisson's ratio were varied with fibre orientation angle from 0° to 90° . The results are shown in Figure 4.1.

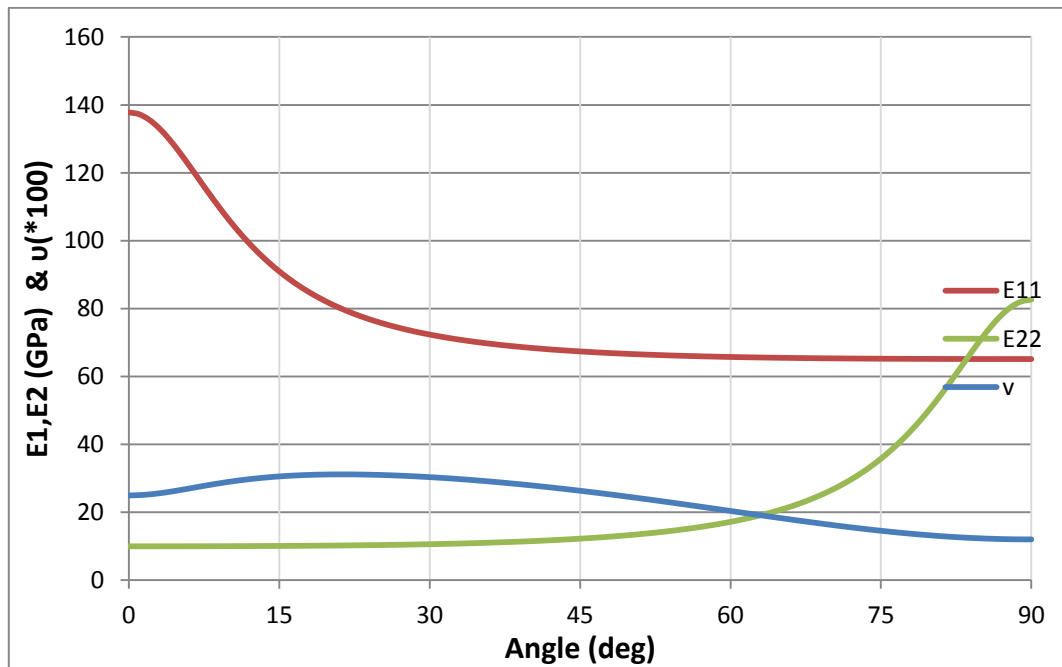


Figure 4.1 Variations of effective Young's modulus and Poisson's ratio with orientation

The effective longitudinal modulus is higher than the rest of the values in the initial stage as it is the fibre property. The variation of Poisson's ratio of the composite is less sensitive to the fibre characteristics. The longitudinal modulus is at its maximum when the 700S and 700 G are at 0° . The transverse modulus reaches its maximum when the 700G is at 90° . The effective shear modulus was varied with fibre orientation angle from 0° to 90° and the results are shown in Figure 4.2

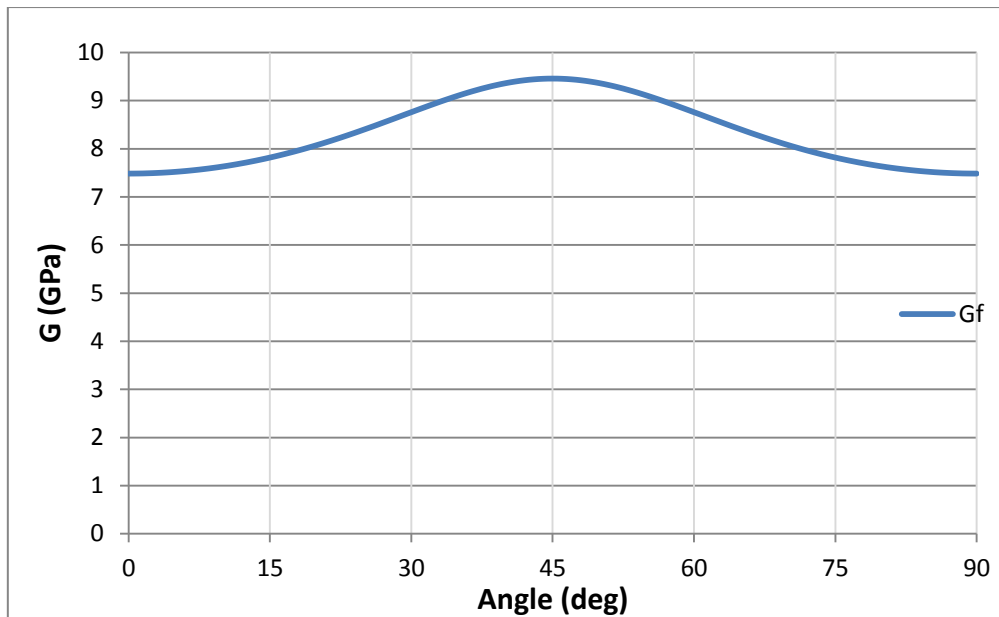


Figure 4.2 Variations of effective shear modulus with orientation

The variation of shear modulus is less sensitive compared to others and thus it is shown in a different graph for better visibility of the effect. The effective shear modulus starts to rise from 0° and reaches its maximum when the $700G$ is at 45° to the fibre axis, the $+45^\circ$ behaviour is fibre dominated and thus this is the ideal angle at which the lamina will resist maximum torsion, and falls to the initial value from $+45^\circ$ to 90° . The shear stiffness of the composite rises as the loading direction shifts away from the matrix axis, to the fibre axis at 45° and drops to the initial value as it shifts back to matrix axis at 90° . The shear stiffness of the composite is less sensitive to the matrix characteristics as angle increases from 0° to 45° , being largely controlled by the fibre rigidity. Thus it will resist maximum shear at 45° angle, which is achievable only in composites by changing the orientation which gives composites its advantage over alloys and pure metals.

4.2.2 For Compression

The effective longitudinal modulus, transverse modulus, shear modulus and Poisson's ratio were varied with fibre orientation angle from 0° to 90° under compression and are shown in Figure 4.3.

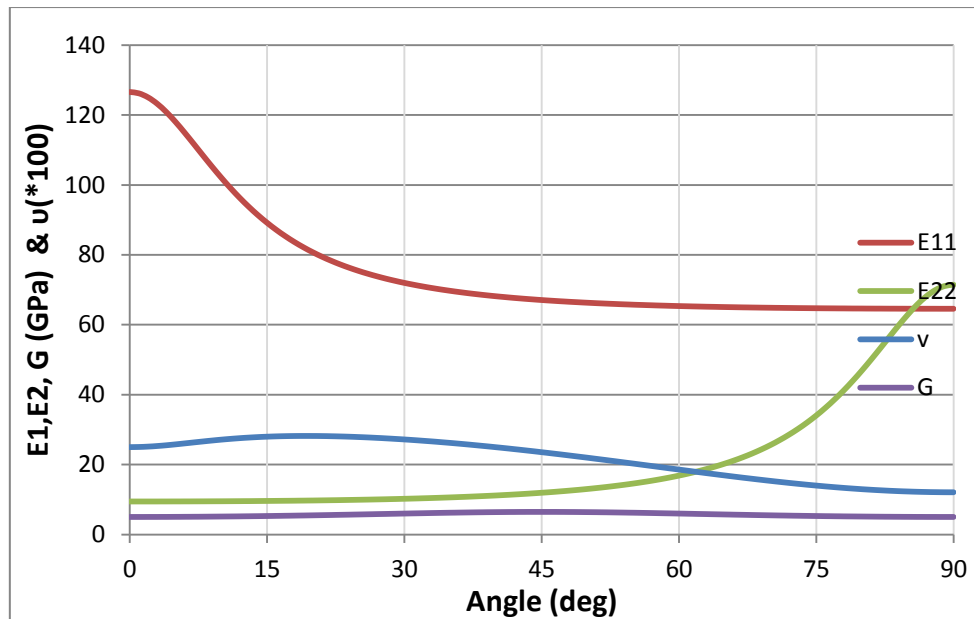


Figure 4.3 Variations of effective elastic constants for compression with orientation

Using fibre orientation, it is possible to create a composite that has high stiffness in all directions by taking advantage of the longitudinal strength. The shear strength variation is one of the principle advantages of composites. Thus the component will be designed to resist all the forces acting in all directions. Since the swingarm must resist forces in all direction the 700S was orientated at 0° and the 700G was orientated at 45° to give maximum strength and stiffness in the shear and transverse direction along with a good longitudinal stiffness. The values for the effective elastic constants of the swingarm for the 12 layers i.e. 6 layers of Toray 700S in $0^\circ/90^\circ$ orientation and 6 layers of Toray 700G in $+45^\circ/-45^\circ$ orientation in tension and compression are given in Table 3.6.

4.3 Effect of Thickness

The effective elastic constants of a composite are a function of the volume fraction which in turn is a function of the thickness of the body [49]. Using a similar approach the effective stiffness of the swingarm was calculated for different thickness of the body. The thickness was varied by changing the number of laminae in each material with the ratio of 1:1 (700s: 700G). The calculated values and the variations of effective elastic constants with thickness are given in [Appendix D.1](#).

It is observed that the elastic constants do not change with thickness, but the strength of the material changes. But the cost of production will rise since more material is being used.

Therefore it is always advisable to use the most effective thickness according to the strength necessary for the body, in the most cost efficient manner.

4.4 Effect of Volume Fraction

According to the rule of mixture model [49] [50] [58], the effective modulus of composites depends upon the volume fraction of the different materials used. A similar approach was carried out to come up with a solution for the effective stiffness of the swingarm. The volume fraction is varied by changing the number of laminae in each material [59], such that $n_1+n_2=12$. The calculated values are given in [Appendix D.2](#). The variations of effective elastic constants with volume fraction of the composite are shown in Figure 4.4 and Figure 4.5.

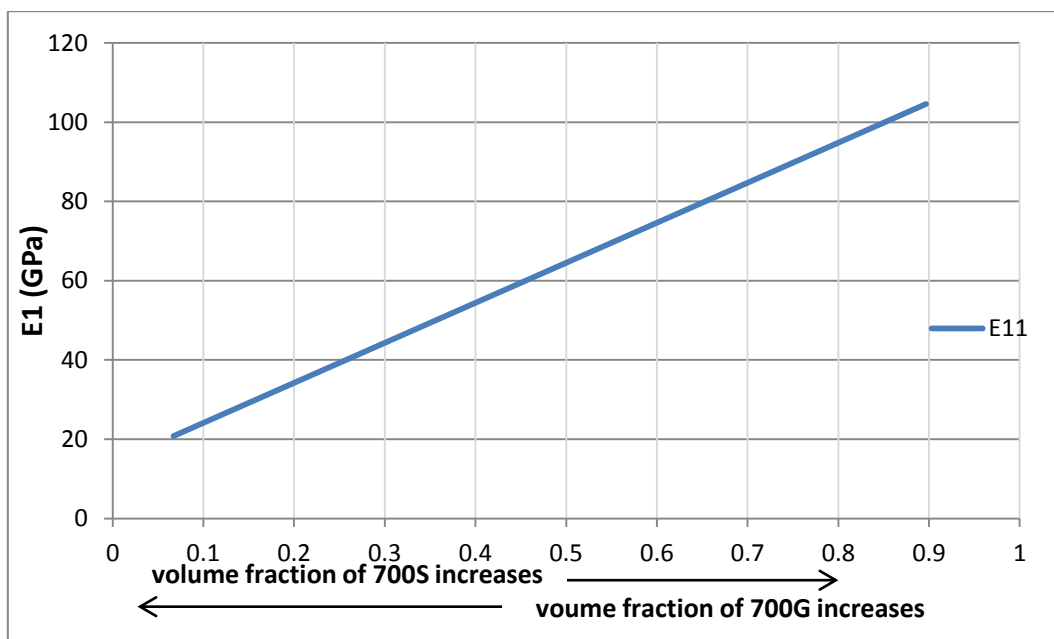


Figure 4.4 Variations of effective Young's modulus with volume fraction

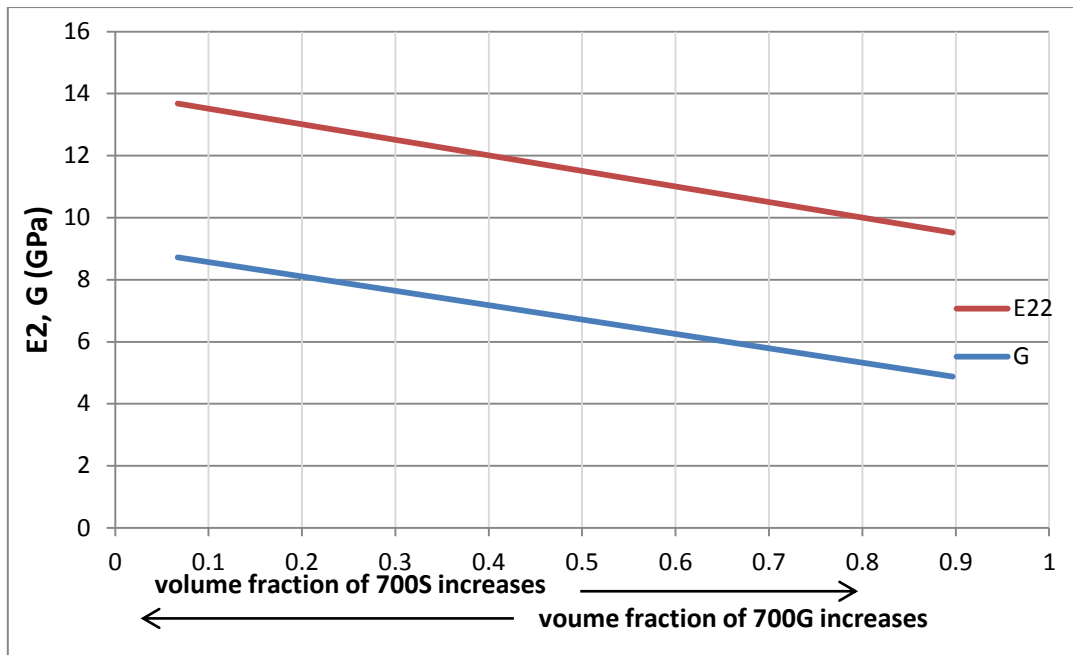


Figure 4.5 Variations of effective transverse and shear modulus with volume fraction

The variation of transverse modulus and shear modulus is less sensitive to volume fraction thus; it is shown in a different graph for better visibility of the effect. As the volume fraction of 700S increases its fibre properties at 0° takes advantage, where by as the volume fraction of 700G increases its fibre properties at 45° takes advantage and thus shear modulus and transverse modulus increases which enables the swingarm to resist shear force.

At low volume fractions of 700G, the whole composite will fail when the 700G fails. At higher volume fractions of 700G, the chances for the composite to fail are low because of the increased shear and transverse strength along with the longitudinal strength of the body. Therefore it is always advisable to determine the optimum volume fraction of the different materials used according to the shear and transverse strength necessary for the product, in the most cost efficient manner. A similar approach was carried out in the design of the carbon fibre swingarm.

4.5 Evaluation of Test Rig

The loading aims to simulate the vertical loading that the swingarm experiences during a real-life test which causes bending in the vertical plane. The load will be applied at the wheel hub interface in the direction which causes vertical bending to the arm as shown in Figure 3.2. This section covers details of the variable loading system for the static and dynamic test rig to overcome the drawbacks of the Leyni test bench.

4.5.1 Static Test

The range of static load applied on the swingarm will depend on the hydraulic ram capacity and thus, the test rig has the potential for future application since it can vary the static load as required. The hydraulic jack which was part of BST bearing assembly department was chosen to be part of the test rig for cost reduction. For this research a maximum static load of 7350 N was used. The load applied was limited since the swingarm test piece was needed for further testing in BST (the component being very expensive) thus there was no failure to the swingarm recorded during this test.

4.5.2 Dynamic Test

For preloading the swingarm during a dynamic test with a static load, a hexagonal bolt (shown in Figure A.2) when tightened compresses the outer spring while the inner spring expands inside the spring housing (Figure 4.6). This action pulls the swingarm towards the motor side as shown in the figure below, thereby preloading the swingarm with the weight of the pilot and his passenger of 2470 N (Eqn. A.4). Thus the pretension of the springs can be changed to get the force range needed for testing.

The test rig replicates the same preloading action that a swingarm experiences on the test track. The cross-section of the springs and spring housing was necessary to explain the concept of the mechanical spring arrangement to get the force range needed, and thus a hand drawn picture of the same is given below.

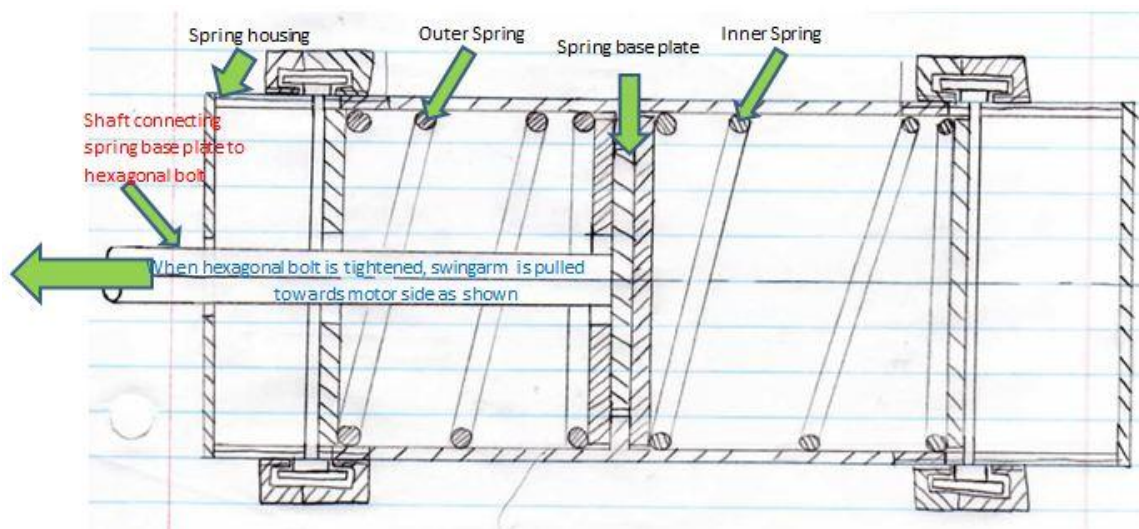


Figure 4.6 Mechanical spring arrangement inside spring housing

The eccentric mechanism gives the test rig its ability to vary the dynamic or cyclic load applied by changing the eccentric radius. The dynamic load is varied by changing the eccentric radius in the eccentric hub and the maximum eccentric radius for the test rig was 0.1 m.

Equation

$$F = \text{eccentric radius} * K \tag{4.1}$$

Where $F =$ force in N
 $K =$ spring rate = 62700 N/m

The calculated values are given in [Appendix D.3](#).

Results

The variation of dynamic load to the eccentric radius is show in Figure 4.7.

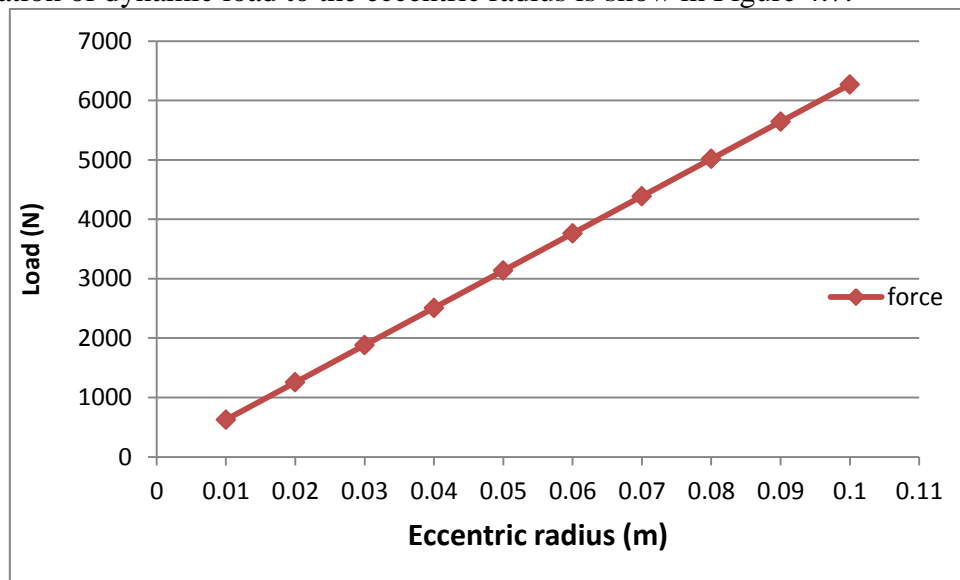


Figure 4.7 Variation of dynamic load to the eccentric radius

It is observed that higher dynamic loads, up to 6270 N, can be applied with this test rig. Thus the test rig has the potential for future application since it can vary the dynamic loads to values as required within the range and thus overcome the drawbacks of the Leyni bench.

4.6 Static Test Results

The positions of the strain gauges on the swingarm are shown in chapter 3. The swingarm was loaded to a static load of 7350 N using the static test rig. The load applied was limited since the swingarm test piece was needed for further testing in BST thus there was no failure to the swingarm recorded during this test.

Classical Laminate Theory

The classical laminate theory is based on the following hypothesis:

- The plate is constructed of an arbitrary number of layers of orthotropic sheets bonded together.
- The thickness (Z) is much smaller than the other physical dimensions.
- In-plane strains ϵ_x , ϵ_y and ϵ_{xy} are small compared to unity.
- Each ply obeys Hooke's law.
- No slip between layers occurs.
- The plate has constant thickness.

Laminate force - deformation equations

The resultant forces (N_i) and moments (M_i) on the laminate are obtained by integration of the stresses in each lamina through laminate thickness. The forces applied to a small part of the laminate, can be described by 6 components in classical shell theory: 3 in-plane forces and 3 moments as shown in Figure 4.8. In a practical notation, the in-plane forces and the moments are calculated per unit length. The in-plane forces are denoted by N_i , ($i = 1; 2; 6$). The 3 moments per length are denoted M_i , ($i = 1; 2; 6$) [60].

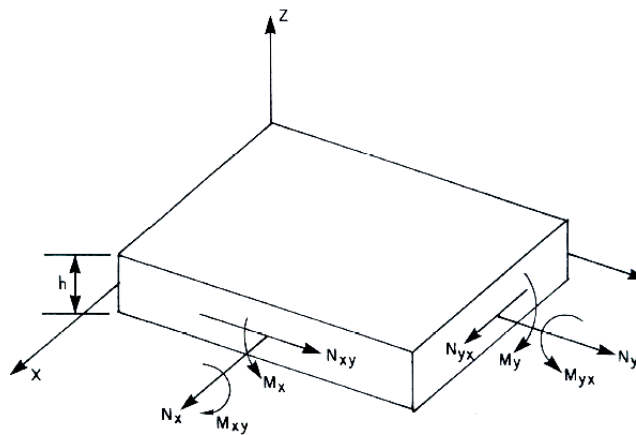


Figure 4.8 Resultant forces and moments acting on the laminate

The matrix notation for the equation relating resultant forces and moments with the strains in the classical laminate theory is given in Eq. 4.1. Since only one strain value was acquired with the data acquisition system, the equation was used to calculate the transverse strain and shear strain acting on the swingarm. It was assumed that the swingarm does not undergo any twisting during the test thus M_1 , M_2 and M_6 were assumed to be zero and the load applied acted in only in one direction (N_1), thus N_2 and N_6 were assumed to be zero.

$$\begin{Bmatrix} N_1 \\ N_2 \\ N_6 \\ M_1 \\ M_2 \\ M_6 \end{Bmatrix} = \begin{Bmatrix} A_{11} & A_{12} & A_{16} & B_{11} & B_{12} & B_{16} \\ A_{12} & A_{22} & A_{26} & B_{12} & B_{22} & B_{26} \\ A_{16} & A_{26} & A_{66} & B_{16} & B_{26} & B_{66} \\ B_{11} & B_{12} & B_{16} & D_{11} & D_{12} & D_{16} \\ B_{12} & B_{22} & B_{26} & D_{12} & D_{22} & D_{26} \\ B_{16} & B_{26} & B_{66} & D_{16} & D_{26} & D_{66} \end{Bmatrix} * \begin{Bmatrix} \varepsilon_x \\ \varepsilon_y \\ \varepsilon_{xy} \\ K_1 \\ K_2 \\ K_6 \end{Bmatrix} \quad (4.2)$$

Where $A_{ij} = \sum_{k=1}^n Q_{ij} * (Z_k - Z_{k-1})$ (4.3)

$$B_{ij} = 0.5 * \sum_{k=1}^n Q_{ij} * (Z_k^2 - Z_{k-1}^2) \quad (4.4)$$

$$D_{ij} = (1/3) * \sum_{k=1}^n Q_{ij} * (Z_k^3 - Z_{k-1}^3) \quad (4.5)$$

K is the laminate number

n is the total number of laminate

Z is the thickness of laminate

The calculations and the Matlab code used to solve for the unknowns are given in [Appendix D.3](#).

Stress – strain relationship

The stresses can be calculated from the know strain and elastic modulus values. The effective elastics modulus values of the swingarm are taken from Table 3.6. Using the equations the stresses ($\sigma_x, \sigma_y, \tau_{xy}$) were calculated. Based on classical laminate theory, the stress-strain relation for composites is expressed as: [50] [49]

$$\{\varepsilon_l\} = [S]\{\sigma_l\},$$

Or

$$\begin{Bmatrix} \varepsilon_{11} \\ \varepsilon_{22} \\ 2\varepsilon_{12} \end{Bmatrix} = \begin{bmatrix} \frac{1}{E_1} & \frac{-\nu_{12}}{E_1} & 0 \\ \frac{-\nu_{12}}{E_1} & \frac{1}{E_2} & 0 \\ 0 & 0 & \frac{1}{G_{12}} \end{bmatrix} \begin{Bmatrix} \sigma_{11} \\ \sigma_{22} \\ \sigma_{12} \end{Bmatrix} \quad (4.6)$$

Alternatively, they can be written as

$$\begin{Bmatrix} \sigma_x \\ \sigma_y \\ \tau_{xy} \end{Bmatrix} = \frac{1}{1-\nu_{12} * \nu_{21}} * \begin{bmatrix} E_{11} & E_{22} * \nu_{12} & 0 \\ E_{22} * \nu_{12} & E_{22} & 0 \\ 0 & 0 & (1 - \nu_{12} * \nu_{21})G_{12} \end{bmatrix} * \begin{Bmatrix} \varepsilon_x \\ \varepsilon_y \\ \gamma_{xy} \end{Bmatrix} \quad (4.7)$$

Where,

E_{11} - Effective longitudinal modulus of elasticity for the 12 layers

E_{22} - Effective transverse modulus of elasticity for the 12 layers

G_{12} - Effective longitudinal in-plane shear modulus for the 12 layers

ν_{12} - Effective major Poisson's ratio for the 12 layers

The above values are taken from [Table 3.6](#).

Minor Poisson's ratio,

$$\nu_{21} = \nu_{12} * \frac{E_{22}}{E_{11}} = 0.06203 \quad (4.8)$$

ϵ_x - was recorded using the NI data acquisition system

ϵ_y - transverse strain from Eq. 4.1.

γ_{xy} - shear strain in the x - y plane from Eq. 4.1.

Results

4.6.1 Load vs. Time

The load applied during the static test is shown in Figure 4.9.

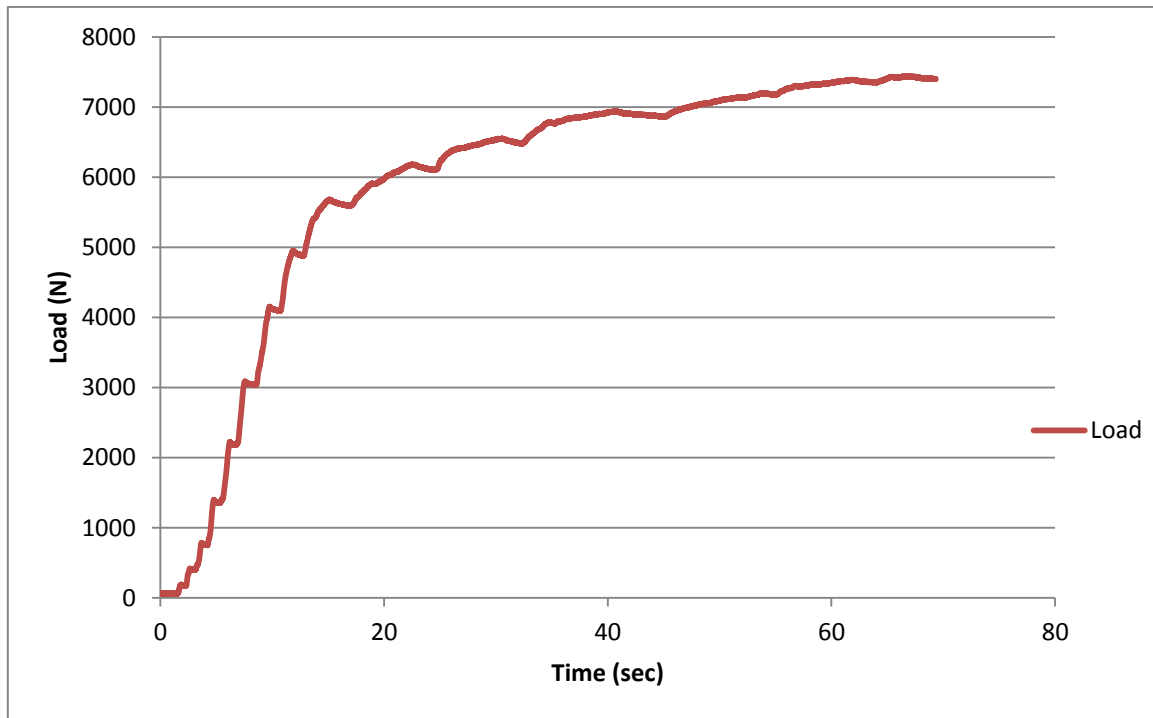


Figure 4.9 Load applied during the static test

Since the load was applied using a hydraulic jack which was hand pumped, the graphs do not follow a smooth curve. After the first 15 seconds, the property of the swingarm to resist force is visible from the above graph as more time is consumed afterwards to apply further loads to the arm. The load was limited to 7350 N since the swingarm was needed for further testing. Thus the failure or fracture point was not attained.

4.6.2 Strains vs. Time

The strains experienced by the body during the static test are shown in Figure 4.10.

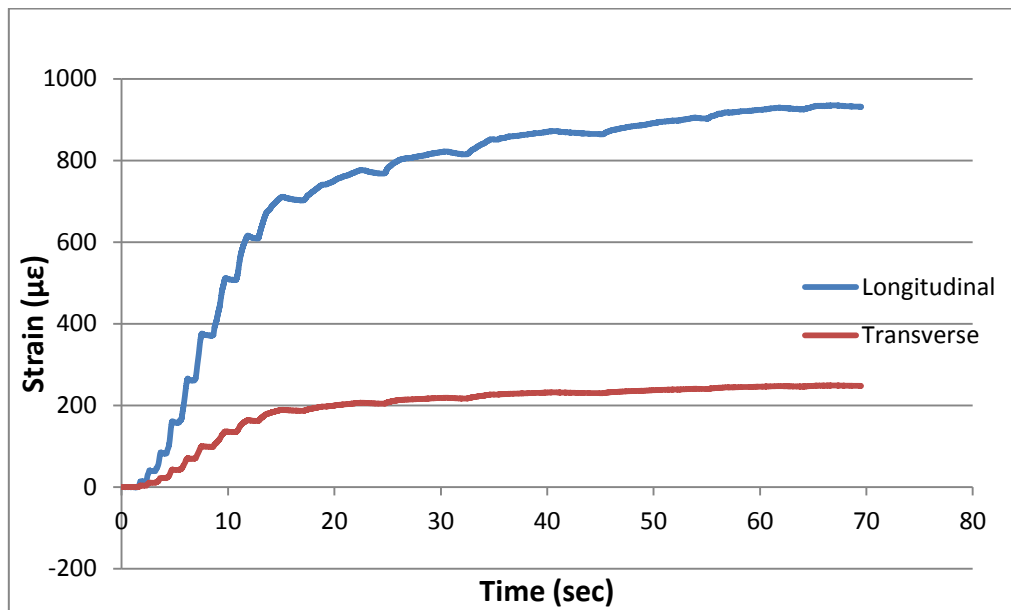


Figure 4.10 Strains experienced during the static test

Here the strains experienced in Strain gauge no-1, channel 7, are shown. The longitudinal strain has the highest value. All strain values exhibited similar paths or increasing trends as the load applied (shown in Figure 4.9). Similarly like the load, the property to resist bending is visible from the graph as more time is consumed afterwards to apply further strain to the body. There is no shear strain ($=0$) acting on the body since no twist (in horizontal or vertical) is experienced by the body as those degrees of freedom are restrained by different components of the rig.

4.6.3 Stresses vs. Time

The stresses experienced by the body during the static test are shown in Figure 4.11.

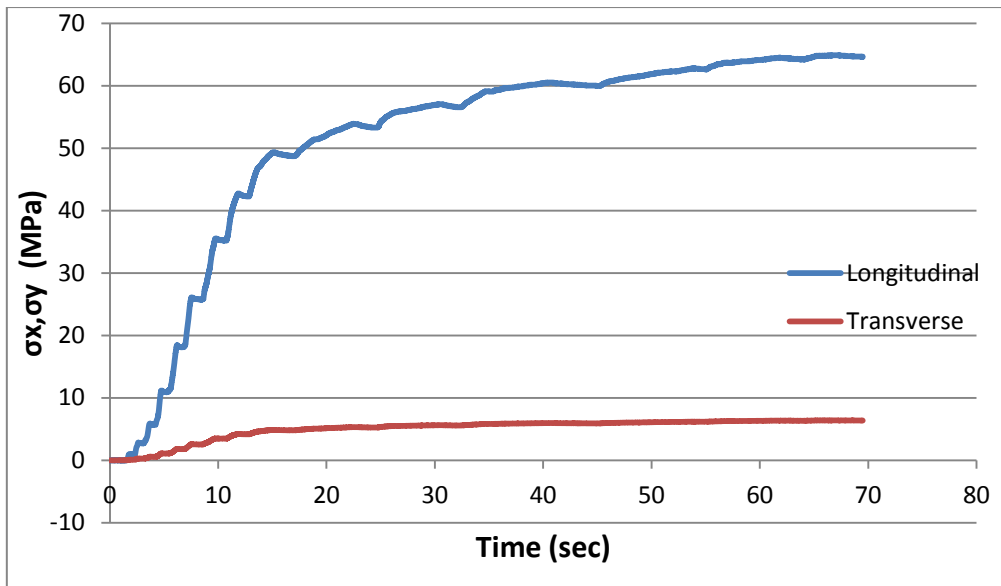


Figure 4.11 Stresses experienced during the static test

Here the stresses experienced in Strain gauge no-1, channel 7, are shown. It is verified that the swingarm has the largest stress in the longitudinal direction and no shear stress ($=0$) acts on the body since there was no twisting on the body.

4.6.4 Stress vs. Strain

A stress-strain graph shown in Figure 4.12 was formed by the combination of all stress-strain values from all 5 strain gauges.

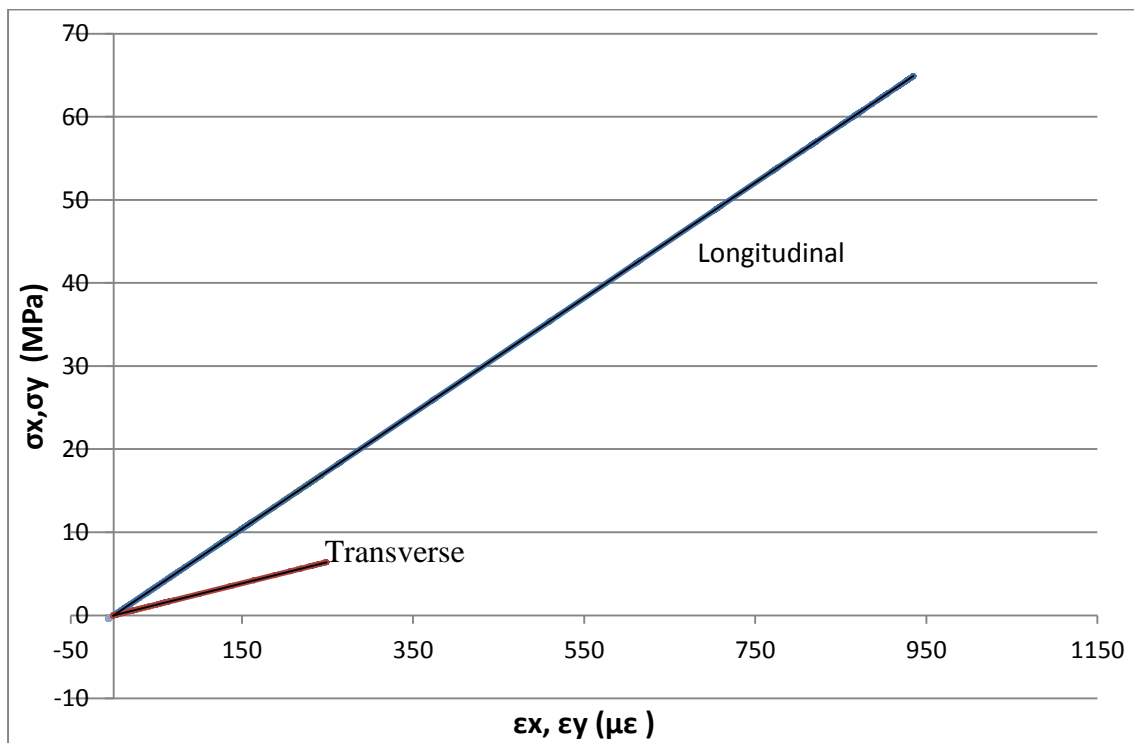


Figure 4.12 Stress-strain graphs for static testing

Here the strains experienced due to the stresses applied while statically testing the swingarm is shown. A linear path is followed for the stress-strain curves in all directions. All points where the gauges were placed exhibit linear elastic behaviour. The stress-strain curve can be divided into two distinct deformation regions, which are the elastic deformation and the plastic deformation. The elastic deformation is temporary and is fully recovered when the load is removed. The plastic deformation is permanent and is not recovered when the load is removed.

The line that is straight (Figure 4.12) shows the elastic deformation region. Within this region if the load is removed the specimen would return to its original length. The slope of the curve in this region (stress/strain) was identified as Young's modulus. There was no record for failure of the swingarm (as seen in graph) because the load applied to the arm was limited as the swingarm test piece was needed for further testing in BST. Thus the plastic deformation region is not shown in the graph. The stress-strain equation based on the classical laminate theory for composites was used (Eqn. 4.7). Using the equations the stresses ($\sigma_x, \sigma_y, \tau_{xy}$) were calculated.

The equations to determine stresses from strains (from graph) are given by:

For longitudinal stress,

$$\sigma_x = 0.0694 * \epsilon_x \quad (4.9)$$

For transverse stress,

$$\sigma_y = 0.0248 * \epsilon_y \quad (4.10)$$

Where, Stresses in MPa and

Strains in micro-strain ($\mu\epsilon$)

4.7 Dynamic Test Results

In design situations, the number of stress cycles a part is designed to undergo is limited by the life of the part. The maximum completely reversing cyclic stress that a material can withstand for indefinite (or infinite) number of stress cycles is known as the fatigue strength or endurance strength of the part material. When a part is subjected to cyclic stress it has been observed that the failure of the part occurs after a number of stress reversals even if the magnitude of the cyclic stress is below the material's yield strength. Generally, higher the cyclic stress, lesser number of reversals is needed for failure.

This section details that the applied load creates stresses below the endurance limit and thus the body will undergo indefinite (or infinite) number of stress cycles. This validates that the arm can successfully withstand the total load applied during a real-life test without failure. The test was done for more than 1.2 million cycles as required by BST standards. After a number of cycles the strains experienced by the swingarm reached a steady state as shown in Figure 4.17. There was no failure to the swingarm during this dynamic test and this proves that the swingarm can withstand a real-life test with infinite life.

Applied load: from eqn. A.3 & A.4.

Preloaded loading – 2470 N

Cyclic loading – 2365 N

4.7.1 Load vs. Time

The total load applied in each second is shown in Figure 4.13.

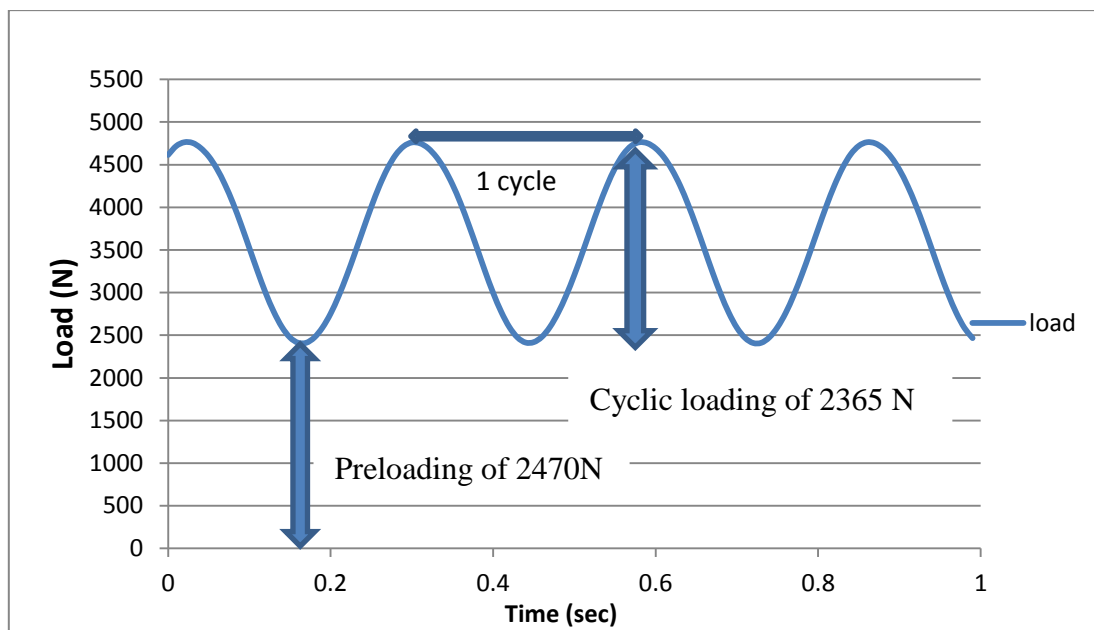


Figure 4.13 Effective load applied in one second

The loading consisted of a 2470 N static value, on which was superimposed a dynamic cyclic load of 2365 N with a frequency of 3.5 cycles/second. The graph proves that the load during each cycle was consistent since the test runs on the basis that the required total load is applied throughout each test cycles.

4.7.2 Transmission History

The longitudinal strain recorded with the NI DAQ system is shown in Figure 4.14. For better visualization the last few cycles are shown [61].

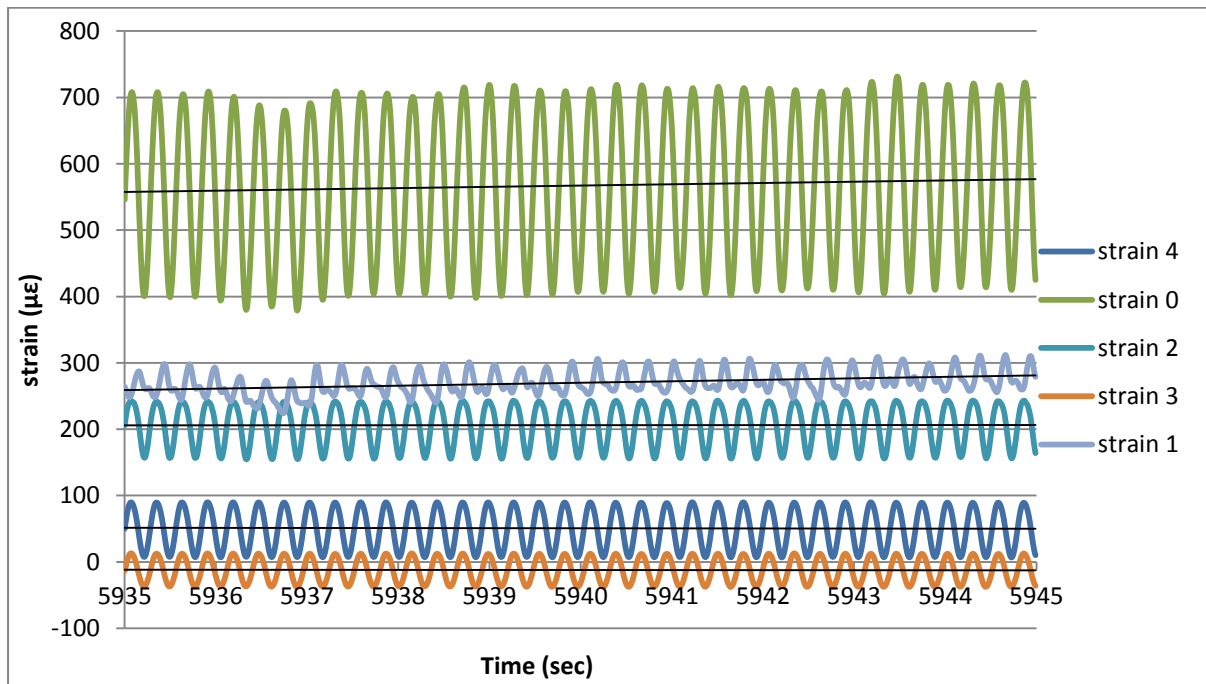


Figure 4.14 Strain readings from the dynamic test

The trend line shows that a steady state was reached. These steady state values will be used for further analysis. The number of cycles when steady state was reached is calculated by:

$$\begin{aligned}
 \text{Number of cycles} &= \text{time (sec)} * \text{Frequency} \\
 &= 20790 \text{ cycles} \\
 \text{Where} \quad \text{Frequency} &= 3.5 \text{ cycles/second} \quad (\text{from Appendix A.3}) \\
 \text{Time} &= 5940 \text{ seconds}
 \end{aligned}$$

4.7.3 Strain in One Second

The strains experienced by the body in a second are shown in Figure 4.15.

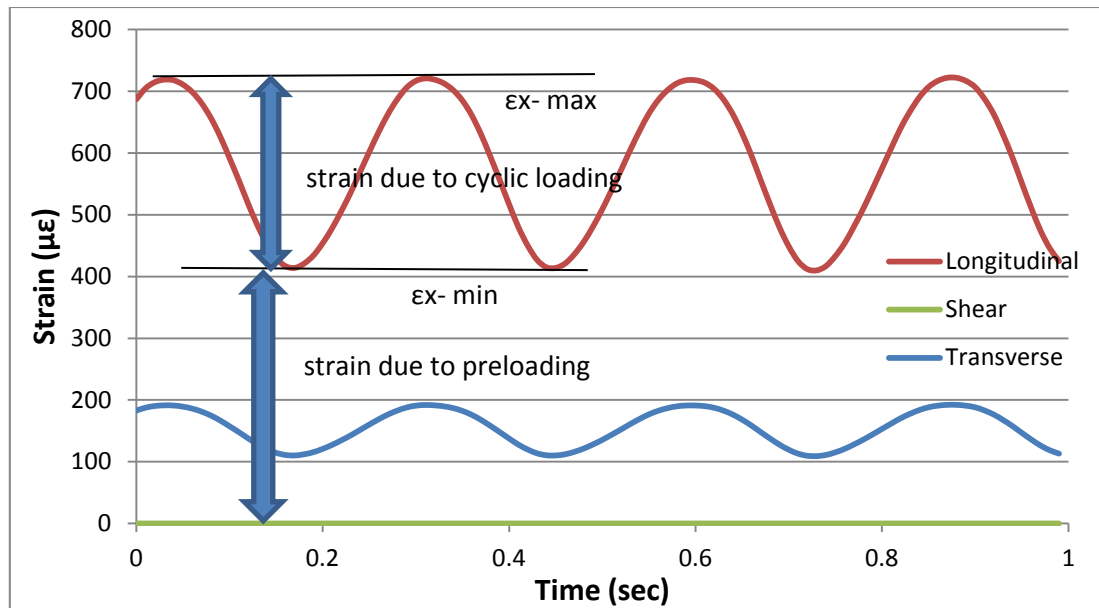


Figure 4.15 Effective strains in one second

Here the strains experienced in Strain gauge no-1, channel 7, are shown. The Longitudinal strain has the highest value as expected. All strains values exhibits a cyclic path since a cyclic load is applied as shown in Figure 4.15. The maximum and minimum longitudinal strain (which is consistent) during each cycle along with the strain due to preloading and cyclic loading is shown for better visualization of the effect of the respective loads on the arm. The strain due to preloading from the initial value of 0 to $\epsilon_{x-\min}$ is not shown on the graph because its effect is only visible during the first cycle of the test. There is no shear strain ($=0$) acting on the body.

4.7.4 Stresses in One Second

The stresses experienced by the body during the dynamic test in each second are shown in Figure 4.16.

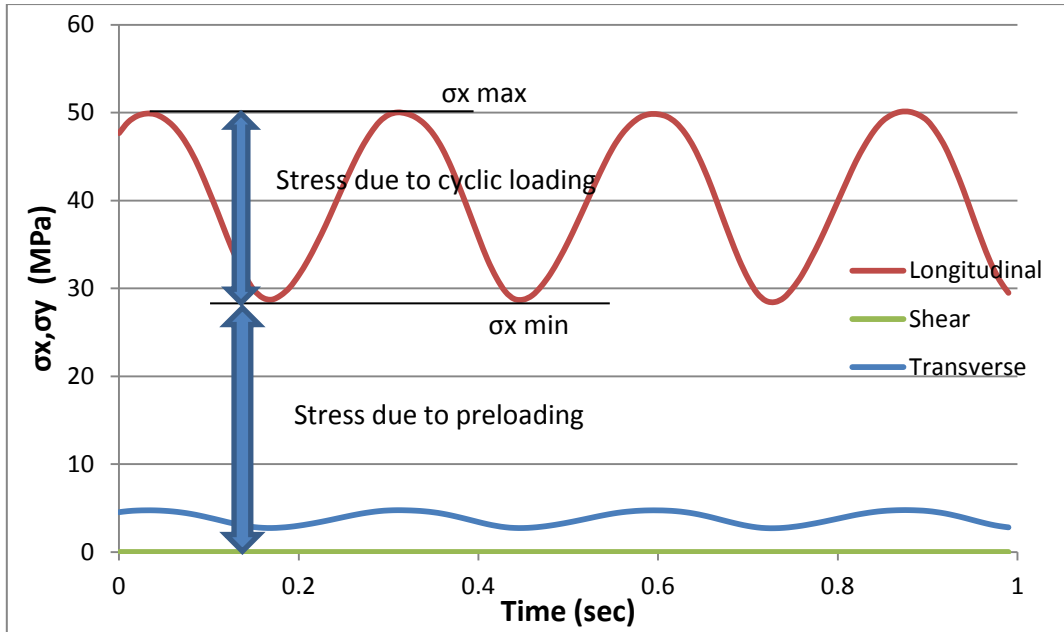


Figure 4.16 Stresses experienced in each second during the dynamic test

Here the stresses experienced in Strain gauge no-1, channel 7, are shown. All stress values exhibit a cyclic path since a cyclic load is applied. A cyclic stress means when the stress alternates between equal peak stresses during each cycle of operation. Cyclic stress over time can be represented by a sinusoidal curve as shown. The maximum and minimum longitudinal stress (which is consistent) during each cycle along with the stress due to preloading and cyclic loading is shown for better visualization of the effect of the respective loads on the arm.

The stress due to preloading from the initial value of 0 to σ_{x-min} is not shown on the graph because its effect is only visible during the first cycle of the test. It is verified that the swingarm has the largest stress in the longitudinal direction and no shear stress ($=0$) acts on the body since there was no twisting on the body.

Some of the findings from the graphs are given below: (for longitudinal stress)

1. Stress range,

$$\Delta\sigma = \sigma_{\max} - \sigma_{\min} = 21.648 \text{ Mpa} \quad (4.11)$$

2. Alternating stress,

$$\sigma_a = \frac{|\sigma_{\max} - \sigma_{\min}|}{2} = 10.824 \text{ Mpa} \quad (4.12)$$

3. Mean stress,

$$\sigma_m = |\sigma_{\max} + \sigma_{\min}| / 2 = 39.272 \text{ Mpa} \quad (4.13)$$

4.7.5 Stresses vs. Number of Cycles

The average stresses experienced by the body during the entire dynamic test are shown in Figure 4.17.

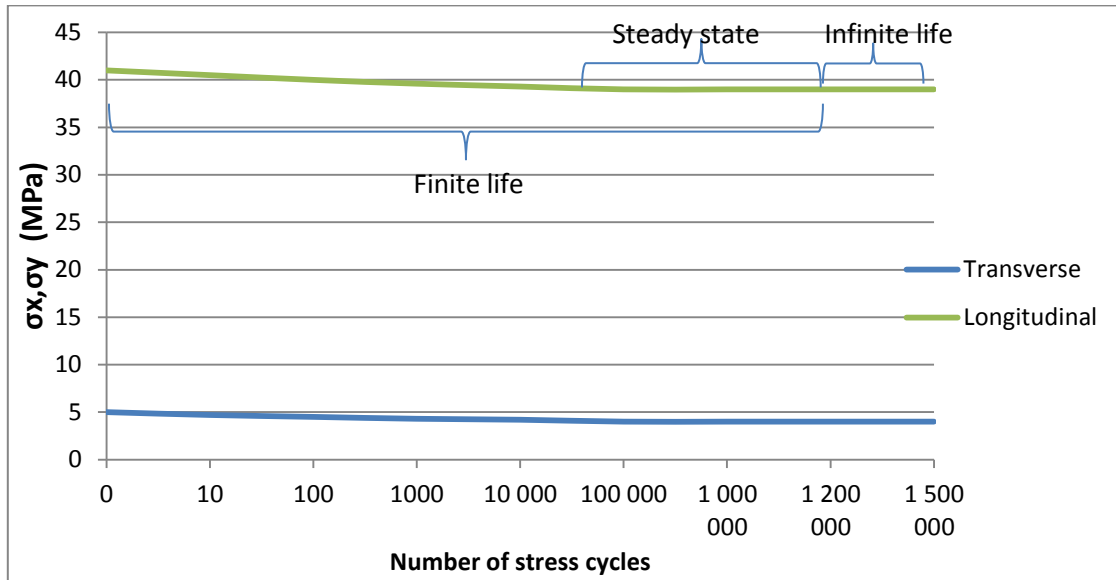


Figure 4.17 Stresses experienced during the dynamic test

Fatigue design methodologies for metallic components have been traditionally based on the stress-life approach [32] and this approach works well for designs involving long life. Here the average stresses experienced in Strain gauge no-1, channel 7, are shown. At this point the swingarm has the largest stress in the longitudinal direction. It has been observed that for most of engineering materials, the rate of reduction of cyclic stress becomes negligible near the vicinity of $N = 10^6$ and the slope of the stresses vs. number of cycles curve becomes more or less horizontal. The fatigue strength of the arm dropped after a first few 10 000 cycles and stabilized afterwards to infinite life. The steady state was reached after 20 000 cycles as shown.

After 1.2 million cycles the swingarm was further tested and validated to be having infinite life. Since the slope of the above curve is horizontal after certain cycles, if we keep the cyclic stress value equal or less than the values of this test, the part will survive indefinitely (infinite number of stress reversals). This proves that the applied load creates stresses below the endurance limit and that the arm can successfully withstand the total load applied during a real-life test without failure. No tests were conducted by applying higher loads to test the

endurance limit of the swingarm since no higher loads are applied on the swingarm during its life.

4.7.6 Stress vs. Strain

A stress-strain graph shown in Figure 4.18 was formed by the combination of all stress-strain values from all 5 strain gauges.

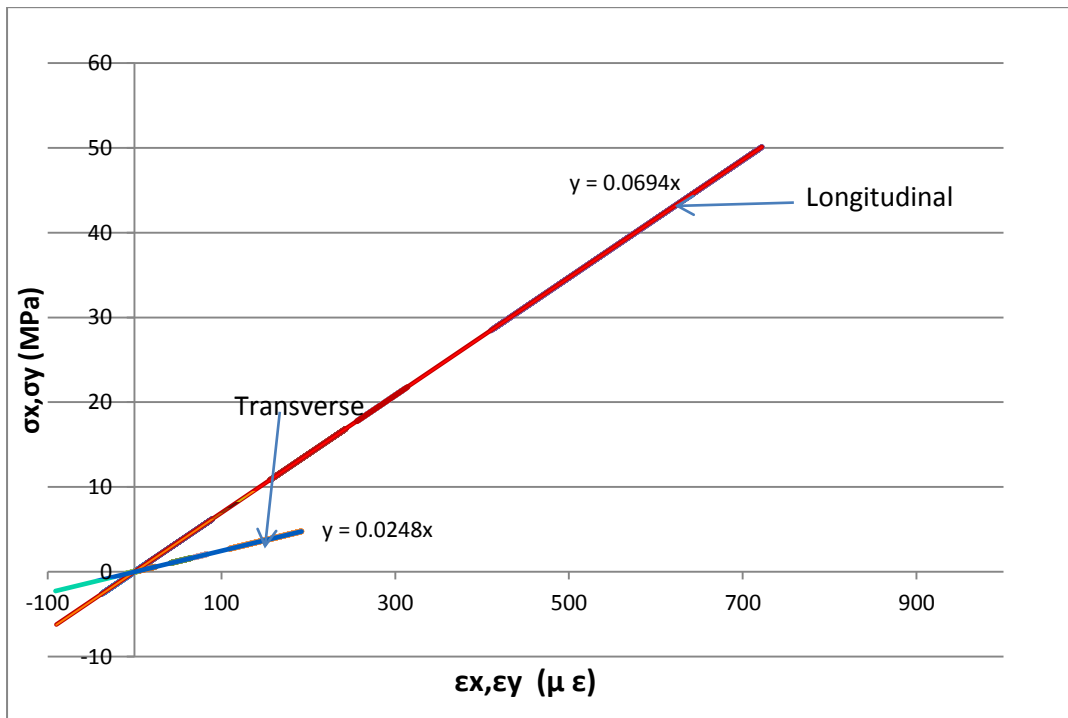


Figure 4.18 Stress-strain graphs for dynamic testing

Here the strains experienced due to the stresses applied while dynamically testing the swingarm is shown. The line that is straight (Figure 4.18) shows elastic deformation which means if you stop pulling, the material will go back to its original size. The slope of the stress-strain curve in the elastic deformation region is the modulus of elasticity, which is known as Young's modulus. It represents the stiffness of the material or resistance to elastic strain. The design of machines is based on component materials operating within this region. Thus the plastic deformation region is not shown in the graph because the component was designed in such a way that the stresses applied to it during its operation are never beyond the elastic deformation region.

The stress-strain equation based on the classical laminate theory for composites was used. Using the equations the stresses ($\sigma_x, \sigma_y, \tau_{xy}$) were calculated. The equations to determine stresses from strains (from graph) are given by:

For longitudinal stress,

$$\sigma_x = 0.0694 * \epsilon_x$$

For transverse stress,

$$\sigma_y = 0.0248 * \epsilon_y$$

Where, Stresses in MPa and

Strains in micro-strain ($\mu\epsilon$)

The equations are the same in both static and dynamic tests (i.e. Eqn. 4.9 and Eqn. 4.10). The results indicate a good correlation between the static and dynamic test to arrive at the same equations.

4.8 Chapter Summary

The structure of this dissertation is such that chapter-specific summary and discussions have, to a large extent, been included in the respective chapters. The results of the swingarm testing were presented and discussed in this chapter.

Parameters that affect the final mechanical properties of composites such as orientation, thickness and volume fraction were discussed with its effect on the current design of the swingarm. The swingarm composite with maximum strength and stiffness in the shear and transverse direction along with a good longitudinal stiffness was created using fibre orientation of the different composite layers. It is also observed that strength and elasticity of the material changes with thickness and volume fraction respectively. But the cost of production will rise since more material is being used. A similar approach was carried out in the design of the carbon fibre swingarm for a cost effective composite with maximum strength and elasticity for its job.

The static test was conducted to analyse the fatigue strength of the arm, but there was no record for any failure of the swingarm since the load was limited as the swingarm test piece was needed for further testing in BST. The dynamic test was done to analyse the safety of the swingarm to withstand a real-life test without failure with a factor of safety of two or more. The test was conducted for 1.5 million cycles with the exact loading as a real-life test and validated that the arm has infinite life at this particular loading since the applied load creates stresses below the endurance limit and never beyond the elastic deformation region. No tests were conducted by applying higher loads to test the endurance limit of the swingarm since no higher loads are applied on the swingarm during its life.

Different aspects such as load, strain and stress were analysed with respect to time to show the steady state of the system after a number of cycles. The results indicate a good correlation between the static and dynamic test to arrive at the same equations for the stress vs. strain curve. But there were no published results available, for the carbon fibre swingarm, in the literature of stresses and strains for comparison and error analysis.

The test rig was the first of its kind for swingarm testing and has highlighted a number of unique aspects of the rig such as variability of the loading using the eccentric mechanism was discussed. The rig helped in understanding the real- life behaviour of a swingarm, especially while going over bumps, in a laboratory. It was possible to study the damper effect of the arm while replicating all degrees of freedom as in real-life. But the interaction between rider and vehicle was not replicated. There is significant scope for further work on this topic by testing other carbon fibre components, by applying higher loads and including more accurate interaction between the rider and vehicle.

Chapter 5: Conclusions and Future Work

The chapter is structured as follows:

1. The overall conclusions of this work are stated.
2. Recommendations for further work are suggested.

5.1 Conclusions

A test rig was designed to experimentally validate a carbon fibre swingarm of a motorcycle. The test rig replicated the suspension of a Ducati 1098. The model builds upon the work of others, selecting and combining the advantages and remedying the disadvantages of previous work. It was able to overcome the drawback of the Leyni test bench (used in previous research studies in the literature) and apply variable loads for static and dynamic tests. The rig was able to test swingarms with a preload of 2470 N and a superimposed dynamic load of 2364 N. The rig can vary the static and dynamic loads to any value required. The model was designed using SolidWorks 2009 and most of the test rig components were made in house for cost saving. The model was computationally very efficient and was able to count the number of cycles performed while storing all the data concerned with load and strain, experienced by the swingarm during the fatigue testing.

The swingarm test rig was designed to give an industrial answer as to whether the swingarm will pass the BS code for fatigue test, before mass production of the swingarms. The test rig was an excellent approximation of a real-life test. It can be used for a deeper analysis and for further development of the component. Since no published results were available for comparison and error analysis, the strain gauge results can be used to compare the designed rig performance to the performance of other rigs else, they can be used for the future work involving FEA.

The model was successfully used to benchmark the swingarm performance. The test rig using static and dynamic loading proved that the swingarm can withstand a real-life test with infinite life. There was no record for the failure of the swingarm during static testing since the load was limited as the swingarm test piece was needed for further testing. And for dynamic testing, it is validated that the body will undergo infinite number of stress cycles since the applied load creates stresses below the endurance limit and never beyond the elastic

deformation region. The test rig was shown to be versatile, accurate and efficient, with potential for future application. This research has shown the benefit of test rigs for testing motorcycle components.

5.2 Recommendations for Further Work

1. A number of improvements to the test rig model are suggested, including:
 - a) An option to place the swingarm in different directions on the test rig so as to test the swingarm for twist and torsional test.
 - b) A different crank mechanism that can adjust the offset from the centreline of the gearbox which can enable the system to be easy to operate with the capability of adjusting the loads in a simpler manner.
 - c) Eliminating some of the rose joints which would improve the accuracy of the whole system.
 - d) An option to place different types of swingarms and other carbon fibre components made at BST on the test rig for fatigue testing.
2. The static test should be conducted until failure and the stresses in the swingarm can then be compared to the swingarm material strength to assess its durability.
3. Work can be carried out towards a new design of the test rig using hydraulic actuators so that higher loads can be applied which can be useful while testing other types of swingarms or carbon fibre components. The purpose is not to replace the current testing machine, but to have better control over the machine and to apply higher loads during the test. The hydraulic servos would eliminate the eccentric mechanism therefore improved reliability and accuracy would be achieved using hydraulics.
4. It was difficult to quantify the actual value and direction of the human damping force on road. Development of suitable instrumentation for this quantification is required.
5. The next step would be to develop an FE model of the swingarm and to compare the results with the test results from this report. The FE model would act as a guide to determine the stress points on the swingarm for further testing with strain gauges.

References

- 1 BlackStone Tek. Official Website, "www.blackstonetek.com". February 2013.
- 2 Grote K. Design of a Torsional Fatigue Testing Machine at BST. South Africa: Blackstone Tek; 2008.
- 3 Mangaraju KV, Yogaraja V, Karthik M, Dora BK, Babu R, Venkatesan R. Kinematic and Dynamic Analysis of Monoshock Rear Suspension. SAE Paper no: 2004-32-0020/20044307; 2004.
- 4 Kharul RV, Pomaje SD. Effect of Human Damping on Two wheeler Fatigue Life and Its Simulation on Two Poster Rig Using Passive Rider. SAE Paper no: 2001-26-0049; 2001.
- 5 Kumar MD. Redesign and Implementation of Motorcycle Rear Swingarm. ERES International Journal of Mechanical, Vol. 1, No. 1; 2013.
- 6 Mangaraju KV, Govardan D, Chavan C, Babu R, Venkatesan R. Optimization of Damping Characteristics for Two Wheelers. SAE Paper no: 2008-32-0068 / 20084768; 2008.
- 7 Meijaard JP, Popov AA. Multi-body Modelling and Analysis into the Non-linear Behaviour of Modern Motorcycles. United Kingdom: School of Mechanical, Materials and Manufacturing Engineering, University of Nottingham; 2006.
- 8 Leal MF, Borg JA, Butkewitsch S. Optimal Robust Design of Motorcycle Suspension Systems. SAE Paper no: 2000-01-3216; 2000.
- 9 Ide R, Ogushi T, Sunayama Y, Kishita Y, Watanabe S. Estimating of Motorcycle Frame Strength by Virtual Durability Test. SAE Paper no: 2009-32-0143/20097143; 2009.
- 10 Carfagni M, Pierini M, Caprioli D. Set Up and Validation for a Simulation of a Scooter Confort Bench. SAE Paper no: 2001-01-1875/4273; 2001.
- 11 Risitano G, Scappaticci L, Grimaldi C, Mariani F. Analysis of the Structural Behavior of Racing Motorcycle Swingarms. SAE Paper no: 2012-01-0207; 2012.
- 12 Piazza SD. Ducati Chassis Design: Simulation and Experiment Testing. Bologna, Italy: Ducati motor holding S.P.A.
- 13 Cassani S, Mancuso A. Shape Optimization of a High Performance Motorbike Single Sided Swingarm. SAE Paper no: 2005-01-0887; 2005.
- 14 Armentani E, Fusco S, Pirozzi M. Numerical Evaluation and Experimental Tests for a Road Bike Swingarm. Italy: Department of Industrial Design and Management, University of Napoli; 2007.
- 15 Dragoni E, Foresti F. Design of a Single Sided Composite Swingarm for Racing Motorcycles. Switzerland: International Journal of Mateils & Product Technology, Vol 13, Pages 411-420; 1998.
- 16 Bruderick M, Denton D, Shinedl M, Kiesel M. Carbon Fiber Composite Body Structures For the 2003 Dodge Viper. DaimlerChrysler Corporation.
- 17 O'Dea N. Motorcycle Swingarm Redesigned in Carbon Composite. Reinforced Plastics, 55 (1), pp 38-41; 2011.
- 18 Gaiani S. Industrialization of an Aluminium Alloy Single Swingarm for Ducati Monster S4 R. Development Trends of Motocycles II, page 288-303.
- 19 Iwasaki H, Mizuta A, Hasegawa T, Yoshitake H. Development of a Magnesium

- Swingarm for Motorcycles. SAE Paper no: 2004-32-0048 / 20044335; 2004.
- 20 Campbell FC. Structural Composite Materials, Introduction to Composite Materials. 2010.
 - 21 Corum JM, Battiste RL, Liu KC, Ruggles MB. Basic Properties of Reference Cross ply Carbon-Fiber Composite. United States: Lockheed Martin Energy Research Corp.; 2000.
 - 22 Eastern Cape Development Corporation. An Overview of the Eastern Cape Automotive Industry. South Africa 2005.
 - 23 Ministry of Heavy Industries & Public Enterprises. Automotive Mission Plan 2006-2016. New Delhi, India 2006.
 - 24 Kharul R, Balakrishnan S, Singa AV, Patil MG. Methodology Adopted to Establish Rig Correlation with Customer Usage for Two Wheelers. SAE Paper no: 2005-32-0029/20056542; 2005.
 - 25 Singanamalli A, Kharul R, Jayaram N, ora B, Anand R. Optimization of Frame Design Through Virtual Simulation of Bump Test. SAE Paper no: 2004-32-0021/20044308; 2004.
 - 26 Balakrishnan S, Muniyasamy K, Singanamalli AV, Kharul R, Jayaram N. Application of Fatigue Life Prediction Techniques for Optimising the Motorcycle Center Stand. SAE Paper no: 2004-32-0046/20044333; 2004.
 - 27 Muniyasamy K, Kharul R, Jayaram N, Govindarajan R. Vibration Fatigue Analysis of Motorcycle Front Fender. SAE Paper no: 2005-32-0030/20056543; 2005.
 - 28 Kharul R, Balakrishnan S, Singanamalli AV, Dora KB. Development of Generic Load Cases for Motorcycle Components for Design Optimisation. SAE Paper no: 2007-32-0095/20076595; 2007.
 - 29 Kharul R, Balakrishnan S, Karedla D, Shawn S. Virtual Testing and Correlation for a Motorcycle Design. SAE Paper no: 2010-01-0925; 2010.
 - 30 Balakrishnan S, Sasun C, Anoop P, Kharul R. Accurate Estimation of Time Histories for Improved Durability Prediction Using Artificial Neural Networks. SAE Paper no: 2012-01-0023.
 - 31 Pawar PR, Karanth NV. Effect of Disc Brake and Drum Brake on the Durability of Front Shock Absorber Tube of a Motorcycle. SAE Paper No: 2003-26-0031; 2003.
 - 32 Lin KY, Chang JM, Wu JH, Chang CH, Chang SH, Hwang JR, Fung CP. Durability Assessments of Motorcycle Handlebars. SAE Paper no: 2005-01-0801; 2005.
 - 33 Kharul R, Patil MG, Balakrishnan S, Risam GS. Methodology for Accelerated Vibration Durability Test on Electrodynamical Shaker. SAE Paper no: 2006-32-0081 / 20066581; 2006.
 - 34 Michiue M, Kawasaki T, Nishio K, Sugiura H, Inamura F, Morikawa M. Prediction of Vibration Fatigue Life for Motorcycle Exhaust Systems. SAE Paper no: 2011-32-0642/20119642; 2011.
 - 35 Muthuveerappan G, Manoj V, Gopinath K. Development of a Power Re-Circulating Gear Test Rig. Chennai, India: Dept. of Mechanical Engineering, IIT Madras.
 - 36 Crump D, Dulieu M, Savage J. Design and Commission of an Experimental Test Rig to Apply a Full-Scale Pressure Load on Composite Sandwich Panels Representative of Aircraft Secondary Structure. Measurement Science and Technology, 21 (1), pp 1-6; 2010.
 - 37 Ismail K, Kadambi R, Thomas S. Development and Implementation of Test Rig setup for Integrated Centre Panel. India: M.S.Ramaiah School of Advanced Studies; 2001.
 - 38 Kumar S, Kundra TK, Modak SV. Model Updating Studies on a Two Wheeler Chassis. SAE Paper no:2007-01-2353; 2007.
 - 39 Carroll P, Carver S. Factors in the Mechanical Design of Motorcycle Laboratory Test

- Systems. SAE Paper no: 2001-01-1879/4296; 2001.
- 40 Maurizio C. Topological Optimization of Side Plates For Rear Swingarm of Mv Agusta F4 1000 My '10. Cagiva Research Center; 2010.
 - 41 Sato S, Sunayama Y, Sakamoto Y. Radiation Noise Analysis for Electric Scooter Swingarm. SAE Paper no: 2011-32-0650/20119650; 2011.
 - 42 Ardiri D, Cammarata A, Sinatra R. Simulation of Roller Test Bench for Fatigue Validation of a Scooter Frame. Italy: Piaggio Brand Unit Vehicle Mechanical System & CAE.
 - 43 Stefano V, Simone P. Structural Optimization of the Rear Swingarm of Ducati HyperMotard. Berlin, Germany: 1st European HyperWorks Technology Conference; 2007.
 - 44 University of the Witwatersrand. Guidelines for Design Reports, MECN2009 Notes. South Africa 2011.
 - 45 Zoerb GC. Strain Gage Instrumentation for Power Measurement. United States: South Dakota State College.
 - 46 National Instruments Corporation. Load and Pressure Measurements, www.ni.com/white-paper/7138/en.. February 2013.
 - 47 New Jersey Institute of Technology, Department of Engineering Technology. Design for Cyclic Loading, MET 301. United States 2013.
 - 48 Bradley E. Reliability Engineering Course notes, MECN 7001. South Africa: University of the Witwatersrand; 2012.
 - 49 Bryan H. Engineering Composite Materials. London, United Kingdom: The Institute of Materials; 1999.
 - 50 University of the Witwatersrand. Mechanics of Composite Materials, MECN4003 Notes. South Africa.
 - 51 Zipp Speed Weaponry. Woven Carbon Vs. Unidirectional, "www.zipp.com". United States July 2013.
 - 52 Oribi Manufacturing. Uni-Directional vs Woven, "www.oribimanufacturing.com". United States July 2013.
 - 53 Adis A, Ujjal KS. Simulating a Tensile Test of a Carbon Fibre Composite Test Specimen in ABAQUS. Sweden: University of Skovde.
 - 54 Department of Defence. Polymer Matrix Composites; Materials Usage, Design and Analysis. United States 1997.
 - 55 Toray Carbon Fibers. Toray Data Sheet: "www.toraycfa.com" & "www.torayca.com". Japan February 2013.
 - 56 TenCate Advanced Composites. Technical Data for RS-36 Resin System: "www.tencate.com". United States July 2013.
 - 57 Tomblin J, Sherraden J, Seneviratne W, Raju KS. A–Basis and B–Basis Design Allowables for Epoxy Based Prepreg. Advanced General Aviation Transport Experiments (AGATE); 2002.
 - 58 Tienie VS. Short Course on Filamentary Composite Materials. South Africa: University of Pretoria; 1998.
 - 59 Tiwari N. Mechanics of Laminated Composite Structures. Kanpur, India: Indian Institute of Technology.
 - 60 Calard V. Formulas and Equations for the Classical Laminate Theory. 2011.

- 61 Socie D. Fatigue Analysis Techniques. United States: University of Illinois.
- 62 Fibro Springs. Round Wire Compression Spring, "www.fibro.de". February 2013.
- 63 Mahadevan K, Reddy K. Design Data Hand Book. India: CBS Publishers and Distributors; 2002.
- 64 Budynas RG, Shigley JE, Nisbett JK. Shigley's Mechanical Engineering Design. McGraw–Hill; 2008.
- 65 Einstein College of Engineering. Course Notes on Design of Machine Elements. Tamil Nadu, India.
- 66 Koyo Bearings. Ball and Roller Bearings, "www.koyousa.com". United States February 2013.
- 67 National Instruments Corporation. Strain Gauge Measurements, "www.ni.com/white-paper/3642/en". February 2013.
- 68 Micro-Measurements. Shunt Calibration of Strain Gage Instrumentation, www.micro-measurements.com. February 2013.
- 69 Vozkova P. Elastic Modulus FEM Modelling of the Layered Woven Composite Material. Czech Republic: Technical University of Liberec.

Appendix A

A.1 Cost of Machined Components

Table A.1 The cost of machined components within the factory

Components machined	Material	Qty. (kg)	Cost (Inc. VAT) (per kg)	Total cost (Inc. VAT) (R)
Eccentric mechanism components (only for electrical test rig)				
Eccentric shaft	En19	1	33	33
Eccentric bolt	En19	0.5	33	16.5
Con-rod	En19	2	33	66
Angle plates (2 numbers)	En19	14	33	462
Hexagonal bolt	En19	1	33	33
Eccentric hub and its shaft (2 numbers)	En19	8	33	264
Essential nuts and bolts				250
Total cost of machined components (only for electrical test rig)				1125
Swingarm attachment components (common for electrical and hydraulic)				
Angle plates (2 numbers)	En19	12	33	396
Swingarm pivot	En19	3.5	33	115.5
Rocker arm	Aluminium	1	60	60
Wheel hub	Aluminium	1	60	60
The two rods	Aluminium	1	60	60
Essential nuts and bolts				250
Slider and spring mechanism components (common for electrical and hydraulic)				
Slider rail	En19	0.5	33	16.5
Slider base	Aluminium	2.5	60	150
Sliding arm	En19	1	33	33
Essential nuts and bolts				120
Spring housing	Aluminium	4	60	240
Total cost of machined components (common for electrical and hydraulic)				1501

The cost of components purchased which are common for electric and hydraulic test rig is given below.

Table A.2 Cost of components purchased

Components and specifications purchased	QTY	Price (Inc. VAT)	Total (R) (Inc. VAT)
Static test rig components (common for electrical and hydraulic)			
Single sided hydraulic Ram	1	950	950
Chain	1	116.28	116.28
Dynamic test rig components (common for electrical and hydraulic)			
Ohlin's springs	2	494	988
2 plumber blocks for angle plates	2	240	480
Linear way for sliding mechanism	1	245	245
IKO Rod End bearing (rose joint)	3	263	789
Base plate	1	6775	6775
Total cost of purchased components (R)			10343

A.2 Load Design

Given data

- Acceleration due to gravity, $g = 9.810 \text{ m/s}^2$
- Motorcycle weight, $W_b = 2158 \text{ N}$
- Weight of rider and passenger, $W_r = 1960 \text{ N}$
- The maximum load to be reached while testing, $F = 5900 \text{ N}$ [18] (Appendix E, test factor (K_r) of 1.431)

Equations and calculations

The cyclic load,

$$F_c = F - W_r = 3940 \text{ N} \quad (\text{A.1})$$

Total preload,

$$F_p = W_b + W_r = 4118 \text{ N} \quad (\text{A.2})$$

Real wheel loads, taking (on rear wheel) 60 % / 40% (one front wheel) split: [14]

Rear wheel cyclic load,

$$F_{rc} = 0.6 \cdot F_c = 241 \text{ kg} = 2364 \text{ N} \quad (\text{A.3})$$

Rear wheel total preload,

$$F_{rp} = 0.6 \cdot F_p = 251 \text{ kg} = 2470 \text{ N} \quad (\text{A.4})$$

Maximum load on the rear wheel is,

$$F_{\max-r} = F_{rc} + F_{rp} = 4835 \text{ N} \quad (\text{A.5})$$

A.3 Spring Design

A spring is an elastic member, which deflects, or distorts under the action of load and regains its original shape after the load is removed. The factor of safety of a selected spring is calculated and it is used for this research if it is greater than one.

Function of the spring.

1. To measure forces in spring balance, meters and engine indicators.
2. To store energy.

Given data

- Spring material: spring steel Class C
- Spring type no : 241.02.44.200 by Fibro springs [62]
- Hard-drawn wire
- Round wire compression spring

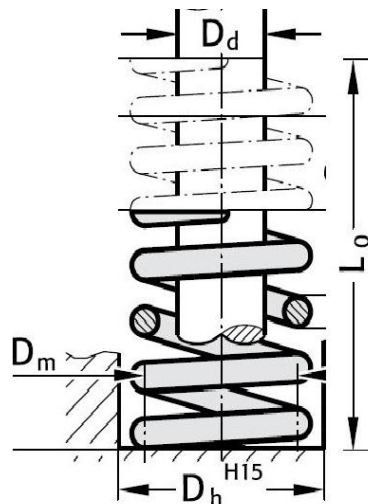


Figure A.1 Dimensions of a spring

- D_h = diameter of guide sleeve = 44 mm
- D_m = mean coil diameter = 34 mm

- $D_d = \text{coil diameter} = 8 \text{ mm}$
- $L_0 = \text{free length of spring} = 200 \text{ mm}$
- $K = \text{the load required per unit deflection of the spring, spring rate} = 62700 \text{ N/m}$
- $N_a = \text{number of active coils} = 17 \text{ turns}$
- Young's modulus, $E = 2.07E+11 \text{ N/m}^2$
- Shear modulus, $G = 8.10E+10 \text{ N/m}^2$
- $\alpha = 0.5$, since spring supported between flat parallel surfaces
- Density, $\rho = 7850 \text{ kg/m}^3$
- Fatigue strength in reversed shear, $S_{sa} = 398 \text{ MPa}$
- Ultimate strength in shear, $S_{sm} = 534 \text{ MPa}$
- Minimum load cycles = $1.20E+06 \text{ cycles}$
- Speed of shaft, $N = 210 \text{ rpm}$
- Torsional frequency, $f = 3.5 \text{ cycles/second}$

Equations and calculations

Forces acting on spring

Maximum force, from Eqn. A.3 and A.4

$$F_{\max} = 2364 + 2470 \approx 5000 \text{ N}$$

Minimum force, (before preloading)

$$F_{\min} = 0 \text{ N}$$

Spring index = mean coil diameter / coil diameter = 4

The maximum shear stress in the spring associated with the maximum force is given by [63]

$$\tau_{\max} = \frac{8WD}{\pi d^3} * F_{\max} = 1163 \text{ MPa} \quad (\text{A.6})$$

Where W is the Wahl correction factor

$$W = \frac{4C-1}{4C-4} + \frac{0.615}{C} = 1.380 \quad (\text{A.7})$$

The total number of spring coils is equal to the active coils in the spring interior plus the 2 coils at the spring ends,

$$n_f = n_a + 2 = 19 \quad (\text{A.8})$$

The solid length of the spring is length of a spring under the maximum compression,

$$L_s = (N_f - 0.75) d = 146 \text{ mm} \quad (\text{A.9})$$

To determine if spring is stable:

Free length, [64]

$$\frac{\pi * D_m *}{\alpha} * \sqrt{\frac{2 * (E - G)}{2E + G}} = 176.540 \quad (\text{A.10})$$

OK since it has a guide to travel in.

Ultimate tensile strength of spring,

$$S_{ut} = \frac{A}{m * d} = 1201 \text{ MPa} \quad (\text{A.11})$$

Where $A = 1783 \text{ MPa} \cdot \text{mm}^2$

$M = 0.190$

The spring mass, M can be found by finding the spring volume and multiplying by its material density,

$$M = \rho * \text{Vol.} = \rho * (L_{\text{wire}} * \frac{\pi}{4} * d^2) \quad (\text{A.12})$$

$$= 0.717 \text{ kg}$$

Where $L_{\text{wire}} = \pi * d * N_s$

The natural frequency of the spring,

$$f_n = 0.25 * \sqrt{\frac{c}{m}} = 74 \text{ Hz} \quad (\text{A.13})$$

To determine the safety factor of spring:

Yield strength in shear,

$$S_{se} = \frac{S_{sa}}{1 - [\frac{S_{sm}}{0.67 * S_{ut}}]^2} = 711.170 \text{ MPa} \quad (\text{A.14})$$

Stress components are given by

$$\tau_m = w * 8 * F_m * C / \pi * d^2 = 581 \text{ MPa}$$

$$\tau_a = w * 8 * F_a * C / \pi * d^2 = 581 \text{ MPa} \quad (\text{A.15})$$

Where $F_a = (F_{\max} - F_{\min}) / 2$

$F_m = (F_{\max} + F_{\min}) / 2$

The factor of safety

$$Sf = S_{se} / \tau_a = 1.2 \quad (\text{A.16})$$

OK, since its Sf is greater than 1

A.4 Motor Design

The electric motor (Figure A.2) provides the required power to the whole dynamic test rig at a given frequency. A gear system is attached to the motor to provide the required torque. This component can be a significant contributor to the cost of the whole test system and is therefore worth the time to properly evaluate it instead of buying an overrated system.

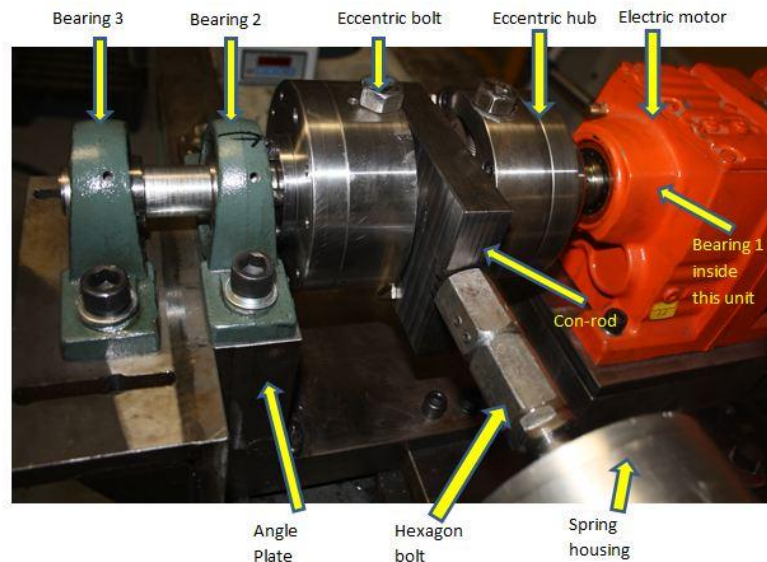


Figure A.2 Eccentric mechanism components and the electric motor

Equations and calculations

Rotating forces:

Maximum rotating force, from Eqn. A.3

$$F_{\max 1} \approx 2500 \text{ N}$$

Minimum rotating force, (when motor is not running)

$$F_{\min 1} = 0 \text{ N}$$

Eccentric radius:

Maximum eccentric radius needed

$$F_{\max 1} / K = 0.040 \text{ m}$$

Minimum eccentric radius needed

$$F_{\min 1} / K = 0 \text{ m}$$

Where K = spring rate

Torque needed for transmission:

Maximum torque that needs to be transmitted

$$F_{\max 1} * \text{Max eccentric} = 99.7 \text{ Nm}$$

Minimum torque that needs to be transmitted

$$F_{\min} * \text{Min eccentric} = 0 \text{ Nm}$$

Power needed by motor =

$$\text{Max torque} * f * 2\pi / 1000 = 2.190 \text{ kW} \quad (\text{A.17})$$

Motor details:

- Power, $P = 4 \text{ kW}$, **OK**, since chosen power is greater.
- Rated speed = 1400 RPM
- Rated Frequency, $R_f = 23.334 \text{ Hz}$
- $I = R_f / f = 6.700$
- Torque,

$$(P * 1000) / (R_f * 2\pi) = 27.3 \text{ Nm} \quad (\text{A.18})$$

A.5 Eccentric Bolt Design

The eccentric bolt (Figure A.3) attaches the eccentric shaft to the eccentric hub. Since the bolt takes a large amount of stress during a test, it is designed with a factor of safety greater than one.

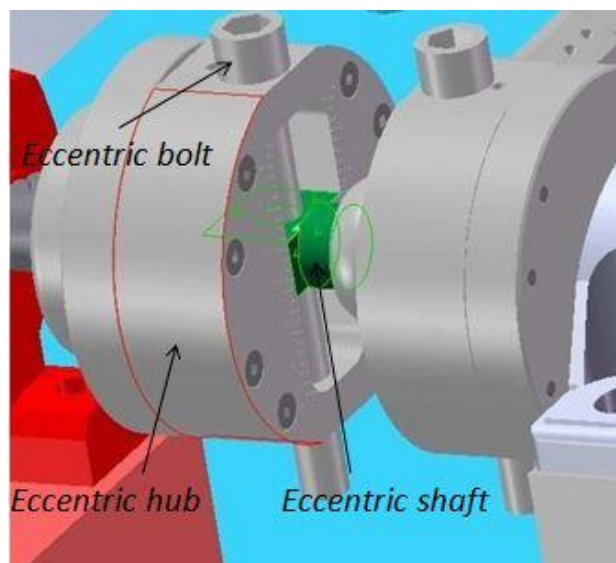


Figure A.3 Eccentric system of the test rig

Given data

- No of bolts = 2
- Material – EN19
- Yield stress, $S_y = 480 \text{ MPa}$
- Tensile stress, $S_{ut} = 690 \text{ MPa}$

- Assume bolt diameter, $D_{as} = 16$ mm
- Assume safety factor, $S_f = 1.3$

Equations and calculations

Endurance limit,

$$S_e' = 0.504 * S_{ut} = 347.760 \text{ MPa} \quad (\text{A.19})$$

Forces acting on bolts:

Max shear force experienced on each bolt

$$F_{\max 2} = F_{\max} / 2 = 2500 \text{ N}$$

Min shear force experienced on each bolt

$$F_{\min 2} = F_{\min} / 2 = 0 \text{ N}$$

Adjustment of the Endurance Limit,

- Surface Condition (K_a): Assume machined,

$$K_a = a * (S_{ut})^b = 0.798 \quad (\text{A.20})$$

Where $a = 4.51 \text{ MPa}$

$$b = -0.265$$

- Size (K_b):

$$K_b = 1.24 * (0.37 * D_{as})^{-0.107} = 1.025 \quad (\text{A.21})$$

- Load (K_c) = 1

- Temperature (K_d): Assume operating temperature, $t = 25$ °C

$$K_d = 0.975 + 0.000432 * t - (1.15) * 10^{-6} * t^2 + (1.04) * 10^{-9} * t^3 \quad (\text{A.22})$$

$$= 0.985$$

- Reliability (K_e): Assume 90% reliable = 0.897

- Miscellaneous (K_f): Assumed reversed bending = 1

Real-World Allowable Cyclic Stress,

$$S_e = k_a * k_b * K_c * k_d * k_e * k_f * S_e' \quad (\text{A.23})$$

$$= 251.310 \text{ MPa}$$

Bending moment,

$$M = (F_{\max 2} * \text{length to disk}) / 1000 = 75 \text{ Nm} \quad (\text{A.24})$$

Where, length to disk = 30 mm

Diameter of bolt,

$$d = \left[\frac{32 * M * S_f * 1000}{\pi * S_e} \right]^{(1/3)} = 15.810 \text{ mm} \quad (\text{A.25})$$

OK, since chosen diameter is greater.

A.6 Eccentric Shaft Design

Similar to the eccentric bolt, the eccentric shaft (Figure A.4) connects the two eccentric hubs together and the double row angular contact ball bearing's inner race fits along the shaft and thus it is designed with a factor of safety greater than one.

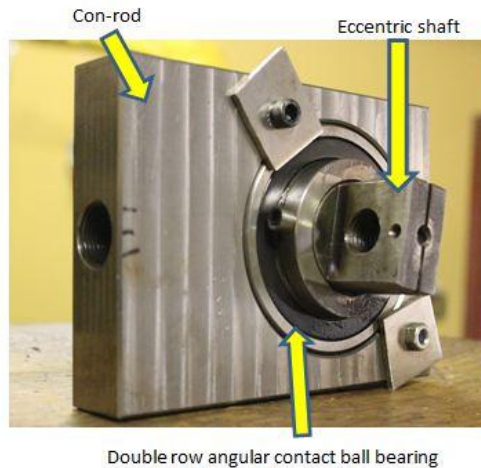


Figure A.4 Eccentric shaft and its components

Given data

- Material – EN19
- Yield stress, $S_y = 480$ MPa
- Tensile stress, $S_{ut} = 690$ MPa
- Assume safety factor, $S_f = 5$
- Shaft diameter, $d = 45$ mm
 $D = d/0.75 = 60$ mm
 $r = D/20 = 3$ mm
- Theoretical stress-concentration-factor for bending, $K_t = 1.750$
- Theoretical stress-concentration-factor for torsion, $K_{ts} = 1.5$

Equations and calculation

Torque transmitted to shaft,

$$\text{Torque of motor} * I = 181.9 \text{ Nm} \quad (\text{A.26})$$

$$\tau_{\max} = 181.9 \text{ Nm}$$

$$\tau_{\min} = -189.9 \text{ Nm}$$

Reversed Bending moment transmitted to shaft = $2M = 150$ Nm

$$M_{\max} = 150 \text{ Nm}$$

$$M_{\min} = -150 \text{ Nm}$$

Endurance limit,

$$S_e' = 0.504 * S_{ut} = 347.760 \text{ MPa}$$

Adjustment of the Endurance Limit,

- Surface Condition (K_a): Assume ground,

$$K_a = a * (S_{ut})^b = 0.906$$

Where $a = 1.580 \text{ MPa}$

$$b = -0.085$$

- Size (K_b):

$$K_b = 1.24 * (0.37 * d)^{-0.107} = 0.825$$

- Load (K_c) = 1

- Temperature (K_d): Assume operating temperature, $t = 25 \text{ }^\circ\text{C}$

$$K_d = 0.975 + 0.000432 * t - (1.15) * 10^{-6} * t^2 + (1.04) * 10^{-9} * t^3 \\ = 0.985$$

- Reliability (K_e): Assume 90% reliable = 0.897

- Miscellaneous (K_f): Assumed reversed bending = 1

Real-World Allowable Cyclic Stress,

$$S_e = k_a * k_b * K_c * k_d * k_e * k_f * S_e' \\ = 229.840 \text{ MPa}$$

Stress-concentration factors:

Fatigue stress-concentration factor for bending,

$$K_f = \frac{K_t}{1 + \frac{2(K_t - 1) \sqrt{a}}{K_t \sqrt{r}}} = 1.590 \quad (\text{A.27})$$

Fatigue stress-concentration factor for torsion,

$$K_{fs} = \frac{K_{ts}}{1 + \frac{2(K_{ts} - 1) \sqrt{a}}{K_{ts} \sqrt{r}}} = 1.390 \quad (\text{A.28})$$

Where, stress concentration at shoulder

$$\sqrt{a} = 139/S_{ut} = 0.201$$

Shaft stresses:

Maximum axial stresses,

$$\sigma_{\max} = \frac{K_f * M_{\max}}{I} * \left(\frac{d}{2}\right) = 26.680 \text{ MPa} \quad (\text{A.29})$$

Minimum axial stresses,

$$\sigma_{\min} = \frac{K_f * M_{\min} * \left(\frac{d}{2}\right)}{I} = - 26.680 \text{ MPa} \quad (\text{A.30})$$

Maximum torsional stresses,

$$\tau_{\max} = \frac{K_f * \tau_{\max} * \left(\frac{d}{2}\right)}{I} = 14.150 \text{ MPa} \quad (\text{A.31})$$

Minimum torsional stresses,

$$\tau_{\min} = \frac{K_f * \tau_{\min} * \left(\frac{d}{2}\right)}{I} = - 14.150 \text{ MPa} \quad (\text{A.32})$$

Midrange axial stresses,

$$\sigma_m = (\sigma_{\max} + \sigma_{\min})/2 = 26.680 \text{ MPa} \quad (\text{A.33})$$

Alternating axial stresses,

$$\sigma_a = |\sigma_{\max} - \sigma_{\min}|/2 = 0 \quad (\text{A.34})$$

Midrange torsional stresses,

$$\tau_m = (\tau_{\max} + \tau_{\min})/2 = 14.150 \text{ MPa} \quad (\text{A.35})$$

Alternating torsional stresses,

$$\tau_a = |\tau_{\max} - \tau_{\min}|/2 = 0 \quad (\text{A.36})$$

Diameter of shaft [65]

$$d = \left[\frac{s.f * 32}{\pi} * \left\{ \frac{M * K_f * 1000}{S_e} + \frac{\tau * K_{fs} * 1000}{S_{ut}} \right\} \right]^{(1/3)} \quad (\text{A.37})$$

$$= 41.520 \text{ mm}$$

OK, since chosen diameter is greater.

A.7 Thread for the Hexagonal Bolt Design

The hexagonal bolt attaches the spring housing to the eccentric mechanism as shown in [Figure A.2](#) through the thread for the hexagonal bolt (Figure A.5). The design for this thread ensures less chance for thread cracks and could lead to higher reliability in the entire test rig.

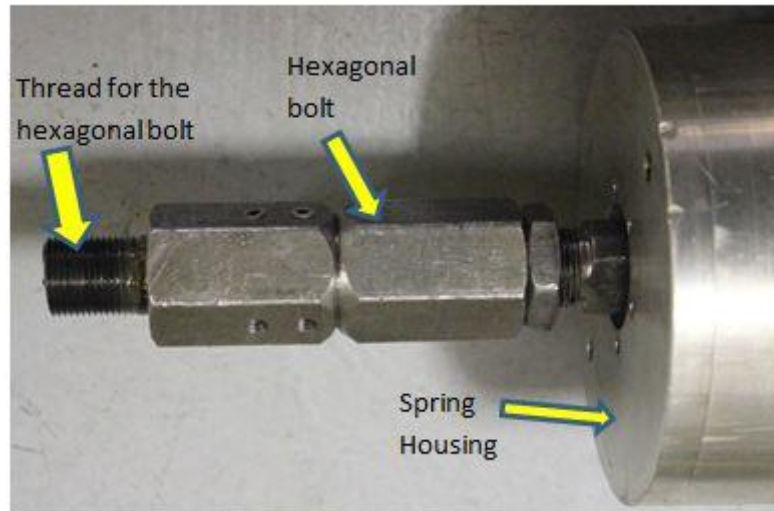


Figure A.5 Hexagonal bolt and its components

Given data

- Material – EN19
- Yield stress, $S_y = 480 \text{ MPa}$
- Maximum force (from Eqn. A.3 and A.4), $F_{\max} = 5000 \text{ N}$
- Assume: Diameter of rod on which thread lies, $d = 20 \text{ mm}$
- Pitch of thread, $p = 1.5 \text{ mm}$
- Length of thread, $L = 25 \text{ mm}$

Equations and calculation

The area under which the stress acts A,

$$\Pi * d * L = 1570 \text{ mm}^2 \quad (\text{A.38})$$

Load capacity of bolt

$$F_a = C * (A)^{1.48} = 23816 \text{ N} \quad (\text{A.39})$$

Where $C = 0.7$ for alloy steel

Shear stress on thread

$$F_{\max}/A = 3.184 \text{ N/mm}^2 \quad (\text{A.40})$$

Safety factor,

$$Sf = S_y/\text{shear stress} = 150 \quad (\text{A.41})$$

OK, since its Sf is greater than 1

A.8 Bearing Design

Bearings enhance the functionality of any machinery and help to save energy. Bearings do their work silently, in tough environments, hidden in machinery where they can't be seen. The purpose of a bearing is to reduce friction, most often on a rotating shaft. The design for these crucial components ensures fewer chances for failures.

A.8.1 Bearing Over the Eccentric Shaft Design

The double row angular contact ball bearing has its inner and outer race along the eccentric rotating shaft and the con-rod respectively as shown in [Figure A.4](#). Maximum load during the dynamic test on the arm is 4835 N (Equation A.5). Thus 5000 N is used for calculations to include a factor of safety greater than one.

Given data

- Assume bearing is a double row angular contact ball bearing [66]
- Inner diameter, $d = 40$ mm
- Outer diameter, $D = 85$ mm
- Specific capacity, $C = 45400\text{N}$
- Basic static load rating, $C_0 = 51400$ N
- Speed of shaft, $N = 210$ RPM

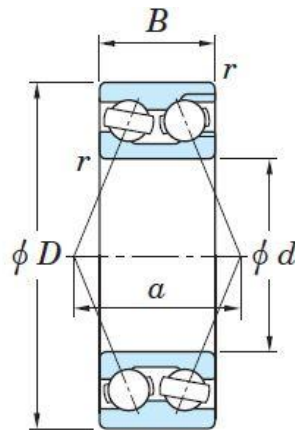


Figure A.6 Dimensions of a double row angular contact ball bearing

Equations and calculation

Forces acting on bearing

Maximum force, from Eqn. A.5

$$F_{\max} \approx 5000\text{N}$$

Minimum force, from Eqn. A.3

$$F_{\min} \approx 2500 \text{ N}$$

The constant mean load for a period of fluctuating loads is,

$$F_m = (F_{\min} + 2 F_{\max})/2 = 4166.6 \text{ N}$$

Radial force,

$$F_r = F_m = 4166.6 \text{ N}$$

Axial force,

$$F_a = 0 \text{ N}$$

Life in millions of revolutions,

$$L_n = (C/F)^3 = 1293.601 \text{ millions of revolutions} \quad (\text{A.42})$$

Life in working hours,

$$L_h = \frac{10^6 * L_n}{60 * N} = 102666.7 \text{ hours} = 11.720 \text{ yrs.} \quad (\text{A.43})$$

OK since the bearing will last long enough.

A.8.2 Bearing Reactions

The 3 bearings which react against the force and friction on the rotation shaft are shown in [Figure A.2](#). The reactions of each bearing are calculated and the bearing with more load acting on it is designed. Similar bearings will be used for all 3 plummer blocks to make the system more reliable.

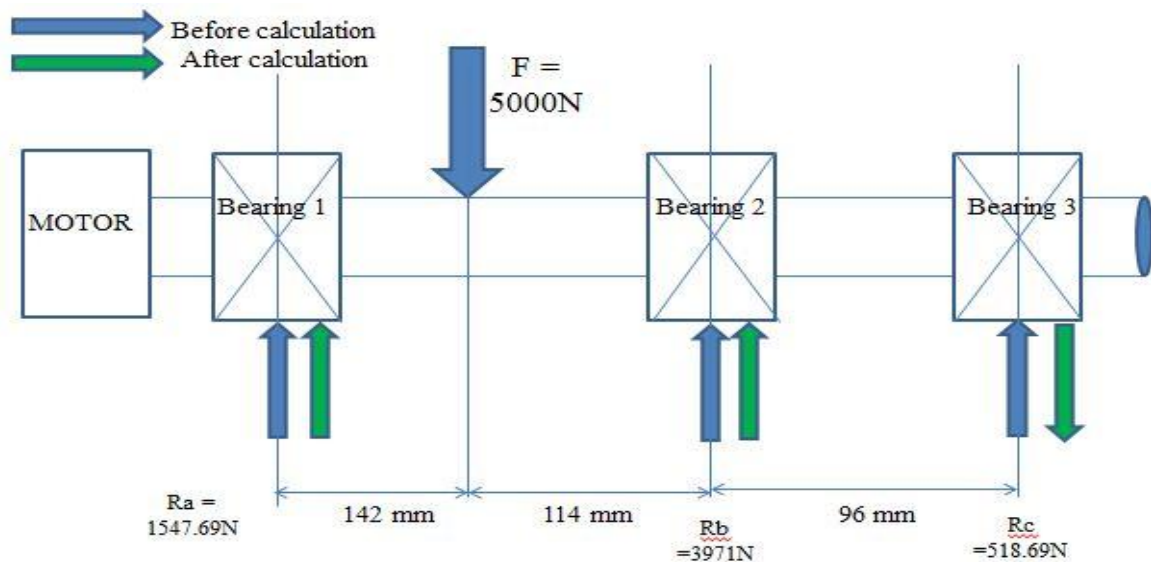


Figure A.7 Bearing reactions

Forces acting:

$$R_a + R_b + R_c = F = 5000 \text{ N}$$

$$\text{At 1: } 0.142 F = 0.256 R_b + 0.352 R_c$$

$$\text{At F: } 0.142 R_a = 0.114 R_b + 0.21 R_c$$

$$\text{At 2: } 0.256 R_a - 0.096 R_c = 0.114 F$$

$$\text{At 3: } 0.352 R_a + 0.096 R_b = 0.011 F$$

Solving,

- $R_a = 1547.690 \text{ N}$, acting on the bearing 1
- $R_b = 3971 \text{ N}$, acting on the bearing 2
- $R_c = -518.690 \text{ N}$, acting on the bearing 3 in reverse direction as shown.

A.8.3 Bearing-2 Design

Since similar plummer blocks consisting of similar bearings are used in the test rig, it would be optimum to design bearing 2 since there is more load acting on it as in Figure A.7.

Given data

- Assume bearing is a deep groove ball bearing
- Inner diameter, $d = 30 \text{ mm}$
- Outer diameter, $D = 72 \text{ mm}$
- Specific capacity, $C = 26700 \text{ N}$
- Basic static load rating, $C_0 = 15000 \text{ N}$
- Speed of shaft, $N = 210 \text{ RPM}$

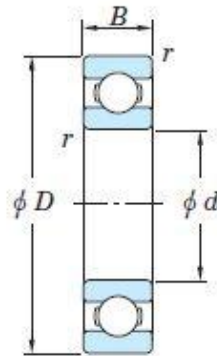


Figure A.8 Dimensions of a deep groove ball bearing

Equations and calculation

Forces acting on bearing

$$\text{Radial force, } F_r = R_b = 3971 \text{ N}$$

$$\text{Axial force, } F_a = 0 \text{ N}$$

Life in millions of revolutions,

$$L_n = (C/F)^3 = 303.972 \text{ millions of revolutions}$$

Life in working hours,

$$L_h = \frac{10^6 * L_n}{60 * N} = 24124.790 \text{ hours} = 2.754 \text{ yrs.}$$

OK since the bearing will last long enough.

Appendix B

B.1 Strain Gauge Calibration

Fatigue test loads

- Rear wheel cyclic load, $F_{rc} = 2364 \text{ N} = 241 \text{ kg}$
- Rear wheel total preload, $F_{rp} = 2470.9 \text{ N} = 251.9 \text{ kg}$

Strain gauge equipment description

Equipment: National Instruments SCXI-1000 chassis, SCXI-1600 control card, SCXI-1521B universal card, SCXI-1317 module

Features of strain gauges used:

- Resistance = 119.8 ohm
- FG = gauge factor of strain gauge = 2.12
- Quarter-bridge circuit with a single active gauge.

Strain Gauge Method

Sample rate: 100 Hz

Low pass filter: 10 Hz

Calibration

The gauges were extremely stable.

Table B.1 Strain gauge calibration chart

Channel Information		Offset Adjustment		Gain Adjustment (with shunt)			
Name	Phys. Channel	Meas. Strain	Err %	Sim. Strain	Meas. Strain	Gain Adj. Val.	Err %
Strain_0	SC1Mod2/ai7	-300.562E-9	0.56	543.182E-6	566.066E-6	0.999	0.57
Strain_4	SC1Mod2/ai11	-133.303E-9	1.72	498.931E-6	567.392E-6	0.999	1.71
Strain_3	SC1Mod2/ai10	-177.132E-9	1.05	523.686E-6	566.091E-6	0.999	1.06
Strain_2	SC1Mod2/ai9	-731.118E-9	0.29	535.904E-6	566.177E-6	1.000	0.30
Strain_1	SC1Mod2/ai8	-164.882E-9	0.57	543.038E-6	566.046E-6	0.999	0.58

Calibration successful

As seen the % error was less than 2% and thus accepted.

B.2 Load Cell Calibration

Load cell calibration Equipment Description

Equipment: National Instruments SCXI-1000 chassis, SCXI-1600 control card, SCXI-1521B universal card, SCXI-1317 module, load cell.

Loading and unloading of 350 kg was done by using weights.

Load cell wiring

EX +	blue
EX -	yellow
CH +	red
CH -	green

Load Cell Dead Weight Calibration

Table B.2 Load cell calibration data

Mass	Load	Voltage	Mass	Load	Voltage
[kg]	[N]	[v]	[kg]	[N]	[v]
0	0.00	-3.20E-04	325	3.18E+03	-1.62E-03
25	2.45E+02	-4.20E-04	300	2.94E+03	-1.52E-03
50	4.90E+02	-5.20E-04	275	2.69E+03	-1.42E-03
75	7.34E+02	-6.10E-04	250	2.45E+03	-1.32E-03
100	9.79E+02	-7.10E-04	225	2.20E+03	-1.22E-03
125	1.22E+03	-8.10E-04	200	1.96E+03	-1.12E-03
150	1.47E+03	-9.10E-04	175	1.71E+03	-1.02E-03
175	1.71E+03	-1.01E-03	150	1.47E+03	-9.20E-04
200	1.96E+03	-1.12E-03	125	1.22E+03	-8.20E-04
225	2.20E+03	-1.21E-03	100	9.79E+02	-7.20E-04
250	2.45E+03	-1.31E-03	75	7.34E+02	-6.20E-04
275	2.69E+03	-1.42E-03	50	4.90E+02	-5.30E-04
300	2.94E+03	-1.51E-03	25	2.45E+02	-4.30E-04
325	3.18E+03	-1.61E-03	0	0.00	-3.30E-04
350	3426.5	-1.72E-03			

Results

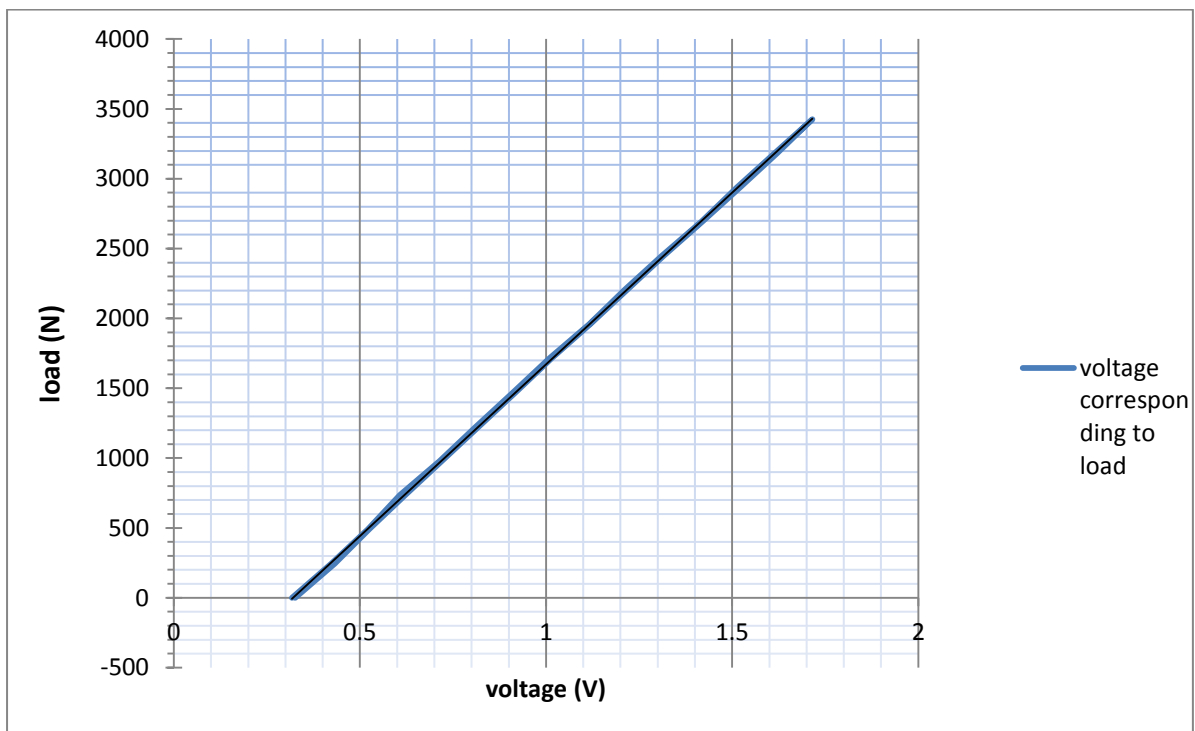


Figure B.1 Load vs voltage graph

From the graph an equation can be derived in the form $Y = M \cdot X + C$

$$Y = -252874 \cdot X - 81.3 \quad (\text{B.1})$$

Where,

Y = load in kg

Y' = load in N = $Y \cdot 9.81$

X = value of voltage in volt

M = slope of the graph = -252874 v

C = Y -intercept of the graph = -81.3 v

B.3 Equations for Strain Gauge Measurements

To simplify the equations and account for unbalanced bridges in the non-strained state, let us introduce the ratio V_r : [67]

$$V_r = (V_{O \text{ (strained)}} - V_{O \text{ (unstrained)}}) / V_{EX} \quad (B.2)$$

Where $V_{O \text{ (strained)}}$ = measured output voltage when strained
 $V_{O \text{ (unstrained)}}$ = initial, unstrained output voltage
 V_{EX} = excitation voltage

Strain before correction takes the lead resistance in to consideration and is given by the equation:

$$\varepsilon = \frac{-4V_r}{GF*(1+2V_r)} * 1 + \frac{R_L}{R_G} \quad (B.3)$$

Where R_G = nominal resistance value of strain gauge
 GF = gauge factor of strain gauge
 R_L = lead resistance

The corrected strain for a quarter-bridge circuit, with a single active gauge at any different strain level can be calculated from: [68]

$$\varepsilon = \frac{2\varepsilon_i}{2+GF(\varepsilon_s-\varepsilon_i)} \quad (B.4)$$

Where ε = corrected strain
 ε_s = calibration strain
 ε_i = indicated strain

Appendix C

C.1 Young's Modulus, Volume Fraction, the Thickness and the Poisson's Ratio of Lamina

Equations used

The rule of mixture model will be selected for the analysis in this research.

1. According to the rule of mixture model [58] [20], if an axial load is applied in the longitudinal direction it will be shared by the fibre and the matrix, therefore longitudinal modulus is given by:

$$E_1 = E_f * V_f + E_m * V_m \quad (C.1)$$

Maximum stiffness is obtained when the stress is applied parallel to the layers.

2. For the transverse modulus, a load is assumed to be applied at right angles to the fibre direction. The simplified equation for transverse stiffness is:

$$E_2 = \frac{E_m E_f}{E_m V_f + (1 - V_f) E_f} \quad (C.2)$$

When the layers are orientated transverse to the applied stress, the effective modulus is lower. Generally the matrix dominated properties of composites material are usually much lower in magnitude than the fibre dominated properties.

3. The major Poisson's ratio refers to the case where a load applied in the fibre direction results in a strain in the fibre direction and a Poisson's contraction transverse to the fibre direction. The major Poisson's ratio is defined as:

$$\nu_{12} = \nu_f * V_f + \nu_m * V_m \quad (C.3)$$

4. For a composite with n layers of fibre with a known areal mass, the total thickness is given by:

$$T_{c1} = n * \frac{m_f}{\rho_f} + \frac{m_m}{\rho_m} \quad (C.4)$$

Total no of lamina, $n = n_1 + n_2 = 12$

5. Volume fraction of each material is the ratio of the thickness contribution of that material to the total thickness.

$$V_{c1} = \frac{T_{c1}}{T_{c1} + T_{c2}} \quad (C.5)$$

C.2 New Stiffness Values According to the Orientation of Ply in Tension and Compression

C.2.1 Equations Used

The elastic constants for a lamina at an orientation to the reference axes were simplified to give the following equations. [49] [69]

1. The longitudinal modulus could be defined as

$$E_x = \left[\frac{\cos^4 \theta}{E_1} + \left(\frac{1}{G_{12}} - 2\frac{v_{12}}{E_1} \right) * \sin^2 \theta * \cos^2 \theta + \frac{\sin^4 \theta}{E_2} \right]^{-1} \quad (C.7)$$

2. Similarly transverse modulus could be defined as

$$E_y = \left[\frac{\cos^4 \theta}{E_2} + \left(\frac{1}{G_{12}} - 2\frac{v_{12}}{E_1} \right) * \sin^2 \theta * \cos^2 \theta + \frac{\sin^4 \theta}{E_1} \right]^{-1} \quad (C.8)$$

3. The shear modulus was defined as

$$G_{xy} = \left[2 \left(\frac{2}{E_1} + \frac{2}{E_2} + 4\frac{v_{12}}{E_1} - \frac{1}{G_{12}} \right) * \sin^2 \theta * \cos^2 \theta + \frac{1}{G_{12}} (\sin^4 \theta + \cos^4 \theta) \right]^{-1} \quad (C.9)$$

4. Finally the Poisson's ratio was defined as

$$v_{xy} = E_x * \left[\frac{v_{12}}{E_1} (\sin^4 \theta + \cos^4 \theta) - \left(\frac{1}{E_1} + \frac{1}{E_2} - \frac{1}{G_{12}} \right) * \sin^2 \theta * \cos^2 \theta \right] \quad (C.10)$$

C.2.2 Variation of Elastic Constants with Fibre Orientation

Using the above equations and the given data from Table 3.3 for the Toray 700G which is in +45⁰/-45⁰ orientation, the following conclusions were formulated.

For tension

The longitudinal and transverse modulus was varied with fibre orientation angle from 0⁰ to 90⁰ [21]. The results are shown in Figure C.1.

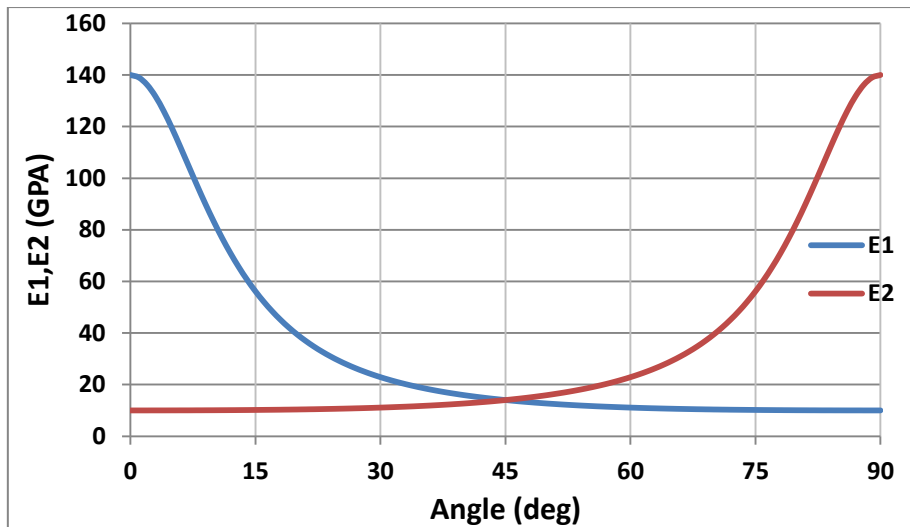


Figure C.1 Variations of Young's modulus for Toray 700G with orientation

The highest and lowest values of E1 and E2 are same and at 45° the value of E1 and E2 will be the same. The stiffness of the composite falls rapidly as the loading direction shifts away from the fibre axis, the effect being marked more, if the stiffness of the reinforcing fibre is higher.

The shear modulus was varied with fibre orientation angle from 0° to 90° . The results are shown in Figure C.2.

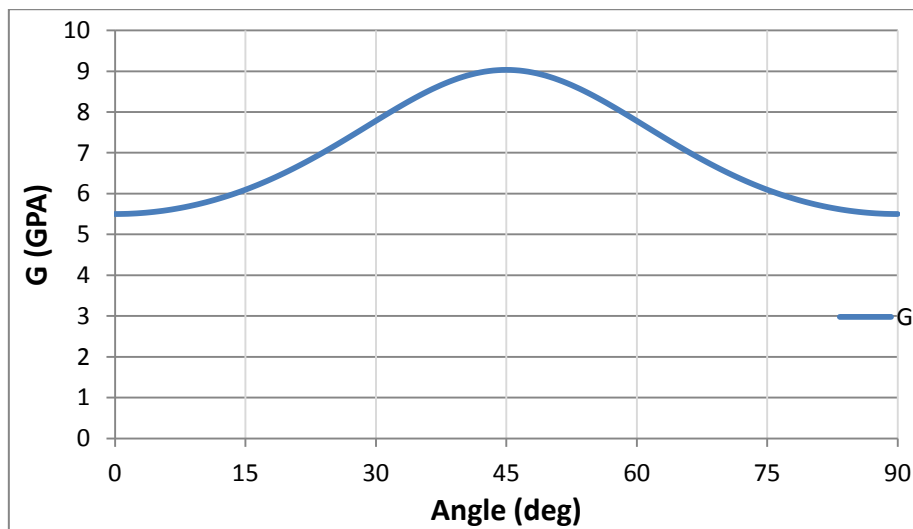


Figure C.2 Variations of shear modulus for Toray 700G with orientation

Since the variation of shear modulus is less sensitive compared to others, it is shown in a different graph for better visibility of the effect. The shear stiffness of the composite is less sensitive to the matrix characteristics as angle increases from 0° to 45° , being largely controlled by the fibre rigidity. The shear modulus is a maximum however in a direction at 45° to the fibre axis thus the lamina will resist torsion.

The Poisson's ratio was varied with fibre orientation angle from 0^0 to 90^0 . The results are shown in Figure C.3.

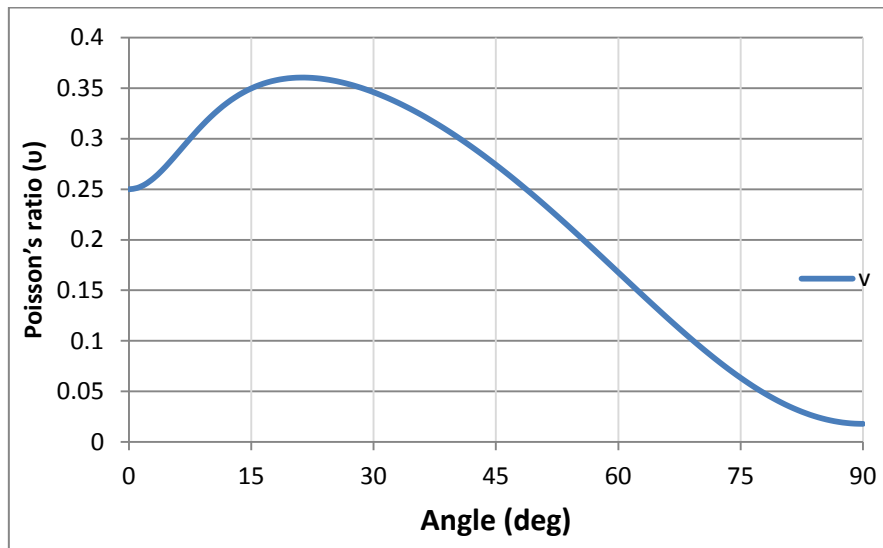


Figure C.3 Variations of Poisson's ratio for Toray 700G with orientation

It is noted that the Poisson's ratio of composites can be relatively large in comparison to a normal isotropic material. This means firstly, that the deformations associated with Poisson's expansion/contraction can be large and secondly, that if these deformations are restrained in any ways, the associated stresses can be quite high.

For compression

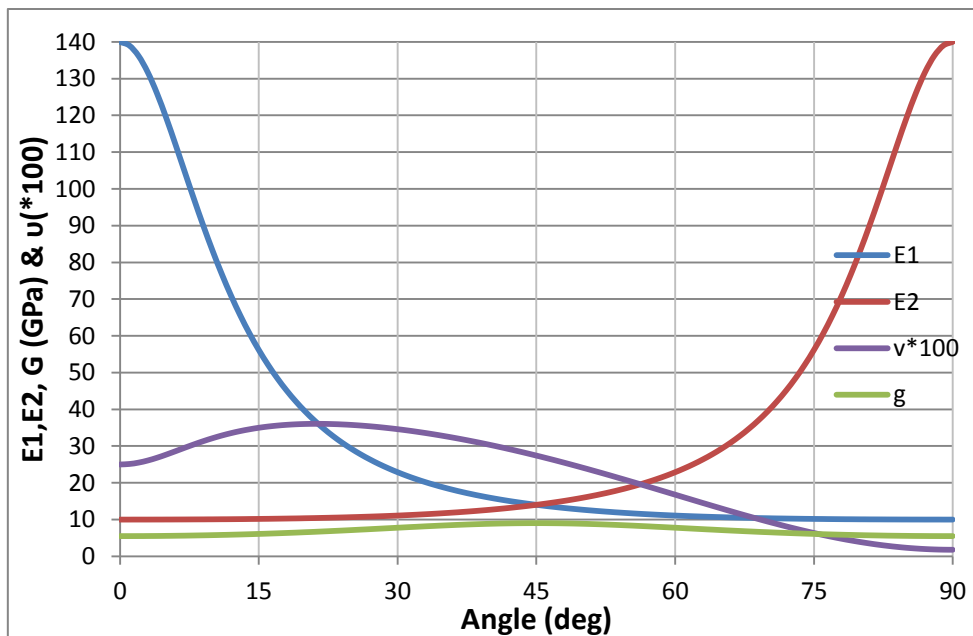


Figure C.4 Variations of elastic constants for Toray 700G with orientation

The Figures indicate that good properties in a particular direction come at the expense of poor properties in another direction. Note that for tension and compression, fibre behaviour

dominates the $0/90^0$ behaviour, while matrix behaviour dominates the $+45^0$ direction. These roles are reversed in the shear case, the $+45^0$ behaviour is fibre dominated. $\pm 45^0$ is the ideal fibre angle to resist pure torsion. The transverse modulus is matrix dominated and tends to be very low in comparison to the fibre dominated longitudinal modulus. Hence a sensible approach to design would be to ensure that transverse stresses are minimised.

C.3 Effective Elastic Constants of the Swingarm for the 12 Layers

Equation used

For simple hybrids consisting of unidirectional plies or mixed, aligned fibre tows, a technique to estimate the effective elastic constants as a function of the volume fraction of the body is done with the following equation. [49] The Young's modulus and shear modulus of most laminate hybrids are predicted satisfactorily by this method. Equation C.1 becomes:

$$E_{\text{hybrid}} = E_A * V_A + E_B * V_B \quad (\text{C.11})$$

$$G_{\text{hybrid}} = G_A * V_A + G_B * V_B \quad (\text{C.12})$$

Where E_A/G_A and E_B/G_B are the moduli of the individual components and V_A and V_B are the volume fractions of the components. As in the case of a simple composite,

$$V_A + V_B = 1.$$

Appendix D

D.1 Effect of Thickness

The thickness is varied by changing the number of laminae in each material with the ratio of 1:1 (700s: 700G) and the new effective stiffness was calculated. The results were then formulated in to a graph to show the effect of thickness on elastic constants.

Results

Table D.1 Effect of thickness on elastic constants

No of layers	Thic kness	Thic kness	Thic kness	Volume fraction	Volume fraction	Elastic modulus	Elastic modulus	Shear modulus
Total	t _{700s}	t _{700G}	Total	t _{700s}	t _{700G}	E11	E22	G
2	0.41	0.52	0.92	0.441	0.559	58.57	11.8	6.99
4	0.81	1.03	1.84	0.441	0.559	58.57	11.8	6.99
6	1.22	1.55	2.77	0.441	0.559	58.57	11.8	6.99
8	1.63	2.06	3.69	0.441	0.559	58.57	11.8	6.99
10	2.03	2.58	4.61	0.441	0.559	58.57	11.8	6.99
12	2.44	3.09	5.53	0.441	0.559	58.57	11.8	6.99
14	2.85	3.61	6.45	0.441	0.559	58.57	11.8	6.99
16	3.25	4.12	7.37	0.441	0.559	58.57	11.8	6.99
18	3.66	4.64	8.3	0.441	0.559	58.57	11.8	6.99
20	4.07	5.15	9.22	0.441	0.559	58.57	11.8	6.99

The variations of effective elastic constants with thickness of the composite are shown in Figure D.1

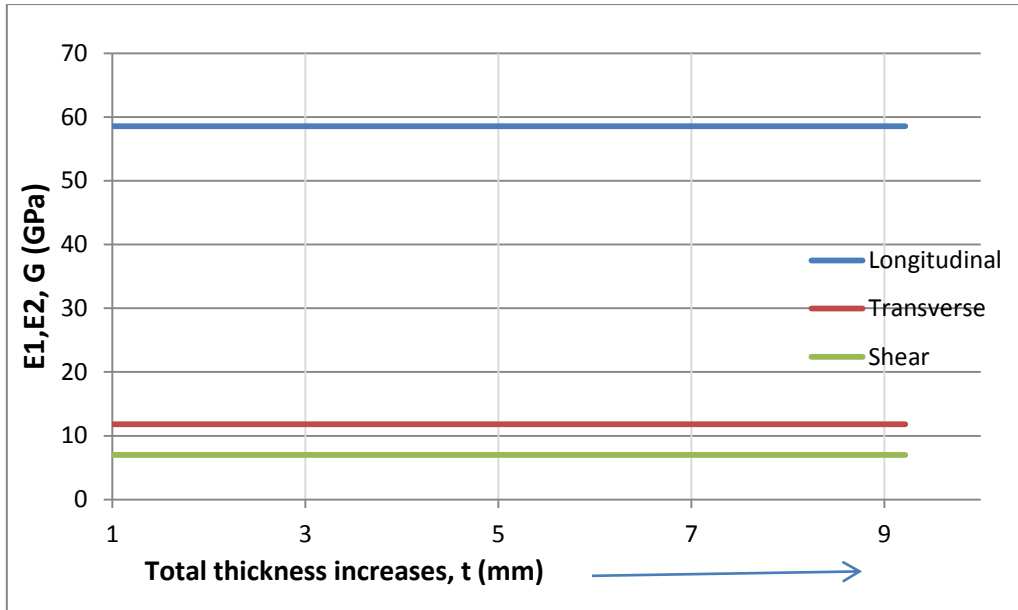


Figure D.1 Variations of effective elastic constants with thickness of composite

The effective longitudinal modulus is higher than all values throughout the system as it is a fibre property followed by effective transverse modulus. The variation of shear modulus is less sensitive than longitudinal modulus but this factor determines the thickness of the body, i.e. based on the total shear the body is meant to resist. It can be observed that the elastic constants do not increase with the increase in thickness since the volume fraction was kept constant as seen in Table D.1. Even though the elastic constants do not change, the strength of the material changes with thickness. But the cost of production will rise since more material is being used. Therefore it is always advisable to use the most effective thickness according to the strength necessary for the product, in the most cost efficient manner.

D.2 Effect of Volume Fraction

The volume fraction is varied by changing the number of laminae in each material, such that $n_1 + n_2 = 12$, and the new effective stiffness was calculated. The results were then formulated in to a graph to show the effect of volume fraction on elastic constants.

Results

Table D.2 Effect of volume fraction on elastic constants

No of layers	No of layers	No of layers	Volume fraction	Volume fraction	Elastic modulus	Elastic modulus	Shear modulus
t_{700S}	t_{700G}	Total	V_{700S}	V_{700S}	E11	E22	G
1	11	12	0.067	0.933	20.78	13.68	8.72
2	10	12	0.136	0.864	27.79	13.33	8.4
3	9	12	0.208	0.792	35.05	12.97	8.07
4	8	12	0.283	0.717	42.6	12.6	7.72
5	7	12	0.361	0.639	50.43	12.21	7.36
6	6	12	0.441	0.559	58.57	11.8	6.99
7	5	12	0.525	0.475	67.03	11.38	6.6
8	4	12	0.612	0.388	75.84	10.94	6.2
9	3	12	0.703	0.297	85.02	10.49	5.78
10	2	12	0.798	0.202	94.59	10.01	5.34
11	1	12	0.897	0.103	104.57	9.52	4.88

D.3 Variation of Dynamic Load

The dynamic load is varied by changing the eccentric radius in the eccentric hub such that the eccentric radius doesn't go beyond the maximum eccentric radius of 0.1 m.

Results

Table D.3 Variation of dynamic load to the eccentric radius

Force (N)	Eccentric radius (m)
627	0.01
1254	0.02
1881	0.03
2508	0.04
3135	0.05
3762	0.06
4389	0.07
5016	0.08
5643	0.09
6270	0.1

D.4 Classical Laminate Theory

The unknowns from Eq. 4.1 (N_1 , ε_y , ε_{xy} , K_1 , K_2 and K_6) are calculated by equating A_{ij} , B_{ij} , and D_{ij} with the know strain (ε_x) in Matlab. The Laminate geometry and ply numbering system used for the calculation of the thickness of laminate are shown in Figure D.2 and the results are shown in Table D.4.

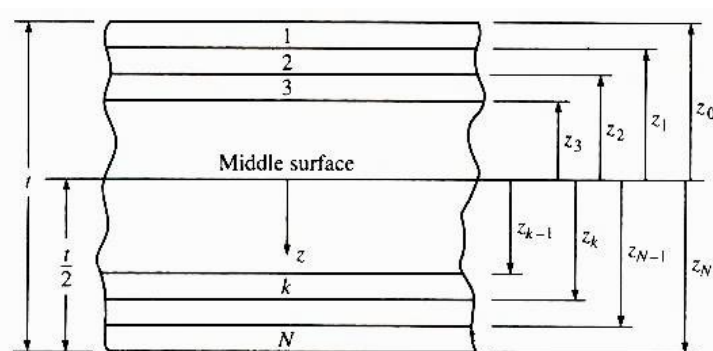


Figure D.2 Laminate geometry and ply numbering system

Table D.4 Calculated values for laminate thickness

Laminate number (K)	Z_k Thickness (mm)	$Z_k - Z_{(k-1)}$	$Z_k^2 - Z_{(k-1)}^2$	$Z_k^3 - Z_{(k-1)}^3$
0	2.7654	-	-	-
1	2.2503	-0.5151	-2.5836	-9.7530
2	1.8436	-0.4067	-1.6650	-5.1290
3	1.3285	-0.5151	-1.6339	-3.9215
4	0.9218	-0.4067	-0.9152	-1.5614
5	0.4067	-0.5151	-0.6843	-0.7160
6	0	-0.4067	-0.1654	-0.0673
7	-0.5151	-0.5151	0.2653	-0.1367
8	-0.9218	-0.4067	0.5843	-0.6466
9	-1.4369	-0.5151	1.2149	-2.1835
10	-1.8436	-0.4067	1.3341	-3.2994
11	-2.3587	-0.5151	2.1646	-6.8564
12	-2.7654	-0.4067	2.0839	-8.0257

For T700S, the lamina stiffness (Q_{ij}) matrix is given as: (from Table 3.4)

$$Q_{ij} = \begin{bmatrix} 140 & 2.5 & 0 \\ 2.5 & 10 & 0 \\ 0 & 0 & 5.5 \end{bmatrix}$$

For T700G, the lamina stiffness (Q_{ij}) matrix is given as: (from Table 3.5)

$$Q_{ij} = \begin{bmatrix} 14.016 & 3.84 & 0 \\ 3.84 & 14.016 & 0 \\ 0 & 0 & 9.032 \end{bmatrix}$$

Using Eq. 4.2, 4.3, 4.4, the A_{ij} , B_{ij} , and D_{ij} were calculated to be:

$$A_{ij} = \begin{bmatrix} -384.94 & -17.969 & 0 \\ -17.969 & -67.719 & 0 \\ 0 & 0 & -41.335 \end{bmatrix}$$

$$B_{ij} = \begin{bmatrix} 167.163 & 0.728 & 0 \\ 0.728 & 3.760 & 0 \\ 0 & 0 & 1.237 \end{bmatrix}$$

$$C_{ij} = \begin{bmatrix} -984.144 & -45.777 & 0 \\ -45.777 & -172.537 & 0 \\ 0 & 0 & -105.29 \end{bmatrix}$$

The Matlab code used to solve the matrix is:

$$A1=Aw(2:end,1);$$

```
for i=1:length(x1)
    b(:,i)=(A1*x1(i)*-1);
    A=Aw(2:end,2:end);
    x(:,i)=mldivide(A,b(:,i));
end
```

Appendix E

E.1 The English code

The English Code

BS AU 50:1

Appendix B

Radial fatigue test

B.1 Test equipment. The test machine shall be one with a means to impart a constant radial force which rotates with respect to the wheel. A suitable form of machine is shown in figure 2, in which the wheel equipped with a tyre is loaded radially against a rotating drum. The drum should

B.3 Test force determination. The test force shall be determined as follows:

$$F_r = F \times K_r \times 9.81$$

where

F_r is the radial test force (in N);

F is the maximum static wheel loading (in kg),
(see 6.7(d));

K_r is a test factor

B.4 Radial test duration. The duration of test shall be 500 000 cycles with F_r applied.

B.5 Accuracy of applied force. The applied test force, as determined by a suitable means of calibration, shall be accurate to within $\pm 5\%$ of its nominal value throughout each rotational cycle.

B.6 Criteria of acceptance. At completion of the test, there shall be no evidence of fatigue cracks (as indicated by a penetrant-dye test) deformation or failure (including looseness) of mechanical fastenings.